PATHOGENESIS OF THEILER'S MURINE ENCEPHALOMYELITIS VIRUS (TMEV) IN AN EXPERIMENTAL MODEL OF EPILEPSY

A Dissertation

by

MEGHA BIJALWAN

Submitted to the Office of Graduate and Professional Studies of
Texas A&M University
in partial fulfillment of the requirements for the degree of

DOCTOR OF PHILOSOPHY

Chair of Committee,	C. Jane R. Welsh
Committee Members,	Louise Abbott
	Farida Sohrabji
	Waithaka Mwangi
Head of Department,	C. Jane R. Welsh

December 2017

Major Subject: Biomedical Sciences

ABSTRACT

Epilepsy is a complex neurological disease composed of two or more unprovoked seizures that occur due to aberrant neuronal hyperexcitability. Detailed analysis of the mechanisms involved in epilepsy is required since there is a lack of adequate preventive therapies and one third of epileptic patients are pharmaco-resistant. Theiler's murine encephalomyelitis virus (TMEV) infection induces a well-characterized experimental model of epilepsy. In response to intracerebral (I.C.) injection of DA or BeAn strain of TMEV in C57BL/6 mice, there is an unregulated immune response that has detrimental effects on neurons, and contributes to acute seizures, rendering mice susceptible to epilepsy. However, the specific contributions of virus and innate immune components to epileptogenesis need to be elucidated. For the first objective, we compared the *in vivo* neurovirulence of two variants of the DA strain, small (DA-D_S) and large (DA-C_L) plaque forming variants, by infecting C57BL/6 mice IC with either DA-D_S or DA-C_L variant. For the latter two objectives, we investigated the function of *Nlrc5* and *Nlrc3* genes as positive or negative regulator of anti-viral immunity and epilepsy by infecting age-matched C57BL/6 wild type, *Nlrc5*$^{-/-}$, and *Nlrc3*$^{-/-}$ mice with BeAn strain of TMEV. The infected mice were monitored for seizures, sickness, weight loss, and cognitive and behavioral deficits during the course of infection. Brains and spinal cords from infected mice were collected to determine viral titers, histopathology, and characterization of cellular infiltration.

We identified that DA-D_S-infected mice exhibited significantly more seizures, sickness behavior, anxiety, weight loss, viral burden, neuroinflammation, and neuronal damage than DA-C_L- infected mice. Thus, DA-D_S variant was found highly neurovirulent, while DA-C_L variant was attenuated in epilepsy.

With respect to NLRs we found that *Nlrc5*$^{-/-}$ infected mice had significantly fewer seizures, lower sickness scores, weight loss and neuroinflammation, than wild type mice. In contrast, *Nlrc3*$^{-/-}$ infected mice were found hypersusceptible to acute seizures, epilepsy, and anxiolytic behavior. Furthermore, we determined that chronic seizures were not the consequence of persistent inflammation. We infer that Nlrc5 significantly upregulated anti-viral inflammation and seizures, while Nlrc3 significantly downregulated acute seizures and chronic epilepsy in C57BL/6 mice.

DEDICATION

This study is dedicated to the people and animals who have been afflicted with epilepsy, my loving parents and brother, and my beloved Nani.

ACKNOWLEDGEMENTS

I am immensely grateful to my advisor, Dr. C. Jane R. Welsh for her constant support, patience and guidance, and for providing the independence to conduct my research. I would also like to thank Dr. Colin Young for introducing me to the disease model and helping me every step of the way. I am thankful to my committee members, Dr. Louise Abbott, Dr. Farida Sohrabji, and Dr. Waithaka Mwangi for their invaluable advice and constructive feedbacks. I would like to express my gratitude to Dr. Jianrong Li for allowing me to use her lab equipment; and her lab members Dr. Sunja Kim, Dr. Andrew Steelman, and Dr. Felix Lu for their advice on troubleshooting the experiments.

To my brother, Shishir, thank you for being my best friend and life "guru". I am forever indebted to my parents, Sunita and Indupati, my mother- and father-in-law, Archana and Ashok, and rest of my big and wonderful family for always believing in me and loving me for who I am. I would like to thank my former professors, Dr. Meena Mrigesh and Dr. A.H. Ahmad for their guidance and support during and after my veterinary medicine program. Additionally, I would like to extend my heartfelt appreciation to my friends, Megha, Pankaj, Rohit, Priyanka, Prerna, Aish, Cameron, Thad, Shehnaz and Abha, for their love and affection. Lastly, I would like to thank my amazing husband, Apurv, for his unwavering patience and love.

CONTRIBUTORS AND FUNDING SOURCES

This work was supervised by a dissertation committee consisting of Dr. C. Jane R. Welsh [advisor] of the Department of Veterinary Integrative Biosciences (TAMU), Dr. Louise Abbott of the Department of Veterinary Integrative Biosciences (TAMU), Dr. Farida Sohrabji of the Department of Neuroscience and Experimental Therapeutics (TAMU), and Dr. Waithaka Mwangi of the Department of Diagnostic Medicine/Pathobiology (Kansas State University). For the first objective (Chapter II), we collaborated with Dr. Julian Leibowitz of the Department of Microbial Pathogenesis and Immunology (TAMU). For the latter two objectives (Chapter III and IV), we collaborated with Dr. Koichi Kobayashi of the Department of Microbial Pathogenesis and Immunology (TAMU).

Mice infections were performed by Dr. Colin Young of the Department of Veterinary Integrative Biosciences (TAMU). The plaque assay and real-time PCR experiments in Chapter II were conducted by Dr. Julian Leibowitz and his postdoctoral fellow Dr. Joseph Tingling. In the Chapter II, Dr. Gus Wright of the Department of Veterinary Pathobiology (TAMU) assisted with flow cytometry; Dr. Raquel Rech of the Department of Veterinary Pathobiology (TAMU) with the analysis of spinal cord sections; and TAMU veterinary student, Alesha R Bullis, and TAMU biomedical undergraduates, Lani, Tara, and Connor with behavioral studies and cell counts. The quantitative real-time PCR analyses depicted in Chapter III were conducted in part by

the former postdoctoral fellow, Dr. Isaac Downs; and flow cytometry in Chapter III and IV were performed by the current postdoctoral fellow, Dr. Tabasum Sidiq at Dr. Koichi Kobyashi's lab. H&E stained brain and spinal cord sections were prepared by Lin Bustamante and Chaitali Mukherjee. All other work conducted for the dissertation was completed by the student independently.

The funding for Chapter II was provided by WHIN (Women's Health in Neuroscience) Dr. Farida Sohrabji of the Department of Neuroscience and Experimental Therapeutics (TAMU) and Dr. C. Jane R. Welsh of the Department of Veterinary Integrative Biosciences (TAMU). The funding for Chapter III and IV was provided by CST*R Clinical Science and Translational Research Institute Pilot Grant, Dr. Koichi Kobayashi of the Department of Microbial Pathogenesis and Immunology (TAMU), and Dr. C. Jane R. Welsh of the Department of Veterinary Integrative Biosciences (TAMU).

NOMENCLATURE

AEDs	Anti-epileptic drugs
AMPA	α-amino-3-hydroxy-5-methyl-4-isoxazolepropionic acid
ANOVA	Analysis of variance
AP-1	Activation protein-1
APCs	Antigen presenting cells
ASC	Apoptosis-associated speck-like protein containing a CARD
ATP	Adenosine triphosphate
Av.	Alveus
β_2-m	β_2-microglobulin
BBB	Blood-Brain Barrier
BHK	Baby hamster kidney
BMDMs	Bone marrow-derived macrophages
BSA	Bovine serum albumin
CITA	MHC class I transactivator
CIITA	MHC class II transactivator
C3	Complement3
CA	Cornu ammonis
CARD	Caspase activation and recruitment domain
CDC	Center for Disease Control and Prevention
cDNA	complementary DNA

CLNs	Cervical lymph nodes
cm	Centimeter
CMV	Cytomegalovirus
CNS	Central Nervous System
DA	Daniel’s
DA-C_L	Large plaque forming variant of DA strain
DA-D_S	Small plaque forming variant of DA strain
DAMPs	Danger-associated molecular patterns
DG	Dentate gyrus
DI	Discrimination Index
EPMT	Elevated plus maze test
EPSCs	Excitatory post-synaptic currents
Et al.	Et alia
FBS	Fetal bovine serum
GABA	Gamma-Amino Butyric acid
GFAP	Glial fibrillary acidic protein
H&E	Hematoxylin and Eosin
HF	Hippocampal fissure
HFF	Human foreskin fibroblast
Hi	High
HRV	Human rhinovirus
HS	Hippocampal sclerosis

HSV-1	Herpes simplex virus-1
IACUC	Institutional Animal Care and Use Committee
IBA1	Ionized calcium-binding adaptor molecule1
I.C.	Intracerebral
IFN	Interferon
IHC	Immunohistochemistry
IκB	Inhibitor of kappa B
IL	Interleukin
ILAE	International League against Epilepsy
iNOS	Inducible nitric oxide synthase
Int	Intermediate
IRF3	Interferon regulatory factor 3
KA	Kainic acid
kg	Killogram
LMP2	Low molecular mass proteasome
LPS	Lipopolysaccharide
LRR	Leucine-rich repeats
Mcp-1	Monocyte chemoattractant protein-1
MEFs	Mouse embryonic fibroblasts
mg	Milligram
MHC	Major Histocompatibility Complex
Mip-2	Macrophage inflammatory protein-1

µl	Microliter
mm	Millimeter
µm	micron
MS	Multiple sclerosis
mTLE	Mesial temporal lobe epilepsy
mTOR	mechanistic target of Rapamycin
Natural Killer	NK
NBD	Nucleotide-binding domain
NDV	Newcastle disease virus
NFAT-1	Nuclear factor of activated T-cells
NF-κB	Nuclear factor kappa-light-chain-enhancer of activated B cells
NLR	Nucleotide-binding oligomerization domain-like receptor
NLRC3	NLR family CARD domain containing 3
NLRC4	NLR family CARD domain containing 4
NLRC5	NLR family CARD domain containing 5
NLRP1	NLR family pyrin domain containing 1
NLRP3	NLR family pyrin domain containing 3
NLRP12	NLR family pyrin domain containing 12
NLRX1	NLR family member X1
NMDA	N-methyl-D-aspartate
NOLT	Novel object location test
NORT	Novel object recognition test

OCT	Optimum cutting temperature
PAMPs	Pathogen-associated molecular patterns
PBS	Phosphate buffer saline
PCR	Polymerase chain reaction
PFA	Paraformaldehyde
PFU	Plaque forming unit
p.i.	Post infection
Poly (I:C)	Polyinosinic:polycytidylic
PRRs	Pattern recognition receptors
PVC	Perivascular cuffing
qRT-PCR	Quantitative real-time PCR
RANTES	Regulated Upon Activation, Normally T-Expressed, And Presumably Secreted
RIG-1	Retinoic acid inducible gene-1
rpm	Revolutions per minute
RSV	Respiratory syncytial virus
SEM	Standard error of the mean
SeV	Sendai virus
SLM	Stratum-lacunosum moleculare
STAT1	Signal transducer and activator of the transcription 1
STING	Stimulator of interferon genes
TAP1	Transporter associated with antigen processing 1

TBK1	TANK-binding kinase 1
TCR	T cell receptor
TGF-β	Tumor growth factor β
TLR	Toll-like receptor
TMEV	Theiler's murine encephalomyelitis virus
TNF-α	Tumor necrosis factor-α
TO	Theiler's original
TRAF6	TNF receptor associated factor 6
UTR	Untranslated region
VEEG	Video-electroencephalogram
vol/vol	Volume/volume
VSV	Vesicular stomatitis virus
WNV	West Nile virus
w/v	Weight/volume

TABLE OF CONTENTS

Page

ABSTRACT ii

DEDICATION iv

ACKNOWLEDGEMENTS v

CONTRIBUTORS AND FUNDING SOURCES vi

NOMENCLATURE viii

TABLE OF CONTENTS xiv

LIST OF FIGURES xvi

LIST OF TABLES xxvi

CHAPTER I INTRODUCTION AND LITERATURE REVIEW 1

Overview of epilepsy 1
Theiler's murine encephalomyelitis virus 7
The nucleotide-binding oligomerization domain-like receptors 12
Objective of this dissertation 19

CHAPTER II CHARACTERIZATION OF PLAQUE-SIZED VARIANTS OF DANIEL'S (DA) STRAIN IN TMEV-INDUCED EPILEPSY 20

Introduction 20
Materials and methods 23
Results 37
Discussion 64

CHAPTER III THE *NLRC5* GENE IS CRITICAL FOR INNATE IMMUNITY AND SEIZURE DEVELOPMENT IN TMEV-INDUCED EPILEPSY MODEL 74

Introduction 74
Materials and Methods 77
Results 87
Discussion 107

CHAPTER IV NLRC3: A NOVEL DOWNREGULATOR INVOLVED IN TMEV-INDUCED EPILEPSY MODEL 113

Introduction 113
Materials and Methods 116
Results 122
Discussion 133

CHAPTER V CONCLUSIONS 139

TMEV-induced murine model of epilepsy 139
TMEV-induced demyelinating disease model 140
Virulence and pathogenicity of plaque-sized variants of DA strain in epilepsy 141
Implication of NLRs in neurological diseases 142
The role of *Nlrc5* gene in TMEV-induced experimental model of epilepsy 143
The role of *Nlrc3* gene in TMEV-induced experimental model of epilepsy 144
Future directions 147

REFERENCES 149

LIST OF FIGURES

Page

Figure 1 Immune responses in the TMEV-induced model of epilepsy. (1) Upon intracerebral (I.C.) injection, TMEV is localized mainly in the hippocampal and cortical neurons. (2) In response to infection, the resident cells of the central nervous system (CNS), microglia and astrocytes, become activated and secrete several cytokines and chemokines. (3) The increased production of pro-inflammatory mediators disrupts the integrity of the Blood-Brain Barrier (BBB), and allows the infiltration of peripheral innate immune cells, monocytes/macrophages, neutrophils, into the CNS. (4) The overzealous inflammation within the CNS causes severe damage to hippocampal neurons, resulting in neuronal hyperexcitability and symptomatic seizures within a week p.i. (5) The T cell-mediated viral clearance occurs within a month p.i., (6) but the acute phase events subsequently lead to the development of epilepsy after an undefined latent period. 11

Figure 2 Experimental timeline. The acute phase of disease is defined as up to day 7 p.i., during which seizures, non-epileptic clinical illness, weights, viral burden, inflammation and CNS pathology were determined. The chronic phase is defined as from week 2 to 11 p.i. or until the termination of mice. Chronic phase measures included clinical scores (spontaneous seizures), weights, elevated plus maze test (EPMT), novel object recognition test (NORT), novel object location test (NOLT), and histological analyses of the CNS 23

Figure 3 Schematic diagram of the elevated plus maze. The maze was made of black plexiglass. It consisted of two opposing open and closed arms placed in the shape of a plus, and a platform at the intersection of the arms. The maze was kept elevated at a height of 50 cm above the ground. 32

Figure 4 Schematic diagram of novel object- and novel location- test setup. The open arena made of plexiglass, and non-edible, odorless objects were used for the tests. The test was conducted over a period of five days, comprising of a 5-min session of habitutation phase, 10 min-session of familiarization phase for NORT and NOLT each, a 10-min session of test phase for NORT and NOLT each, with a rentention delay of 24 h between the phases. 33

Figure 5 Seizures induced by infection with DA-D_S were significantly more frequent and more severe than those induced by DA-C_L. (A) Significantly higher number of mice developed seizures following DA-D_S infection. In contrast, the DA-C_L plaque-variant failed to induce seizures in most of the infected mice (**** $p<0.0001$ by Fisher's exact test). The % of seized mice in each

group was calculated as (number of seized mice/total number of infected mice) x 100. (B) The seizure frequency was significantly higher due to infection by DA-D_S than DA-C_L (**** $p<0.0001$ by unpaired t test with Welch's correction). The data are only from seized mice in DA-C_L and DA-D_S groups, N= 4 and 31, respectively. (C) In the DA-C_L group, most of the mice (denoted as %) did not seize and hence, were given Racine score 0, while very few mice exhibited Racine stage 4 or 5 seizures. In comparison, in the DA-D_S group the majority of mice (denoted as %) exhibited seizures of Racine stage 5, and few mice had seizures of Racine stage 3 and 4. (D) Seizures in DA-C_L group were only seen on day 3 p.i., while seizures in DA-D_S group began from day 2 p.i. and lasted till day 7 p.i. with most mice seizing on days 3, 4 and 5 p.i. (E) The duration of seizures that occurred on day 3 p.i. were not significantly different between the groups. However, the duration of seizures in the DA-D_S group showed a significant linear trend over days p.i. (**** $p<0.0001$ by one-way ANOVA with post test for linear trend). Graphs (A, B, C and D) show pooled results from four separate experiments expressed as number/ percent/ mean ± SEM, N=33 per infected group. Graph (E) shows pooled results from three separate experiments expressed as mean ± SEM, N=23 per infected group.....40

Figure 6 Mice infected with DA-D_S plaque variant displayed severe non-epileptic clinical signs in the acute phase. Mice were observed daily for signs of non-epileptic clinical disease during the acute phase. Both the virus infected groups showed clinical signs, but clinical scores were significantly higher in DA-D_S-infected group compared to that in DA-C_L-infected group (* $p<0.05$, ** $p<0.01$, *** $p<0.001$, **** $p<0.0001$ by Mann-Whitney rank sum test). The clinical scores lowered in DA-C_L group, but they remained persistently high in DA-D_S group. Graph shows pooled results from four separate experiments expressed as mean ± SEM, N=33 per infected group. ...41

Figure 7 Mice infected with DA-D_S plaque variant had a significant delay in their recovery. Mice from the control and infected groups were weighed daily until day 7 p.i. and then once weekly until week 5 p.i. (A) We found that the infected mice lost weight following infection during the acute phase, but the highest weight loss was found in the DA-D_S-infected group. (B) DA-C_L-infected mice recovered by week 3 p.i., while recovery among DA-D_S-infected mice was not seen until week 5 p.i. (* $p<0.05$, **/$^{\#\#}$ $p<0.01$, ***/$^{\#\#\#}$ $p<0.001$, ****/$^{\#\#\#\#}$ $p<0.0001$ by Repeated Measures two-way ANOVA with Tukey's multiple comparisons test). Graph A shows pooled results from four separate experiments expressed as mean ± SEM, N=4 in control group and N=32 per infected group. Graph B shows pooled results from two separate experiments expressed as mean ± SEM, N=4 in control group and N=13 per infected group. 43

Figure 8 DA-D_S infection induced significant neuro-edema in mice. To determine the effects of plaque-variants on neuro-edema, brains from infected and control mice were collected and weighed at day 7 p.i. The brains from DA-D_S-infected group weighed significantly more compared to that from control or DA-C_L-infected group. (*** $p<0.001$ by One-way ANOVA with Tukey's multiple comparisons test). Graph shows pooled results from two separate experiments expressed as mean ± SEM, N=3 in control group and N=19 per infected group. 44

Figure 9 Increased viral burden in mice infected with DA-D_S plaque-variant. At day 7 p.i., brains from DA-D_S-infected mice had significantly higher viral titers than DA-C_L-infected mice. Viral load was also detected in their spinal cords at this time point, but no significant difference was observed between the groups. (*** $p<0.001$ by Unpaired t test with Welch's correction). Graph shows mean ± SEM, N=10 in DA-C_L group and N=11 in DA-D_S group. 45

Figure 10 Increased number of viral-antigen positive cells in the hippocampus of DA-D_S-infected mice. At day 7 p.i., (A and B) viral-antigen was primarily detected in the CA1 and CA2 pyramidal layers (white arrows) of the hippocampus in both the infected groups. Some of the cortical neurons surrounding the CA1 and CA2 pyramidal layers also stained positive for viral-antigen. (C) The number of viral-antigen positive cells in the hippocampus was significantly higher in the DA-D_S-infected group than that in the DA-C_L-infected group. (** $p<0.01$ by Unpaired t test with Welch's correction). Graph shows mean ± SEM, N=4/infected group. Cornu ammonis1 (CA1), Cornu ammonis2 (CA2), Cornu ammonis3 (CA3), and dentate gyrus (DG).....46

Figure 11 Heterogeneous astroglial pathology among infected mice. (A) Schematic diagram of the coronal section of hippocampus depicting different areas of CA1 field. (B) In comparison to the control mice that express resting/quiescent astrocytes, viral-infected mice exhibit reactive astrocytes that appear hypertrophied and have increased expression of GFAP protein. Among the infected mice, the CA1 region of the hippocampus showed varied astroglial pathology. In both the infected groups, activated astrocytes were found at the SLM area of CA1. The astrocytes were also found lining the PVCs at SLM. At the CA1-A area of the hippocampus, we found activated, but fewer astrocytes (possible astroglial degeneration) near the damaged CA1 pyramidal layer in both groups. At the CA1-B area, astrocytes were more reactive in the DA-D_S-infected group than that in the control or DA-C_L-infected group. Images were taken under 200x magnification. (C) The total astrocyte count within the hippocampus was not found to be significantly different between the infected groups (Unpaired t test with Welch's correction). Graph shows mean ± SEM,

N=4/infected group. Cornu ammonis1 (CA1), dentate gyrus (DG) and stratum lacunosum-moleculare (SLM). 48

Figure 12 Extensive inflammation and neuronal damage in the hippocampus of mice infected with DA-D_S variant. (A) H&E stained coronal section of hippocampus from control mice. Hippocampal regions from the infected groups were analyzed at days 3 (B and F) and 7 (C and G) and weeks 5 (D and H) and 11 (E and I) p.i. for histopathology. B-E are the representative images from DA-C_L-infected group and F-I are the representative images from DA-D_S-infected group. By day 3 p.i., both the infected groups (B and F) showed increase in cellularity and PVCs at alveus, hippocampal fissure and stratum lacunosum-moleculare area of CA1 and CA2 regions. However, the loss of CA1 and CA2 pyramidal neurons was found only in the DA-D_S-infected group at this time-point. At day 7 p.i., both the inflammation, and CA1 and CA2 neuronal loss, were extremely severe in the (G) DA-D_S-infected mice and greater than that in the (C) DA-C_L-infected mice. (C) A representative section of hippocampus from DA-C_L-infected group presenting CA1-CA2 damage score 2. (G) A representative section of hippocampus from DA-D_S-infected group presenting CA1-CA2 damage score 10. By week 5 p.i., the inflammation mostly resolved in the (D) DA-C_L-infected mice, while it remained high in the (H) DA-D_S-infected mice. At week 11 p.i., no inflammation was found in the (E) DA-C_L-infected group and the intensity of inflammation appeared to decrease in the (I) DA-D_S-infected group. The arrowheads depict neuronal loss and the asterisks depict inflammation in the images. All images were taken under 100X magnification. At day 7 p.i., (J) the damage to the CA1 and CA2 pyramidal layers (** $p<0.01$ by Mann-Whitney test. Sum of ranks) and (K) the intensity of inflammation (* $p<0.05$ by Unpaired t test with Welch's correction) were found to be significantly higher in the DA-D_S-infected group in comparison to that in the DA-C_L-infected group. Graphs show mean ± SEM, N=5 per infected group. Cornu ammonis1 (CA1), cornu ammonis2 (CA2), cornu ammonis3 (CA3), dentate gyrus (DG), alveus (Av.), hippocampal fissure (HF) and stratum lacunosum-moleculare (SLM)..50

Figure 13 Acute inflammation was more pronounced at the lumbar segment of spinal cord following DA-D_S-infection. H&E stained lumbar segments from the (A and C) control group, (B) DA-C_L-infected group, and (D) DA-D_S-infected group. (A and C) No lesions were found in the control group. (B and D) The most affected lumbar segments showing meningitis, PVC, and inflammatory foci in the gray and white matter, and representing scores 3. (E) The degree of inflammation was similar at the cervical, thoracic and sacral segments, while the lumbar segments from the DA-D_S-infected group were found significantly more inflamed than that in the DA-C_L-infected group (* $p<0.05$ by Kolmogorov-Smirnov test). All images were taken

under 100X magnification. Graph shows mean ± SEM, N=5 in DA-C_L group and N=6 in DA-D_S group. Arrowhead indicates possible neuronophagia and arrows indicate inflammation. 53

Figure 14 Increased immune cell infiltration into the CNS of mice following DA-D_S-infection. Brain leukocytes from control and infected mice were collected at day 3 p.i. and stained for cell specific markers. (A) Our results showed that DA-D_S infection significantly increased the expression levels of CD45.2+ in the brain. Upon further analysis, we found that (B and D) neither of the plaque-variants significantly altered CD45.2int and CD45.2int CD11b+ expression levels, while (C) the expression levels of CD45.2hi were DA-D_S > DA-C_L > control group, and (E and F) DA-D_S plaque variant significantly increased the expression levels of CD45.2hi CD11b+ and CD45.2hi Gr1+ in mice brains during the acute phase. Graphs show pooled results from five separate experiments expressed as mean ± SEM, N=5 in control group and N=13 per infected group. (* $p<0.05$, ** $p<0.01$, *** $p<0.001$ by One-way ANOVA with Tukey's multiple comparisons test). 55

Figure 15 Mice with DA-D_S infection developed anxiety-like behavior in the chronic phase. (A) Neither of the plaque-variants affected locomotor activity, but (B) only DA-D_S plaque-variant induced anxiety-like symptoms as infected mice hesitated to enter open arms of the elevated plus maze. Graphs show results expressed as mean ± SEM, N=4 in control group and N=8 per infected group. (* $p<0.05$ by one-way ANOVA with Tukey's multiple comparisons test). 57

Figure 16 The two plaque-variants had no effect on the context-associated memory, but they significantly impaired spatial-associated memory in mice. The results from cognitive tests conducted in the chronic phase showed that (A and B) DI and exploration time (novel object) in NORT remained unaffected following viral infection. (C) DI in NOLT was relatively lower following DA-D_S-infection, but (D) both DA-C_L and DA-D_S plaque-variants significantly decreased exploration time of the displaced object in NOLT. Graphs show results expressed as mean ± SEM. N=4 in control group and N=8 per infected group. (* $p<0.05$, ** $p<0.01$ by Two-way ANOVA with Tukey's multiple comparisons test). Discrimination index (DI), novel object recognition test (NORT), and novel object location test (NOLT). 60

Figure 17 TMEV-induced acute seizures were significantly reduced due to Nlrc5 deficiency. (A) Acute phase results revealed a significant decrease in the proportion of *Nlrc5*$^{-/-}$ infected mice with seizures in comparison to wild type infected mice. The % seized mice in each group was calculated as (number of seized mice/total number of infected mice) x 100. No seizures were

observed in the control groups. (B) Daily examinations of mice showed that *Nlrc5*$^{-/-}$ infected group had significantly fewer seizures than wild type infected group from days 2-5 p.i. The % seized mice per day was calculated as (number of seized mice in a day /total number of infected mice) x 100. (C and D) In both the infected groups, seizures were mostly of highest intensity, i.e. stage 5, while few mice had seizures of stage 3 and 4 on the Racine scale. (**** $p<0.0001$, ** $p<0.01$, * $p<0.05$ by Fisher's exact test). Graphs (A, B, C, D and E) show pooled results from six separate experiments expressed as percent or mean ± SEM, N=4 per control group and N=30-37 per infected group. Graph F shows pooled results from three separate experiments expressed as mean ± SEM, N=12 in wild type infected group and N=3 in *Nlrc5*$^{-/-}$ infected group. 89

Figure 18 Knocking out *Nlrc5* gene alleviates non-epileptic clinical disease following TMEV infection. Mice were observed daily for signs of non-epileptic clinical disease during the acute phase. Both the wild type and *Nlrc5*$^{-/-}$ infected groups showed clinical signs of illness, but clinical scores were significantly lower in *Nlrc5*$^{-/-}$ infected group compared to that in wild type infected group (* $p<0.05$, *** $p<0.001$ by Mann-Whitney rank sum test). Graph shows pooled results from six separate experiments expressed as mean ± SEM, N=30-41 per infected group. 90

Figure 19 The *Nlrc5* gene had a significant effect on mice weights following infection. To determine recovery post infection, mice from the control and infected groups were weighed daily until day 6 p.i. Both the infected groups exhibited significant weight loss immediately following TMEV infection in comparison to their respective controls. However, the body weight comparisons between the infected groups showed that *Nlrc5*$^{-/-}$ mice weighed significantly more than the wild type mice at earlier time-points, indicating better recovery among *Nlrc5*$^{-/-}$ infected mice. (Between wild type control and infected groups: δδδδ $p<0.0001$; between *Nlrc5*$^{-/-}$ control and infected groups: $^{\#}$ $p<0.05$, $^{\#\#}$ $p<0.01$, $^{\#\#\#}$ $p<0.001$; between wild type and *Nlrc5*$^{-/-}$ infected groups: * $p<0.05$, ** $p<0.01$ by Unpaired t test with Welch's correction). Graph shows pooled results from five separate experiments, expressed as mean ± SEM, N=4/control group and N=26/infected group. 92

Figure 20 The *Nlrc5* gene had variable effects on different leukocyte populations in the brain and CLNs. To examine the extent of inflammation at the time of peak seizures, we analyzed the expression of leukocyte subsets in the brain and CLNs at day 3 p.i. In the brain, the deficiency of *Nlrc5* gene caused a significant reduction in the expression of CD45.2hi NK1.1+ (NK) cells, and mild reduction in the expression of CD45.2hi CD11c+ cells (dendritic cells) and CD45.2hi CD4+ CD69+ cells (activated T helper cells), while it led to a slight increase in the expression of CD45.2hi CD11b+ cells

(monocytes/macrophages, granulocytes, etc.) and CD45.2hi Gr1+ cells (granulocytes). In the CLNs, the deficiency of *Nlrc5* gene only mildly downregulated the expression of CD45.2hi CD8+ cells (cytotoxic T cells). (* $p<0.05$ by Unpaired t test with Welch's correction). Graphs (A-E) show results expressed as mean ± SEM, N=3 per infected group. 94

Figure 21 Nlrc5 deficiency induced a significant reduction in the number of GFAP+ cells, but not IBA+ cells, following infection. To assess the effect of Nlrc5 deficiency on the proliferation and activation of astrocytes, microglia/macrophages, and virus-infected cells in the hippocampus, we stained 10 μm coronal sections of fixed brain with antibody against GFAP, IBA, and TMEV-antigen, respectively. (A-F) are the representative images (400x) of CA1, CA3, and DG regions of hippocampus showing GFAP+ astrocytes. (G) The number of astrocytes was significantly reduced in the hippocampus, specifically in the CA1 and dentate gyrus regions, of *Nlrc5*$^{-/-}$ infected mice than wild type infected mice. (H-M) are the representative images (400x) of CA1, CA3, and DG regions of hippocampus showing IBA+ macrophages/microglia. (N) The infected groups had no significant differences in the number of macrophages and microglia in the hippocampus. (O and P) are the representative images (100x) from infected groups showing that TMEV-antigen positive cells were mainly localized in the CA1 and CA2 pyramidal neurons, while TMEV-antigen was not detected in the DG and CA3 neurons. (* $p<0.05$, ** $p<0.01$, **** $p<0.0001$ by Unpaired t test with Welch's correction). Graphs (G and N) show results expressed as mean ± SEM, N=7-9 per infected group. Cornu ammonis1 (CA1), cornu ammonis2 (CA2), and dentate gyrus (DG). 97

Figure 22 Nlrc5 deficiency mitigates hippocampal damage in TMEV-induced seizure model. To determine the effect of Nlrc5 on the extent of inflammation and damage in the hippocampus following infection, we compared the cresyl violet-stained 10 μm coronal sections of fixed brain. (A-C) are the representative images (20x) from wild type control, wild type infected and *Nlrc5*$^{-/-}$ infected group, respectively. The preliminary results indicate that TMEV-infection induced CA1 neuronal damage was less severe in *Nlrc5*$^{-/-}$ than that in wild type infected mice. Cornu ammonis1 (CA1), cornu ammonis2 (CA2), dentate gyrus (DG), and hippocampal fissure (HF).....98

Figure 23 Knocking out *Nlrc5* gene did not alter the resistance to TMEV-induced demyelinating disease. To investigate whether Nlrc5 gene affects the resistance of C57BL/6 mice to TMEV-induced demyelinating disease, we compared the H&E-stained four μm transverse sections from cervical, thoracic, lumbar and sacral segments of spinal cords from infected mice and compared the histological condition with their respective controls. At day 52 p.i., we did not find active inflammation or demyelinating lesions in the

spinal cords from any of the infected mice. (A-D) are the representative images (100x) from thoracic segment of the spinal cord from wild type control, *Nlrc5*$^{-/-}$ control, wild type infected and *Nlrc5*$^{-/-}$ infected groups. 99

Figure 24 Expression of target genes in the brain following TMEV infection: To assess the effects of Nlrc5 deficiency on the expression of virus and inflammatory mediators, we compared the mRNA levels of target genes from the brains of infected mice at day 7 p.i. The comparisons between control and infected groups, and between wild type and *Nlrc5*$^{-/-}$ infected groups showed that (A) TMEV infection caused a significant increase in the expression of *Nlrc5* in wild type mice. (B) The mRNA levels for virus were similar between the infected groups. (C-E) Nlrc5 deficiency caused a significant reduction in the expression of MHC class I and its associated genes, (F-G) while it did not affect the expression of MHC class II and its related genes following TMEV infection. Nlrc5 deficiency significantly downregulated the expression of pro-inflammatory cytokines, (H) *Ifn-β,* (J) *Ifn-β*, but had minimal or no effects on the expression of (I) *Ifn-γ*, (K) *Il-6*, and (L) *Tnf-α*. (M) The expression of anti-inflammatory cytokine, *Tgf-β* was only mildly increased in wild type infected mice, but Nlrc5 deficiency significantly upregulated its expression following infection. The mRNA levels of chemokines, (N) *Mcp-1*, (O) *Rantes*, and (P) *Mip-2*, were highly upregulated in wild type infected mice, but Nlrc5 deficiency only slightly decreased the expression of *Mcp-1* and *Mip-2* following infection. (Q) When compared to the controls, the expression of *iNos* was significantly increased in wild type infected mice, but not in *Nlrc5*$^{-/-}$ infected mice. (Between control and infected groups: $^{\#}$ $p<0.05$, $^{\#\#}$ $p<0.01$, $^{\#\#\#}$ $p<0.001$, $^{\#\#\#\#}$ $p<0.0001$; between wild type and *Nlrc5*$^{-/-}$ infected groups: * $p<0.05$, ** $p<0.01$, *** $p<0.001$, **** $p<0.0001$ by Unpaired t test with Welch's correction or Two-way ANOVA with Tukey's multiple comparisons test). Graphs (A-Q) show results expressed as mean ± SEM, n=1-4/control group and n=3-5/infected group.....105

Figure 25 Mice did not exhibit anxiety-like symptoms following infection. To determine the effects of neuronal damage and *Nlrc5* gene on the development of anxiety-like symptoms in mice, we conducted EPMT at one-month p.i. (A) % time spent in open arms, (B) number of entries in open arms, and (C) number of entries in closed were similar among the groups, suggesting that the infected mice did not show any behavioral or locomotor abnormality, with the exception of one wild type infected mouse. The % time spent in open arms was calculated as (time spent in open arms/time spent in open and closed arms) x 100. The number of entries in open and closed arms was recorded manually at the time of the experiment. (One-way ANOVA with Tukey's multiple comparisons test). Graphs (A-C)

show results expressed as mean ± SEM, N=3-4 per control group and N=5 per infected group. 107

Figure 26 Nlrc3 deficiency increased the susceptibility of mice for TMEV-induced seizures. (A) Acute phase results revealed a significant increase in the proportion of *Nlrc3*$^{-/-}$ infected mice with seizures in comparison to wild type infected mice. The % seized mice in each group was calculated as (number of seized mice/total number of infected mice) x 100. No seizures were observed in the control groups. (B) Daily examinations of mice showed that *Nlrc3*$^{-/-}$ infected group had significantly more seizures that lasted a day longer than wild type infected group. The % seizures per day was calculated as (number of seizures in a day /total number of infected mice) x 100. (C and D) In both the infected groups, seizures were mostly of highest intensity, i.e. stage 5, while few mice had seizures of stage 3 and 4 on the Racine scale. (**** $p<0.0001$, *** $p<0.001$, ** $p<0.01$ by Fisher's exact test). Graphs (A, B, C, and D) show pooled results from four separate experiments expressed as percent, N=4 per control group and N=23-24 per infected group. 124

Figure 27 *Nlrc3*$^{-/-}$ infected mice had increased susceptibility to TMEV-induced epilepsy compared to wild type infected mice. Weekly examinations of the mice showed that chronic seizures in *Nlrc3*$^{-/-}$ infected group started as early as week 2 p.i. and were recorded until the termination of mice, i.e. week 30 p.i. In contrast to *Nlrc3*$^{-/-}$ mice, chronic seizures were only documented at week 28 p.i. in the wild type infected group. The seizure frequency in each group was calculated as number of seizures per week during chronic phase. Graph shows pooled results from two separate experiments expressed as seizure frequency, N=12 per infected group.....125

Figure 28 *Nlrc3*$^{-/-}$ infected mice showed better recovery than wild type infected mice. Mice from the control and infected groups were weighed daily until day 6 p.i. and then once weekly until day 56 p.i. Both the infected groups exhibited significant weight loss immediately following TMEV infection in comparison to their respective controls. However, *Nlrc3*$^{-/-}$ infected mice started to regain weight earlier than wild type infected group, indicating faster recovery in *Nlrc3*$^{-/-}$ infected group. Both the infected groups showed complete recovery by day 21 p.i., when their weights matched with those of their respective controls. (Between wild type control and infected groups: δδ $p<0.01$, δδδδ $p<0.0001$; between *Nlrc3*$^{-/-}$ control and infected groups: ## $p<0.01$, #### $p<0.0001$; between *Nlrc3*$^{-/-}$ infected and wild type infected groups: * $p<0.05$, **** $p<0.0001$ by Repeated Measures two-way ANOVA with Tukey's multiple comparisons test). Graph shows pooled results from acute phase (days 0-6 p.i.) and chronic phase (days 14-56 p.i.) studies, expressed as mean ± SEM. During acute phase, results are from four

separate experiments, N=22-23 per infected group, during chronic phase, result is from one experiment, N=6-7 per infected group. For control groups, N=4 during acute and chronic phase.....127

Figure 29 Nlrc3 deficient mice developed aberrant emotional behavior following TMEV infection. We conducted EPMT to determine behavioral abnormalities among infected mice during chronic phase. Graphs A-C are from study conducted on day 17 p.i., and graphs D-F are from study conducted on day 34 p.i. The EPMT results show that *Nlrc3*$^{-/-}$ infected mice spent significantly more time exploring the open arms, and had significantly higher open and closed arms entries than the other groups, indicating hypermobility and development of anxiolytic behavior. The % time spent in open arms was calculated as (time spent in open arms/time spent in open and closed arms) x 100. The number of entries in open and closed arms was recorded manually at the time of the experiment. Graphs show results expressed as mean ± SEM, N=4 per control group and N=5 per infected group. (* $p<0.05$, ** $p<0.01$, *** $p<0.001$ by one-way ANOVA with Tukey's multiple comparisons test).....130

Figure 30 Seizures in the chronic phase were not mediated by neuro-inflammation. To determine whether chronic inflammation contributed to epileptic seizures, innate and adaptive leukocyte populations were analyzed from brain and CLNs of infected mice at week 30 p.i. Surprisingly, we found minimal or no expression of peripheral immune cells in the brain during the chronic phase. In addition, the expression levels of leukocytes populations from brain and CLNs were similar between the infected groups, indicating that epileptic seizures were not the result of chronic inflammation. Graphs show results expressed as mean ± SEM, N=3 per infected group. (Unpaired t test with Welch's correction).....132

Figure 31 Nlrc3 deficient mice sustain their resistance to demyelinating disease following TMEV infection. To assess the effect of the *Nlrc3* gene on susceptibility of C57BL/6 mice to TMEV-induced demyelinating disease, the spinal cords from *Nlrc3*$^{-/-}$ mice were collected at week 30 p.i., stained with H&E and compared to that of wild type mice. A and B are the representative images (100x) of the thoracic segment of the spinal cord from wild type and *Nlrc3*$^{-/-}$ mice, respectively. Unlike in the susceptible SJL mice, we did not find any pathological condition in the spinal cords from either *Nlrc3*$^{-/-}$ or wild type group, indicating that the *Nlrc3* gene does not regulate the resistance of C57BL/6 mice to TMEV-induced demyelinating disease.....133

LIST OF TABLES

Page

Table 1 cDNA Synthesis Primers.....35

Table 2 PCR products amplified for sequencing.....35

Table 3 Sequencing Primers.....36

Table 4 Summary of sequence differences between DA-C_L and DA-D_S and Genbank Accessions M20301, JX443418, and KF680264. 63

Table 5 Primer sequences for target genes.....85

CHAPTER I

INTRODUCTION AND LITERATURE REVIEW

Overview of epilepsy

Epilepsy and its clinical relevance

Epilepsy is the fourth most common neurological disease in the USA following migraine, stroke, and Alzheimer's disease [1]. Recently, the International League against Epilepsy (ILAE) proposed a new definition of epilepsy to better suit its clinical relevance. They recommended, "epilepsy be considered to be a disease of the brain defined by any of the following conditions: (1) At least two unprovoked (or reflex) seizures occurring >24 h apart; (2) one unprovoked (or reflex) seizure and a probability of further seizures similar to the general recurrence risk (at least 60%) after two unprovoked seizures, occurring over the next 10 years; (3) diagnosis of an epilepsy syndrome" [2]. Further, ILAE defined seizures as "a transient occurrence of signs and/or symptoms due to abnormal excessive or synchronous neuronal activity in the brain" [3]. The current statistics from the Center for Disease Control and Prevention (CDC), estimates 4.1 million adults who have had a diagnosis of epilepsy or seizure disorder, including 2.3 million adults with active epilepsy in the USA [4], and this number escalates to approximately 70 million people in the world. Epilepsy affects people of all ages, but is more frequently seen during childhood and older adulthood, and among people from low- and middle-income countries, possibly due to their increased susceptibility to

cerebral infections and trauma [5]. Currently available anti-epileptic drugs (AEDs) provide only symptomatic relief to patients, may lack efficacy and have several undesirable effects. Non-availability of adequate preventive therapy and pharmaco-resistance among one third of epileptic patients necessitates further understanding of the mechanism of epilepsy [6,7].

According to the ILAE, epileptic seizures can be classified into two groups. The first are generalized seizures where both cerebral hemispheres of the brain are involved. However, the location and lateralization of each seizure onset may vary. The second group includes focal seizures where seizures originate from one focal region of the brain, and each seizure type share the same site of ictal onset. There is no distinct classification of epilepsy, but being a multi-factorial disease, it could be characterized based upon its etiology: (a) genetic, where the cause of the epileptic seizures is a known or presumed genetic defect(s) such as Dravet syndrome; (b) structural/metabolic, where epileptic seizures are caused by an acquired central nervous system (CNS) lesion such as by an infection or trauma; or (c) of unknown cause, where the trigger for epileptic seizures is unidentified [8].

Viral infection-induced seizures or epilepsy

Patients who suffer from encephalitis accompanied with acute seizure(s) have an increased risk of developing epilepsy, and this risk is known to be 10% by 5 years and 22% by 20 years after the onset of the CNS infection. Moreover, patients with viral

encephalitis have a 16-fold increased risk of developing epilepsy, and this risk can persist for about 15 years after the occurrence of the initial viral infection [9]. In most cases of viral encephalitis, the patients may experience seizure(s) during viraemic phase, and 4-20% of the patients, who survive the encephalitic phase, may regress to develop epilepsy [10].

There are a number of viruses that may alter the neuronal circuits of the brain especially in the hippocampus. West Nile virus (WNV), Japanese encephalitis virus, Herpes simplex virus-1 (HSV-1), Enterovirus, Epstein-Barr virus, etc., are some of the common viruses that may cause seizures or epilepsy in humans and/or animals. Most of these viruses may cause generalized tonic-clonic seizures, which is characterized by the loss of consciousness and stiffening of the muscles followed by repetitive jerking movements of arms and/or legs. The viral infection could be a direct or indirect cause, as the virus itself and/or host immune responses developed against the virus may trigger seizures or epilepsy [10]. In many cases of viral-induced epilepsy, the etiology remains unidentified. This could be due to a short period of viremia, lack of adequate viral diagnostic tests and/or unavailability of the affected brain tissue through biopsy [11].

Use of the animal models to study seizures & epilepsy

There are various animal models that could be used to study the cellular and molecular mechanisms of epilepsy and seizures. Existing animal models have been crucial in the development of currently available therapies. Yet, there is a need for new and improved

experimental models due to lack of any existing preventive therapy or "cure" [6]. Most of the available animal models mimic only the acute phase of the disease or lack the development of spontaneous recurrent episodes of epileptic seizures; others may be costly, laborious, non-specific, non-reproducible or may involve long latent periods, lower number of epileptic animals or high animal mortality [12,13].

Nevertheless, different forms of epilepsy with their variable pathophysiologies add complexity to the validation of new AEDs. A single model of epilepsy cannot recapitulate all the clinical signs and symptoms of human epilepsy. Therefore, understanding the mechanisms of epilepsy from different aspects requires studying multiple experimental epilepsy models [14].

The immune responses in epilepsy

The immune system plays a pivotal role in protecting the host against foreign pathogens or toxins. The innate immune responses aid in protecting the host against pathogens, and provide the signals for the activation of the adaptive immune cells. The CNS resident immune cells, microglia and astrocytes (glial cells) share a bidirectional relationship with each other. Their activation and localization near the site of injury/lesion is the hallmark of inflammation in various neurological diseases including epilepsy. But, the prolonged activation of microglia and astrocytes may have detrimental effects on the viability of neurons and the integrity of the blood-brain barrier (BBB). The glial cells can secrete several chemical mediators that affect each other's activation and

recruitment, and the recruitment of peripheral immune cells into the CNS. The damaged BBB further allows the infiltration of peripheral immune cells (macrophages/monocytes, granulocytes, T cells, etc.) into the CNS, thereby exacerbating neuroinflammation [15-18].

Activated microglia, reactive astrocytes and infiltrating macrophages can secrete various pro-inflammatory cytokines such as tumor necrosis factor (TNF-α) and interleukin (IL)-1β, IL-6, which further contribute to inflammation by inducing neuronal cell death [16,19-21]. Microglia can also upregulate the expression levels of the major histocompatibility complex (MHC) class I molecules on neurons through the secretion of various chemical mediators. Besides, microglia and macrophages themselves act as the professional antigen presenting cells (APCs) by expressing the MHC class II molecules on their surface [16]. In addition to secreting pro-inflammatory cytokines, reactive astrocytes may become dysfunctional or lose their typical function of maintaining K^+ and glutamate (excitatory neurotransmitter) homeostasis, thus further contributing to seizure development [19,22].

Cells of the adaptive immune system also play a role in epilepsy. During viral encephalitis, CD8+ (cytotoxic) T cells secrete cytotoxic granules to kill virus-infected cells. These cytotoxic granules can also induce over-activation of glutamate receptors (N-methyl-D-aspartate [NMDA] receptors) leading to neuronal degeneration and seizures [10]. Interestingly, epileptic patients have been found to have a significant

increase in the circulating levels of Natural Killer (NK) and CD8+ T cells during their transition from the ictal to the post-ictal phase [18].

Apart from microglia, macrophages, and astrocytes, pro-inflammatory cytokines can also be produced by cerebral endothelial cells, and in some cases, by neurons [19]. Development of epilepsy could be due to increased expression level of cytokine(s) or an imbalance between pro- and anti-inflammatory cytokine levels. For instance, elevated expression of IL-1β may affect seizure activity by increasing the extracellular concentration of glutamate (major excitatory neurotransmitter) and/or by increasing the function of glutamate receptors (NMDA receptors). Furthermore, IL-1β can dampen the inhibitory current transmission by inhibiting gamma-amino butyric acid (GABA)-mediated Cl^- fluxes thus further increasing neuronal excitability. Besides IL-1β, TNF-α can also increase the neuronal expression of glutamate receptors (α-amino-3-hydroxy-5-methyl-4-isoxazolepropionic acid [AMPA] receptors) [19,23]. Moreover, TNF-α can stimulate its own production (autocrine effect), and can promote the production of other pro-inflammatory cytokines such as IL-1β and IL-6. Additionally, it can activate microglia in an autocrine and paracrine fashion, and has a positive- feedback effect on NF-κB (nuclear factor kappa-light-chain-enhancer of activated B cells) signaling [16].

Thus, excessive and prolonged neuroinflammation may promote seizures, contribute to epileptogenesis, and may favor seizure recurrence by allowing the activation of resident

immune cells and the infiltration of peripheral immune cells into the brain through the damaged BBB [18].

Theiler's murine encephalomyelitis virus

Introduction to virus

Theiler's murine encephalomyelitis virus (TMEV) is a non-enveloped, positive-sense ssRNA virus. It belongs to the Cardiovirus genus of the *Picornaviridae* family. Picornaviruses are cytolytic in nature and may cause tissue damage either by inhibiting host transcription and translation machinery and/or by altering the apoptotic machinery of host cells. TMEV is a natural pathogen of mice and is thought to be transmitted by the fecal-oral route [24-26].

Based on the neurovirulence, different strains of TMEV can be classified into two subgroups, GDVII and Theiler's original (TO). The GDVII subgroup consists of highly neurovirulent strains, GDVII and FA, that cause acute fatal polioencephalomyelitis in all strains of mice including SJL mice, and fatal encephalitis associated with seizures in C57BL/6 mice upon intracerebral infection (I.C.). The TO subgroup is comprised of less virulent strains, DA, BeAn 8386 (BeAn), WW, Yale, and TO4. Among the TO strains, I.C. injection of DA or BeAn strain induces non-fatal but different neurological diseases depending upon the genotype of mice used in the study [24,27-32,33-35]

TMEV-induced demyelinating disease of the CNS

In the SJL strain of mice, TMEV causes T helper (Th1/Th17) cell-mediated chronic demyelinating disease of the CNS within 2-3 months post infection (p.i.). TMEV causes a biphasic disease in SJL mice where the polio-encephalomyelitis-like symptoms appear during the acute phase, and inflammatory demyelination and axonal degeneration in the spinal cord occur during the chronic phase of the disease. In this experimental model, the virus first infects neurons and later persists in astrocytes, microglia and oligodendrocytes. At this stage, the host's autoreactive T cells and antibodies attack the mouse myelin protein resulting in demyelination of the CNS. The TMEV-induced mouse model of demyelinating disease mimics human multiple sclerosis (MS), hence is commonly used to study the mechanism of MS [24,26,29,30].

TMEV-induced epilepsy

Disease pathogenesis

Libbey et al. were the first group to report that TMEV induces epilepsy in C57BL/6 mice [34]. Intracerebral (I.C.) injection of $3x10^5$ plaque forming unit (pfu) DA or BeAn strain of TMEV induces acute symptomatic, afebrile seizures in approximately 65% of the adult infected C57BL/6 mice. The number of mice suffering seizures increases to 80% when a higher dose of virus ($3x10^6$ pfu) is used [35]. The seizures begin from day 3 p.i. and eventually subside by day 7 p.i. The seized mice usually show severe signs of the clinical disease, hence attain the score of 3 or above on the Racine scoring system [34,35]. Following acute seizures, mice acquire increased excitatory post-synaptic currents

(EPSCs), permanent reduction in the seizure threshold, and hippocampal sclerosis. After an indefinite latent period, 40-64% of acutely seized mice proceed to exhibit spontaneous behavioral seizures (epilepsy) and 100% of them exhibit epileptiform activity during 2nd, 4th and 7th month p.i. as reported via video-electroencephalogram (VEEG) monitoring [36]. Thus, the clinical features of TMEV-induced epilepsy model resemble that of mesial temporal lobe epilepsy (mTLE), the most common form of epilepsy in humans [37]. In addition, TMEV infected-seized mice also display anxiety-like behavior and cognitive impairment. Such symptoms are often exhibited by human epileptic patients [38].

Immune responses in the TMEV-induced model of epilepsy

During the first week of infection (acute phase), TMEV mainly resides in the hippocampal and cortical neurons of C57BL/6 mice brains. In addition, a few infected cells are also found in the frontal lobe, caudoputamen, septum, thalamus and hypothalamus. The hippocampus from infected mice exhibits excessive elevation in the activation of astrocytes and microglia, and increased infiltration of granulocytes, macrophages, etc. Additionally, there is pronounced damage to hippocampal neurons, which could be the cumulative result of infection, seizures, and/or inflammation [34,35,39].

C57BL/6 mice attain viral clearance within 2-4 week p.i., with the help of MHC class I-restricted CD8+ T cells and MHC class II-restricted CD4+ T cells. The virus is mainly cleared by MHC class I-restricted CD8+ T cells. β_2-microglobulin (β_2m) knock out

C57BL/6 mice that are devoid of MHC class I-mediated CD8+ T cell signaling, develop severe pathology in their cerebellum, cortex, brain stem and corpus callosum. Whereas, Aβ° knock out mice that lack MHC class II-mediated CD4+ T cell signaling, develop no cerebellar damage, and show comparatively less damage in their cortex, brain stem and corpus callosum. Both MHC class I- and MHC class II-mediated immune responses are important in preventing any damage in the hippocampal and striatal regions of the brain. This suggests that the MHC class I-dependent CD8+ mediated immune responses protect most regions of the mouse brain against TMEV infection [40]. The expression of MHC class I molecules is highly upregulated in the choroid plexus of the brain within 1 day p.i. and in the gray matter of the brain and spinal cord by day 7 p.i. And after the clearance of virus, the MHC class I expression subsides to its normal level as determined on day 28 p.i [41]. Moreover, infected C57BL/6 mice that lack β_2m do not show any clinical signs of the demyelinating disease. But these mice develop inflammatory demyelinating lesions, have a slight increase in the infectious viral titers and a significant increase in the CD4+ T cell-mediated immune responses in comparison to that in wild type mice. This suggests a compensatory role of CD4+ T cells in viral clearance in the absence of functional CD8+ T cells. Alternatively, CD8+ T cells regulate the proliferation of CD4+ T cells by mediating effective viral clearance from the CNS [42,43].

Following infection of C57BL/6 mice with TMEV, there is increased production of pro-inflammatory cytokines and chemokines by macrophages, microglia, astrocytes, etc. [39].

Although, generation of an anti-viral immune response and viral clearance render these mice resistant to the demyelinating disease, development of "bystander" inflammation in the brain makes them susceptible to epilepsy [36]. Previous studies have shown that aberrant activation of complement 3 (C3) and increased production of IL-6 and TNF-α by infiltrating macrophages and resident microglia are considered to be the major contributors in the development of acute seizures in C57BL/6 mice (Figure 1) [20,44].

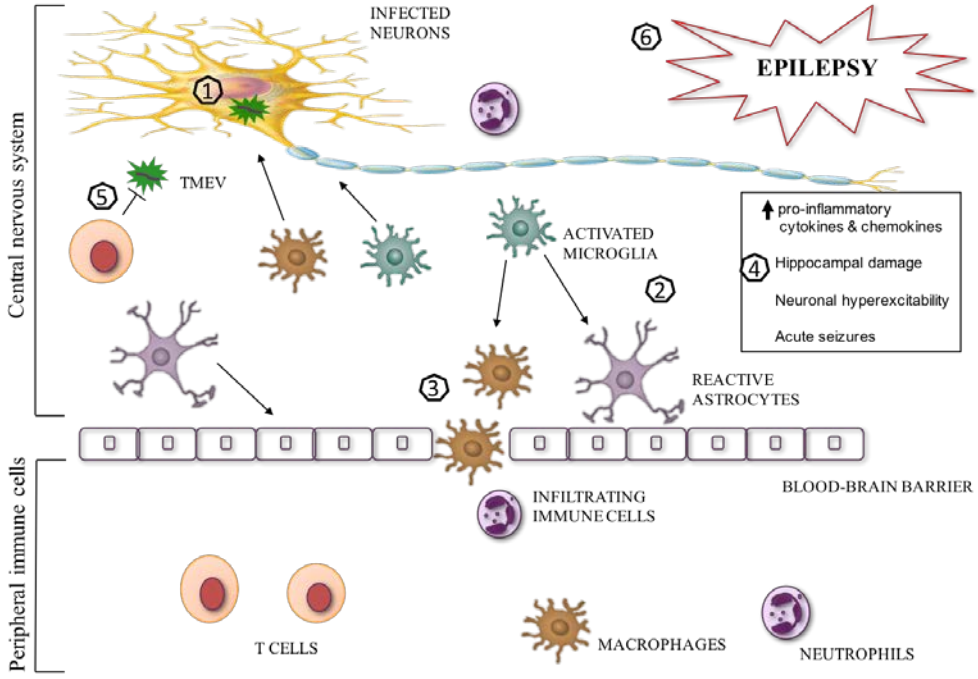

Figure 1 Immune responses in the TMEV-induced model of epilepsy. (1) Upon intracerebral (I.C.) injection, TMEV is localized mainly in the hippocampal and cortical neurons. (2) In response to infection, the resident cells of the central nervous system (CNS), microglia and astrocytes, become activated and secrete several cytokines and chemokines. (3) The increased production of pro-inflammatory mediators disrupts the integrity of the Blood-Brain Barrier (BBB), and allows the infiltration of peripheral innate immune cells, monocytes/macrophages, neutrophils, into the CNS. (4) The overzealous inflammation within the CNS causes severe damage to hippocampal neurons, resulting in neuronal hyperexcitability and symptomatic seizures within a week p.i. (5) The T cell-mediated viral clearance occurs within a month p.i., (6) but the acute phase events subsequently lead to the development of epilepsy after an undefined latent period.

Strengths and limitations of TMEV-induced epilepsy model

The TMEV-induced epilepsy model proves to be clinically relevant to study structural forms of epilepsy, as many cases of human and animal epilepsy are triggered due to environmental factors (such as CNS infection). The greatest strength of this model is that, unlike other infection-driven epilepsy models, TMEV infection runs a non-fatal disease course in C57BL/6 mice, giving investigators the opportunity to understand the mechanisms of epileptogenesis, and the acute and chronic forms of seizures. Moreover, the seizures observed in this model are mostly of severe intensity and resemble the tonic-clonic forms of seizures frequently diagnosed in cases of human epilepsy. However, the limitation of the current epilepsy model is the phenotypic variability observed among TMEV-infected mice, since only ~60% of the infected mice develop acute seizures, and a fraction of the acutely seized mice proceed to develop unprovoked seizures (epilepsy). Furthermore, this phenotypic variability may mask the true effects of potential AEDs tested using the disease model.

The nucleotide-binding oligomerization domain-like receptors

Description of NLRs

The nucleotide-binding oligomerization domain-like receptors (or NLRs) are a family of intracellular pathogen sensors or Pattern Recognition Receptors (PRRs). These innate immune receptors are expressed by a variety of cell types in the body, including those of

both the innate and adaptive immune system. There are 22 types of NLRs in humans and 34 types in mice [45,46].

NLRs serve diverse functions. They may aid in the activation of inflammasomes (multi-protein inflammatory complexes), inflammatory transcription factors and/or MHC molecules or in the inhibition of inflammatory signaling pathways [47]. NLRs can be categorized as pro-inflammatory or anti-inflammatory depending upon their stimulatory or inhibitory effect(s) on the immune responses. The pro-inflammatory NLRs promote immune response against inflammatory stimuli (pathogen-associated molecular patterns [PAMPs]) by either activating the NF-κB signaling pathway (as in case of NLR, domain containing 1 [NOD1], NLR, domain containing 2 [NOD2]) or by forming an inflammasome (as in case of NLR family, pyrin domain containing 3 [NLRP3]), which further activates the production of NF-κB and pro-inflammatory cytokines. On the other hand, the anti-inflammatory NLRs (such as NLR family, pyrin domain containing 12 [NLRP12], NLR family member X1 [NLRX1]) can attenuate inflammation by directly or indirectly inhibiting the activation of inflammatory pathways such as NF-κB and/or type I IFN signaling pathways [48]. Since NLRs have only recently been discovered, many of their functions remain unclear.

The role of NLRC5 gene in inflammation

The NLR family, caspase activation and recruitment (CARD) domain containing 5 (NLRC5), also known as NOD27, NOD4 or CLR16.1, is a member of the NLR family.

It has a tripartite domain that consists of a caspase activation and recruitment domain (CARD) at the N-terminus, a nucleotide-binding domain (NBD) at the center and leucine-rich repeats (LRR) at the C-terminus. The LRR domain of NLRC5 consists of 1,855 amino acids, which makes it the largest protein in the NLR family. Most of the NLR proteins are localized in the cytoplasm but NLRC5 can shuttle between the nucleus and cytosol depending on its activation state. NLRC5 is most closely related to MHC class II transactivator (CIITA) based on its structure and function [46].

NLRC5 is highly expressed in hematopoietic cells with its highest expression in lymphocytes (CD4+ T cells, CD8+ T cell, CD19+ B cells, NK cells, NKT cells) and moderate expression in CD14+ cells (monocytes) and CD11b+ splenic myeloid cells. IFN-γ is a potent stimulator of NLRC5 expression, which is dependent on the signal transducer and activator of the transcription 1 (STAT1) signaling pathway. The expression of NLRC5 can also be upregulated in response to viral infections, polyinosinic:polycytidylic [poly (I:C)], lipopolysaccharide [LPS] and Type I IFN (IFN-β) [46].

The MHC class I molecule is expressed by all nucleated cells. Its expression is critical for antigen presentation and activation of CD8+ T cells. In turn, the expression of MHC class I molecule is tightly regulated by NLRC5, hence NLRC5 is known as the major transactivator of the MHC class I gene (CITA). NLRC5 upregulates the expression levels of MHC class I gene, non-classical MHC class I gene and MHC class I accessory

genes such as *β2m*, *LMP2* (low molecular mass proteasome) and *TAP1* (transporter associated with antigen processing 1). It does not affect the expression of MHC class II or its accessory genes, thereby maintaining its exclusivity in the regulation of genes involved in the antigen presentation and processing in MHC class I pathway. Thus, by regulating the expression of MHC class I genes, NLRC5 plays an important role in immune regulation [45,49-52].

Although, the function of NLRC5 as the MHC class I transactivator has been well defined, its function as the positive or negative regulator of antiviral immunity and inflammation is still unclear. Certain groups have reported NLRC5 as a pro-inflammatory NLR as it mediates immune responses against influenza virus [53], Sendai virus (SeV) [54], Cytomegalovirus (CMV) infected human foreskin fibroblast (HFF) [55], and poly (I:C) stimulated human acute monocytic cell line (THP-1) and human dermal fibroblasts [54]. Other researchers have reported NLRC5 to have anti-inflammatory role in response to vesicular stomatitis virus (VSV) infection, where it downregulates NF-κB and Type I IFN signaling pathways, production of proinflammatory cytokines and antiviral immunity [56,57]. While the third group of researchers have reported that NLRC5 may be dispensable for NF-κB and Type I IFN signaling pathways [50], and may play no role in Toll-like receptor [TLR], retinoic acid inducible gene-1 [RIG1] -like receptor, or DNA (Newcastle disease virus) sensor signaling [58]. In addition, NLRC5 has been suggested to regulate the activation of inflammasome in response to bacterial PAMPs

and crystals [59], and/or partly regulate the activation of NLRP3-mediated inflammasome against intracellular infections [50].

Most studies describing the role of the *Nlrc5* gene have been conducted *in vitro* or *ex vivo*. The conflicting results obtained from the above mentioned studies could be due to the use of different types of cell lines, cell lines obtained from different species, cell lines with variable expression levels of NLRC5, different gene deletion strategies, and/or variable doses and duration of stimuli [53].

The role of NLRC3 gene in inflammation

The NLR, caspase activation and recruitment (CARD) domain containing 3 (NLRC3), also called NOD3 or CLR16.2, belongs to the NLR family of PRRs. Like most NLRs, it is localized in the cytoplasm. It has a tripartite domain consisting of LRR at the C-terminus, NOD/NBD at the center and a less developed CARD3 domain at the N-terminus [60]. It is highly expressed in human T cells and NK cells and mouse T cells. Additionally, human and mouse B cells also express some amount of NLRC3 [61].

NLRC3 is evolutionary conserved. Its expression has been determined in the leukocyte cell lines (including macrophage, cytotoxic T cell and B cell) and various tissues (head kidney, trunk kidney, intestine and spleen) of channel catfish (*Ictalurus punctatus*) [62], where it contributes to innate immunity in response to various bacterial and viral infections [63]. A homologue of NLRC3 in the nervous system of the leech (*Hirudo*

medicinalis), has been suggested to participate in CNS injury and infection in the invertebrates [64]. The NLRC3-like NLR, which shares similarities with the human NLRC3, have been shown to be important for the development of microglia from primitive macrophages during embryogenesis, and in regulating systemic inflammation in zebrafish in the absence of inflammatory stimuli [65].

In vitro studies have shown that NLRC3 expression significantly reduces upon T cell receptor complex (TCR)- and CD28-mediated T cell activation. However, exogenous NLRC3 can attenuate T cell signaling, and reduce the expression levels of IL-2 and CD25 genes, the genes that are important for T cells activation and in preventing T cell anergy. NLRC3 also downregulates the activation of NF-κB transcription factor by either delaying the degradation of inhibitor of kappa B (IκB) a [61] or by blocking the ubiquitination of TNF receptor associated factor 6 (TRAF6). In the resting phase, association of NLRC3 with TRAF6 prevents the activation of NF-κB and production of inflammatory cytokines. However, under pathological conditions, expression levels of NLRC3 decrease resulting in the activation of NF-κB -dependent inflammatory pathway. Nonetheless, NLRC3 expression restores to its normal levels after the resolution of inflammation, suggesting its role in negatively regulating inflammatory responses [66]. NLRC3 may also impair activation of other transcription factors, such as activating protein-1 (AP-1) and nuclear factor of activated T-cells (NFAT), that activate upon T cell stimulation [61].

Additionally, interaction between NLRC3 and Toll-like receptor 4 (TLR4) has been studied using *Nlrc3* deficient (*Nlrc3*$^{-/-}$) mice. One hour following LPS (TLR4 agonist) stimulation, peritoneal macrophages obtained from *Nlrc3*$^{-/-}$ mice had increased expression of pro-inflammatory cytokine-encoding genes and no significant changes in the expression of *Tlr4* and *Traf6* in comparison to wild type cells. But, the expression levels of these genes were found to be similar between the two groups at later time-points. This study suggests a role of NLRC3 in negatively regulating TLR4-mediated inflammation, specifically at earlier time-points [66]. Furthermore, NLRC3 has been reported to downregulate the production of stimulator of interferon genes (STING)-dependent type I IFN, IL-6 and TNF-α, thereby delaying viral clearance. This response is exclusively seen in the case of DNA virus infections (such as HSV-1) but not with RNA virus infections (such as SeV, VSV) or viral mimic poly (I:C) stimulation [67]. NLRC3 may also negatively regulate pro-IL-1β maturation by inhibiting the activation of NLRP3-inflammasome. NLRC3 achieves this by replacing NLRP3 and forming its own complex with apoptosis-associated speck-like protein containing a CARD (ASC) and caspases 1 and 5. The resultant (NLRC3-ASC- caspases 1 and 5) complex, however, does not follow the typical functions of inflammasome in activating pro-inflammatory pathways [60]. Recently, Nlrc3 has been reported to provide partial protection to mice against colitis-associated colorectal cancer by reducing the activation of mechanistic target of Rapamycin (mTOR)-signaling pathways at earlier time-points, thus decreasing cellular proliferation and stem-cell-derived organoid formation at later time-points. Nlrc3 expression significantly decreases in tumor tissue of wild type mice. However,

Nlrc3$^{-/-}$ mice show increased susceptibility to colitis and colorectal tumorigenesis due to increased expression levels of innate immune cells, pro-inflammatory cytokines and chemokines, and increased activation of immune signaling pathways in colon tissue [68]. These studies suggest that NLRC3 negatively regulates both innate and adaptive immune responses by targeting several immune-signaling pathways. Consequently, NLRC3 may have a protective role in preventing autoimmune diseases and inflammatory disorders.

Objective of this dissertation

Overall hypothesis: We hypothesize that viral persistence and viral infection-driven host immune responses are crucial for causing seizures in TMEV-induced murine model of epilepsy.

The viral infection-driven host immune responses are critical in causing acute neuronal damage and seizures in TMEV-induced murine model of epilepsy. Therefore, it is interesting to investigate the influence of distinct virus-variants and inflammatory components on disease pathogenesis. The first aim of this dissertation is to characterize the genomic differences between the two plaque-sized variants, DA-C_L and DA-D_S, of the DA strain of TMEV, and to determine their virulence and pathogenicity in epilepsy. In the latter aims, we examine the independent roles of *Nlrc5* and *Nlrc3* genes in regulating inflammation and epileptogenesis, using BeAn (TMEV strain)-infected *Nlrc5*$^{-/-}$ and *Nlrc3*$^{-/-}$ mice on C57BL/6 background.

CHAPTER II

CHARACTERIZATION OF PLAQUE-SIZED VARIANTS OF DANIEL'S (DA) STRAIN IN TMEV-INDUCED EPILEPSY

Introduction

Theiler's murine encephalomyelitis virus (TMEV) is a single stranded RNA virus that belongs to the *Picornaviridae* family [24]. It is found naturally in the enteric system of mouse [27,69]. TMEV is divided into two serologically related but biologically and neuropathologically distinct subgroups, GDVII and Theiler's original (TO). The GDVII subgroup contains highly neurovirulent GDVII and FA strains, while the TO subgroup contains less neurovirulent DA, BeAn 8386 (BeAn), WW, Yale, and TO4 strains [24,27-29,33,70].

Intracerebral (I.C.) infection with TMEV induces different neurological diseases in mice based upon either the virus strain or mouse strain used [24,30-32,34,70-74]. The GDVII subgroup causes acute fatal polioencephalomyelitis in all strains of mice including SJL mice [30,70], and acute fatal encephalitis accompanied with seizures in C57BL/6 mice [34,73]. DA and BeAn are the two most commonly studied virus strains in the TO subgroup. DA- or BeAn- infected SJL mice develop biphasic disease characterized by early (weeks 1-2 post-infection [p.i.]) mild poliomyelitis and late (~ 2 months p.i.) demyelinating disease [24,71]. In this strain of mice infectious virus is not cleared and persists at low titer,

primarily in the spinal cord [24,75-77]. In contrast to developing demyelinating disease, DA- or BeAn- infected C57BL/6 mice develop acute (within a week p.i.) seizures [34] that progress into epilepsy after an indefinite latent phase (~1-2 months p.i.) [78]. In C57BL/6 mice infectious virus is cleared from the CNS within a month p.i. [79]. Interestingly, tonic-clonic seizures or hyperexcitabilty were also observed in FA-, and occasionally in GDVII- infected Swiss mice [30]. However, like the SJL mice, DA-infected Swiss mice develop demyelinating disease [31,72]. This suggests some phenotypic overlap among the TMEV strains, and among the mouse strains, in spite of their genotypic differences.

TMEV subgroups also differ from one another based upon their *in vitro* characteristics. The GDVII viruses form large plaques (1 to 5 mm), whereas the TO viruses usually form small plaques (0.2-1 mm) on baby hamster kidney (BHK) cells [28,70]. Dr. Leibowitz and colleagues observed that their DA strain of TMEV produced a mixture of large and small sized plaques when assayed on L2 cells. The large plaques were 1.51±0.16 mm, while small plaques were 0.75±0.13 mm in size. The genetically stable, large and small sized plaques forming variants of the DA strain were isolated and called DA-C_L and DA-D_S, respectively [80].

The growth kinetics and neurovirulence of DA-C_L and DA-D_S plaque variants have been well documented in TMEV-induced demyelinating disease. The DA-C_L variant yields higher titer *in vitro*, but replicates to lower titers in the CNS and is unable to induce any clinical disease in SJL mice even though it is able to persist in the CNS. In contrast, the

DA-D_S variant yields lower titers *in vitro*, but replicates efficiently in the CNS and induces demyelinating disease in SJL mice. Following infection with DA-D_S, there is higher viral growth in the CNS and increased severity of demyelinating disease compared to the parental DA virus. [80]. However, no further studies have been carried out to determine the relative virulence of these DA variants in TMEV-induced epilepsy model.

The TMEV-induced epilepsy model is the first viral infection-driven animal model developed to understand both the acute and chronic forms of seizures. Infection in C57BL/6 mice with the DA or BeAn strain of TMEV stimulates a vigorous host immune response (central and peripheral) that targets the virus but could also cause damage to the pyramidal neurons of the hippocampus in the process. The unregulated host immune response and neuronal damage triggers hippocampal excitability, acute seizures, and reduced seizure threshold. The T cell-mediated virus clearance occurs within a month p.i. Nonetheless, the acute phase events pave the way for the development of recurrent spontaneous seizures (epilepsy) in the chronic phase [20,21,34,78,81,82].

Here, we characterized the genetic differences between the two plaque variants, DA-C_L and DA-D_S, and their neurovirulence and pathogenesis in the epilepsy model. We showed that the DA-C_L variant was relatively avirulent as it induced reduced neuroinflammation, neuropathology and minimal seizures in infected mice. Conversely, the DA-D_S variant was highly neurovirulent as it provoked pronounced

neuroinflammation, hippocampal damage and seizures in infected mice. Thus, DA-C was attenuated in both the epilepsy and late demyelinating models. Moreover, our results suggest that the neurovirulence of the DA variants is independent of the genotype of SJL and C57BL/6 mouse strain. A sequence [83] comparison of the DA-C_L and DA-D_S genome sequences revealed two differences between the two variants resulting in three coding differences at the protein level, in the L, L*, and 2C proteins.

Materials and methods

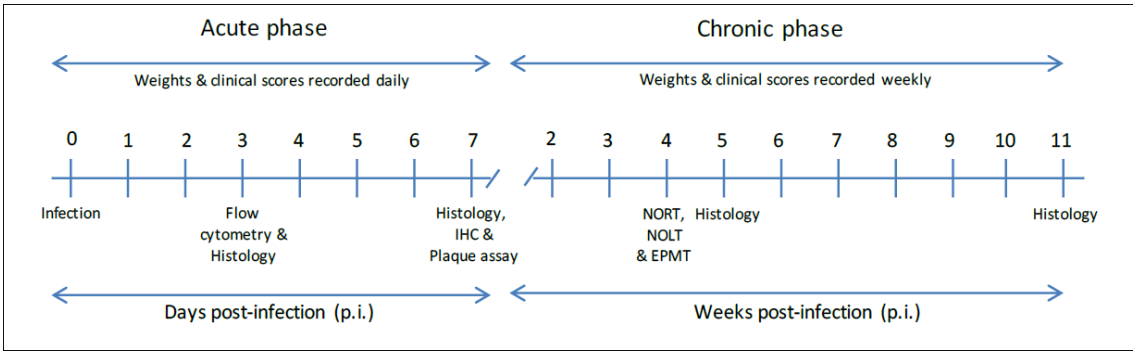

Figure 2 Experimental timeline. The acute phase of disease is defined as up to day 7 p.i., during which seizures, non-epileptic clinical illness, weights, viral burden, inflammation and CNS pathology were determined. The chronic phase is defined as from week 2 to 11 p.i. or until the termination of mice. Chronic phase measures included clinical scores (spontaneous seizures), weights, elevated plus maze test (EPMT), novel object recognition test (NORT), novel object location test (NOLT), and histological analyses of the CNS.

Mice

Three-week-old female C57BL/6 mice were purchased from Envigo Laboratories (Indianapolis, IN). They were caged in groups of four or five, under constant room temperature of 70±0.5° F and relative humidity of ~50% with 12 hours of light and dark

cycle. *Ad libitum* feed and water were provided to the mice throughout the experiment. Mice were given a week to acclimate to their housing environment prior to infection. All animal experiments (Figure 2) were conducted in accordance with the protocols approved by the Institutional Animal Care and Use Committee (IACUC) of the Comparative Medicine Program at Texas A&M University.

Virus

The DA-C_L (large) and DA-D_S (small) plaque variants of the DA strain of TMEV have been described previously [80]. The plaque variants were grown in BHK cells and stored at -80°C, until used for infection. Virus titrations were performed as described previously [77]

Infection

Mice were placed into 3 groups according to the virus used for infection: controls, DA-C_L, and DA-D_S. Mice in the infected groups were injected I.C. with 2.0 x 10^5 plaque forming units (pfu) of either DA-C_L or DA-D_S plaque variant in 20 µl of Dulbecco's modified eagle medium (DMEM) (Sigma, Life Science, St. Louis, MO). Mice in the control group were injected I.C. with 20µl of sterile 1x Phosphate Buffer Saline (PBS). All injections were performed under isoflurane (IsoFlo, North Chicago, IL) anesthesia.

Body weight measurement

Mice were weighed daily until day 7 p.i. (acute phase), and then once a week until the termination of the experiment (chronic phase). % weight loss was calculated as percent of daily or weekly weights of mice compared to their baseline weights i.e. weights at day 0 p.i.

Clinical scores

For clinical scores, mice were observed twice daily for two hours between 9 AM to 6 PM until day 7 p.i. (acute phase). Additionally, two cages of infected mice (n=9/infected group) were video recorded 24/7 and the resulting videos analyzed for acute seizures. Mice were scored for seizures based on the Racine scoring system; (1) Mouth and facial movements; (2) Head nodding; (3) Forelimb clonus; (4) Rearing; and (5) Rearing and falling progressing to tonic-clonic seizure [84]. For non-epileptic clinical signs, mice were scored as: score (0) no clinical signs; score (1) mildly ruffled, hunched, and/or ataxic; score (2) moderately ruffled, hunched, and/or ataxic; score (3) severely ruffled, hunched, and/or ataxic; score (4) paralysis; and score (5) moribund. Moreover, three cages of mice were kept for chronic phase studies until week 5 or 11 p.i. In the chronic phase, mice were observed once weekly for spontaneous seizures and symptoms of demyelinating disease.

Tissue isolation

For tissue isolation, mice were euthanized with 150 mg/kg beuthanasia-D special (Schering-Plough Animal Health Corp. Union, NJ) and perfused intracardially with 10 ml of sterile PBS. For plaque assay experiments, brains and spinal cords were collected at day 7 p.i., snap frozen and stored at -80°C until use. For immunohistochemistry (IHC), brains were collected at day 7 p.i., fixed in freshly prepared 4% paraformaldehyde (PFA) for 24-48 hours at 4°C, and cryoprotected in 30% sucrose for 72 hours at 4°C. Then brains were embedded in optimum cutting temperature (OCT) compound (Tissue-Tek 4583, Torrance, CA) and stored in -80°C until they were ready for sectioning. For histology, brains and spinal cords were collected at days 3 and 7, and weeks 5 and 11 p.i., fixed in 10% formaldehyde for 4-5 days at room temperature, processed and embedded in paraffin wax. Each brain was cut to obtain coronal sections containing dorsal hippocampus and each spinal cord was sectioned to retrieve at least one transverse slice from the cervical to sacral segments. For flow cytometry, brains were collected at day 3 p.i. in ice cold RPMI 1640 (Gibco, Life Technologies, Grand Island, NY), and immediately processed to analyze leukocyte populations as described later.

Brain weight

Increased brain weight could be indicative of neuro-edema. For this, brains were collected from control (n=3) and infected mice (n=19/group) at day 7 p.i. and weighed.

Plaque assay

Brains and spinal cords were collected separately and 10% w/v homogenates in DMEM were prepared and sonicated by three 20 second pulses in a cup sonicator (Heat Systems, Sonicator Ultrasonic Processor, model XL2020). Homogenates were centrifuged at 2000-3000 rpm for 10 minutes at 4°C, and the supernatant containing virus was titrated by plaque assay as described previously [80,85].

Immunohistochemistry (IHC)

10-micron (μm) coronal sections were cut from OCT blocks of mouse brain (n=4/ infected group) on a cryostat (Leica CM 1950). Serial sections containing dorsal hippocampus were collected on plus-charged coated slides, and stored at -80°C until further use. For each immunostain, four rostral-caudal matched sections were analyzed per mouse.

Before staining, the cryosections were incubated for 1 hour at 37°C, hydrated with PBS, and blocked for 1 hour with 5% goat serum (16210-064; Gibco, Life Technologies, Grand Island, NY) and 0.1 or 0.3% Triton X-100 (9002-93-1; Sigma-Aldrich, St. Louis, MO) in PBS. The cryosections were incubated overnight at 4°C with primary antibodies for astrocytes, chicken anti-glial fibrillary acidic protein [86] [1:500, AB5541; EMD Millipore, Temecula, CA], or for TMEV-antigen positive cells, rabbit anti-TMEV [87] [1:50; Welsh lab]. The next day, cryosections were washed and then incubated for 1 hour with either Alexa Fluor 488 goat anti-chicken IgG [1:1000, A11039; Invitrogen,

Life Technologies, Eugene, OR] or Alexa Fluor 594 goat anti-rabbit IgG [1:1000, A11037; Invitrogen, Life Technologies, Eugene, OR]. Later, cryosections were washed, counterstained with Hoechst 33342, trihydrochloride, trihydrate [1:1000, H3570; Life Technologies, Eugene, OR] and mounted with Fluoromount-G (0100-01; SouthernBiotech, Birmingham, AL). All images were acquired using a HRD076-NIK camera attached to OLYMPUS VANOX AHBS3 microscope. Activated astrocytes and TMEV-antigen positive cells were enumerated both in the left and right hippocampi and totaled.

Histology: brain

Four μm paraffin-embedded sections of brains from control (n=3) and infected mice (n=4-5/group) from acute (days 3 and 7 p.i.) and chronic (weeks 5 and 11 p.i.) phase were stained with H&E. To determine the extent of acute (day 7 p.i.) inflammation in hippocampus, we enumerated and totaled the number of inflammatory foci and perivascular cuffs in right and left hippocampi from each mouse. Previous studies have shown that acute neuronal loss in TMEV-infected C57BL/6 mice mainly occurs in the CA1 and CA2 regions of the hippocampus [81]. Therefore, we estimated the percent loss of CA1 and CA2 neurons and ranked it on a scale of 0 to 10. Scores from the left and right hippocampi were totaled, such that the highest possible cumulative score for each mouse was 20 [88]. H&E stained brain sections from day 3 and weeks 5 and 11 p.i. were examined for the progression of neuropathology in the hippocampus.

Histology: spinal cord

Four μm paraffin-embedded transverse sections of the spinal cords from control (n=3) and infected mice (n=4-6/group) from acute (days 3 and 7 p.i.) and chronic (weeks 5 and 11 p.i.) phase were stained with H&E. The cervical, thoracic, lumbar and sacral segments of the spinal cords were examined for the presence of inflammatory foci, axonal/neuronal degeneration, and/or meningitis. Each spinal cord segment was graded separately on a scale of 0 to 4: score (0) the absence of any pathology; score (1) minimal pathological lesions (<10%); score (2) mild pathological lesions (10% to <30%); score (3) moderate pathological lesions (30% to <70%); and score (4) severe pathological lesions (≥ 70%).

Flow cytometry

Whole brains (n=5/control group and n=13/infected group) were homogenized in RPMI 1640, filtered using 70-μm FALCON cell strainers (21008-952; VWR, Sugarland, TX), and centrifuged at 500 x *g* for 5 min at room temperature. After discarding the supernatant, each pellet was suspended in 10 ml of 30% Percoll (17-0891-01; GE healthcare, Uppsala, Sweden) in PBS. This solution was gently overlaid onto 2 ml of 70% Percoll in PBS, and centrifuged 500 x *g* for 30 min at 18°C. The buffy coat containing leukocytes was collected from the interphase of the 30% and 70% Percoll layers, washed, and suspended in flow buffer containing 2% fetal bovine serum (FBS) [16000-044; Gibco, Invitrogen, Grand Island, NY] in PBS. Cells were treated with Anti-Mouse CD16/CD32 (1:100, 14-0161-82; eBioscience, San Diego, CA) for 10 min at 4°C

to prevent any non-specific binding. For phenotyping, cells were stained with the anti-mouse antibodies as indicated below for 30 min at 4°C, washed and fixed with 2% PFA prior to flow cytometric analysis on a Beckman Coulter MoFlo® Astrios™ High-Speed Cell Sorter machine. Data were analyzed using FlowJo® software V10.0.8r1 (Mac OS X, FlowJo, LLC, Ashland, OR). Ly-6G (Gr-1) was detected with clone RB6-8C5 (1:500, 12-5931-82; eBioscience, San Diego, CA). CD11c was detected with clone N418 (1:250, 17-0114-81; eBioscience, San Diego, CA). NK1.1 was detected with clone PK136 (1:500, 12-5941-63; eBioscience, San Diego, CA). CD11b was detected with clone M1/70 (1:500, 101224; BioLegend, San Diego, CA). CD45.2 was detected with clone 104 (1:100, 109805; BioLegend, San Diego, CA). CD8a was detected with clone 53-6.7 (1:250, 100711; BioLegend, San Diego, CA). CD4 was detected with clone GK1.5 (1:500, 100428; BioLegend, San Diego, CA). Cell viability was assessed with Ghost dye Red 780 (1:100, 13-0865; Tonbo Biosciences, San Diego, CA). For compensation controls, UltraComp eBeads (01-2222-41; eBioscience, San Diego, CA) were used [89].

Behavioral and cognitive tests

Behavioral and cognitive tests were conducted at week 4 p.i., since C57BL/6 mice are known to clear TMEV by this time [81]. Experiments were performed in an isolated room with dim lighting to minimize environmental distractions. Mice were given 30 min to acclimate to the room prior to any testing. All experiments were performed during the day.

Elevated Plus Maze test (EPMT)

EPMT was performed by the standard protocol as previously described by Komado et al. with some modifications. The elevated plus maze was made of black Plexiglass. It consisted of two opposing open (25x5x0.5 cm^3) and closed (25x5x16 cm^3) arms placed in a perpendicular fashion, with a central platform (5x5x0.5 cm^3). The maze was kept elevated at a height of 50 cm above the floor (Figure 3).

Mice were individually placed on the central platform with their heads facing towards the same closed arm. Each mouse was given a 5-min test period to freely explore the maze. During this period, we recorded the number of times the mouse entered the open and closed arms. An arm entry was defined as the placement of all four paws of the mouse in that arm of the apparatus. The number of entries in open arms was used as a measure of anxiety-like behavior in the mice. The number of entries in closed arms was used as a measure of locomotor activity. The maze was cleaned with 70% (vol/vol) ethanol between the tests to remove any feces, urine or animal odor [90].

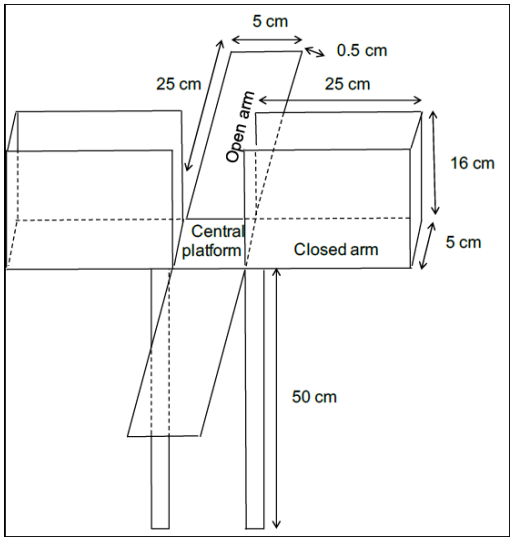

Figure 3 Schematic diagram of the elevated plus maze. The maze was made of black plexiglass. It consisted of two opposing open and closed arms placed in the shape of a plus, and a platform at the intersection of the arms. The maze was kept elevated at a height of 50 cm above the ground.

Novel object recognition test (NORT) and Novel object location test (NOLT)

Mice were tested for object- and place-recognition memory to determine any seizure-associated memory loss. We modified the original protocol as described by Jiang et al. [91] by increasing the period of object exploration time from 5 to 10 min, and retention delay from 90 min to 24 h. The open arena (50x50x50 cm^3) was made of Plexiglass and different sets of objects were used for each test.

As illustrated in Figure 4, the test was conducted over a period of 5 days. On the first day, the habituation phase, mice were individually placed in the open arena and allowed to freely explore it for 5 min. On the second day, the familiarization phase for NORT, mice were allowed to explore the first set of identical objects. On the third day, the test phase for NORT, mice were placed back in the arena with one of the familiar objects

replaced by a novel object. On the fourth day, the familiarization phase for NOLT, mice were allowed to explore the second set of identical objects in the same arena. On the fifth day, the test phase for NOLT, mice were returned to the arena with one of the identical objects displaced to a novel location. A retention delay of 24 hours was used between the phases. The total time for the familiarization and test phases were 10 min for both NORT and NOLT. Touching or sniffing the objects, but not climbing them, at a distance of less than 2 cm was considered as an explorative behavior. Objects and arena were cleaned with 70% (vol/vol) ethanol between the tests to avoid any olfactory cues.

Tests were video recorded and later analyzed for the time spent exploring each object and discrimination index (DI). DI was calculated as the ratio of time spent on novel object or location to the time spent on familiar object or location.

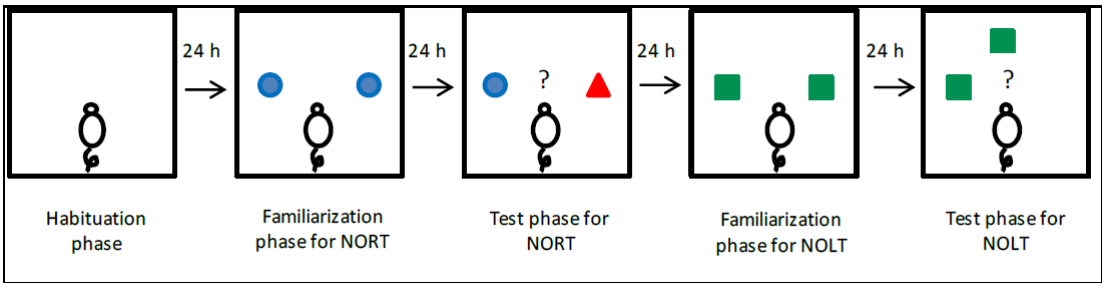

Figure 4 Schematic diagram of novel object- and novel location- test setup. The open arena made of plexiglass, and non-edible, odorless objects were used for the tests. The test was conducted over a period of five days, comprising of a 5-min session of habitutation phase, 10 min-session of familiarization phase for NORT and NOLT each, a 10-min session of test phase for NORT and NOLT each, with a rentention delay of 24 h between the phases.

Sequencing of plaque variants

Tissue culture dishes (60 mm diameter) of confluent L2 cells were infected with DA-D_S and DA-C_L at an multiplicity of infection [92] of 3 and incubated for 16 hours at 37° C and total intracellular RNA extracted using the Omega Bio-Tek Total RNA Kit as per the vendor's directions. cDNA synthesis was performed with Superscript III (Invitrogen) using the primers listed in, Table 1. The resulting cDNAs were amplified by PCR to produce the overlapping amplicons listed in Table 2. PCR was performed with ONETAQ DNA polymerase (New England Biolab) and the PCR primers listed in, Table 2. The most 3' amplicon was amplified using the 3'RACE procedure [93]. The PCR conditions used for each amplicon were those recommended by the New England Biolab web tool (http://tmcalculator.neb.com/#!/) [94] for each primer pair with ONETAQ DNA polymerase. Amplified cDNAs were purified by 1% agarose gel electrophoresis, visualized on a Clare Dark Reader and recovered from the gel using Bioline PCR and Gel Extraction kits, according to the vendor's instructions. Purified PCR products were then sequenced commercially (Eurofins) using the primers shown in, Table 3. Sequences were viewed and aligned using Sequencher (version 4.8) and a consensus sequence determined. The DA-C_L and DA-D_S sequences were aligned and compared for differences using L-align and ClustalOmega web platforms.

Primer Sense and Position	Use	Primer Sequence*
(-) 1170-1151	cDNA synthesis	TGG GAA CCA TTC ACC GTC TG
(-) 2538-2520	cDNA synthesis	TGA GGT CGT CGG GAC AGA A
(-) 3083-3065	cDNA synthesis	GGT AGT TTC ACG GGT TCT G
(-) 4612-4593	cDNA synthesis	GGC AAA CTG GGG GAG GAG TA
(-) 6312-6293	cDNA synthesis	CTT ACT ACG ACA GTG GCC CT
(-) 7835-7813	cDNA synthesis	AGT TTC TCT TTA AGT GTT CCT GG
3' RACE-OligoT	cDNA synthesis	GAC TCG AGT CGA CAT CGA $(T)_{17}$

Table 1 cDNA Synthesis Primers

*Primer positions and sequences are from Genbank Accession M20301

PCR Primer	**Primer Sequence**	**cDNA Used for PCR**	**Amplified cDNAs**
(+)123-142	ACT CCC GAC TCC GCA CCC TA	DA (-) 1170-1151	123-1170
(-)1170-1151	TGG GAA CCA TTC ACC GTC TG		
(+)750-769	ACA CAA AGG CAG CGG AAC CC	DA (-) 2538-2520	750-1760
(-)1760-1741	GGG AGA GGA ATG CGG ATG TG		
(+)1087-1106	CCA GAT GTG TGC CCT ATT TG	DA (-) 3083-3065	1087-3083
(-)3083-3065	GGT AGT TTC ACG GGT TCT G		
(+)1862-1881	CTC AAT TTC ACG CCG GCT CT	DA (-) 2538-2520	1862-2538
(-)2538-2520	TGA GGT CGT CGG GAC AGA A		
(+)2806-2825	TCC CCT ACT CAC TAT CGC CA	DA (-) 4612-4593	2806-4612
(-)4612-4593	GGC AAA CTG GGG GAG GAG TA		
(+)2946-2965	GTC TCC GCG GGA GAT GAT TT	DA (-) 4612-4593	2946-4612
(-)4612-4593	GGC AAA CTG GGG GAG GAG TA		
(+)3753-3772	CTT CTT TCC CTG GCC TGT GT	DA (-) 6312-6293	3753-5839
(-)5856-5839	CTC AAC TCT CAC GGG CGA A		
(+)4229-4248	CCC TGT GCA GTC GGT TTT TC	DA (-) 6312-6293	4229-6312
(-)6312-6293	CTT ACT ACG ACA GTG GCC CT		
(+)6031-6050	CCT GAC AAG GCT GAA GTG AC	DA (-) 7835-7813	6031-7835
(-)7835-7813	AGT TTC TCT TTA AGT GTT CCT GG		
(+)6031-6050	CCT GAC AAG GCT GAA GTG AC	3' RACE	6031-poly(A)
(-)3'RACE	GAC TCG AGT CGA CAT CGA		
(+)6066-6079	GCT CCG TGC CCA CC	3'RACE 6031-poly(A)	6066-poly(A)
(-)3'RACE	GAC TCG AGT CGA CAT CGA		

Table 2 PCR products amplified for sequencing.

Primer Name Position	Polarity	Sequence (5'->3')	Length
DA (+)123-142	+sense	ACT CCC GAC TCC GCA CCC TA	20
DA (-)450-431	-sense	TCA CAT AAT CGG GGA GAC AT	20
DA (-)625-606	-sense	AAG GAA GGG GCA ACA CAT AC	20
DA (+)750-769	+sense	ACA CAA AGG CAG CGG AAC CC	20
DA (+)1087-1106	+sense	CCA GAT GTG TGC CCT ATT TG	20
DA (-)1170-1151	-sense	TGG GAA CCA TTC ACC GTC TG	20
DA (+)1428-1447	+sense	CCC CCA AAA CAA CGG ACA AT	20
DA (+)1737-1756	+sense	CTC CCA CAT CCG CAT TCC TC	20
DA (-)1760-1741	-sense	GGG AGA GGA ATG CGG ATG TG	20
DA (+) 1862-1881	+sense	CTC AAT TTC ACG CCG GCT CT	20
DA (-) 2538-2520	-sense	TGA GGT CGT CGG GAC AGA A	19
DA (+)2806-2825	+sense	TCC CCT ACT CAC TAT CGC CA	20
DA (+)2946-2965	+sense	GTC TCC GCG GGA GAT GAT TT	20
DA (-)3083-3065	-sense	GGT AGT TTC ACG GGT TCT G	19
DA (-)3538-3520	-sense	CAG CAC CGA CGA GCC ACA T	19
DA (+)3753-3772	+sense	CTT CTT TCC CTG GCC TGT GT	20
DA (-)3905-3886	-sense	CCG TGA ACC TTG TAG TCA AA	20
DA (+)4229-4248	+sense	CCC TGT GCA GTC GGT TTT TC	20
DA (-)4612-4593	-sense	GGC AAA CTG GGG GAG GAG TA	20
DA (+)4740-4759	+sense	ACG TGA GGC CAA TGA AGG TT	20
DA (-)5328-5309	-sense	AAC AGC AGG GTA ATG GGC AA	20
DA (-)5856-5837	-sense	CTC AAC TCT CAC GGG CGA A	19
DA (+)6031-6050	+sense	CCT GAC AAG GCT GAA GTG AC	20
DA (-)6312-6293	-sense	CTT ACT ACG ACA GTG GCC CT	20
DA (+)6660-6679	+sense	TCA TGA TGT TTT CCA ACC CA	20
DA (+)7766-7787	+sense	CTC AAA TGG ATG CTG TCA ACT T	22
DA (-)7835-7813	-sense	AGT TTC TCT TTA AGT GTT CCT GG	23

Table 3 Sequencing Primers

Statistical analysis

Comparison of seizure duration within the group was analyzed using the one-way analysis of variance (ANOVA) with the post test for linear trend, and comparison of seizure duration between the infected groups was performed using the unpaired t-test with the Welch's correction. Body weights were analyzed using the repeated measures two-way ANOVA with the Tukey's multiple comparisons test. Cognitive tests were analyzed using the two-way ANOVA with the Tukey's multiple comparisons test. For rest of the parametric analysis, one-way ANOVA with the Tukey's multiple comparisons test or the unpaired t-test with the Welch's correction was used. For non-parametric analysis, the unpaired Mann-Whitney rank sum test or Kolmogorov-Smirnov test was used. For nominal data (presence or absence of seizures), the Fisher's exact test was used. For all cases, significance was determined when $p \leq 0.05$. Statistical analysis was done using GraphPad Prism version 6.0d (Mac OS X, GraphPad Software, La Jolla, CA).

Results

Seizures induced by infection with DA-D_S were significantly more frequent and more severe than those induced by DA-C_L.

Groups of 4-week-old C57BL/6 were infected with DA-C_L, DA-D_s, or mock infected by I.C. injection as described in Materials and Methods. To efficiently record seizures, we observed mice twice a day (mornings and evenings) for a week following infection.

During the first 7 days of infection mice infected with the DA-D_S variant had a much higher incidence of seizures (31/33 mice) than the DA-C_L variant (4/33) (Figure 5A) and this difference reached a high level of statistical significance (Fisher's exact test, $p<0.0001$). No seizures were found in the control group (not shown).

The infected mice usually seized within the first few minutes of observation, suggesting that handling-associated stress played an important role in triggering seizures. Seizures occurred both in the mornings and in evenings indicating that there was no association between seizures and circadian rhythm. Moreover, 64% of the DA-D_S-infected mice experienced more than one seizure during the day, compared to only 3% in the DA-C_L-infected group. Additionally, seized mice were individually monitored for the total number of seizures (frequency) during the acute phase (Figure 5B) the seizure frequency was significantly higher in the DA-D_S-infected group compared to that in the DA-C_L-infected group (Unpaired t test with Welch's correction, $p<0.0001$).

The intensity of seizures was greater in DA-D_S-infected mice with approximately 88% of the mice exhibiting Racine stage 5 level seizure activities, whereas only 9% of the DA-C_L-infected mice had seizures of that severity. These severe seizures started with head nodding and rapidly progressed to tonic-clonic seizures. Seizures in the DA-D_S-infected group started from day 2 p.i., the majority of seizures occurred on days 3, 4 and 5 p.i., and seizures completely ceased after day 7 p.i. (Figure 5D). In comparison, seizures in the DA-C_L-infected group occurred only on day 3 p.i., The duration of

seizures in the DA-D_S-infected group significantly increased over time and showed a significant linear trend (Figure 5C) (One-way ANOVA with post test for linear trend, $p<0.0001$). However, the duration of seizures that occurred on day 3 p.i. was not significantly different between the DA-D_S- and DA-C_L-infected groups (Figure 5E) (Unpaired t test with Welch's correction, $p=0.6511$).

To confirm our findings, we video-recorded two cages of mice from each infected group 24/7 for a week, and analyzed videos in a blinded-fashion. As expected, we did not find any seizures in the DA-C_L-infected groups, while a total of 8 seizure episodes, at the Racine stage 4 or 5, were recorded in the DA-D_S-infected groups during the acute phase. To investigate for occurrence of delayed seizures or epileptic episodes, we examined three cages of mice per infected group for chronic phase (day 8 till week 5 or 11 p.i.) studies. We did not observe any seizures in any of the infected groups during the chronic phase. However, this does not rule out the possibility of the development of epilepsy in the infected mice, since epileptic seizures are sporadic and in our study, mice were not video monitored during the chronic phase.

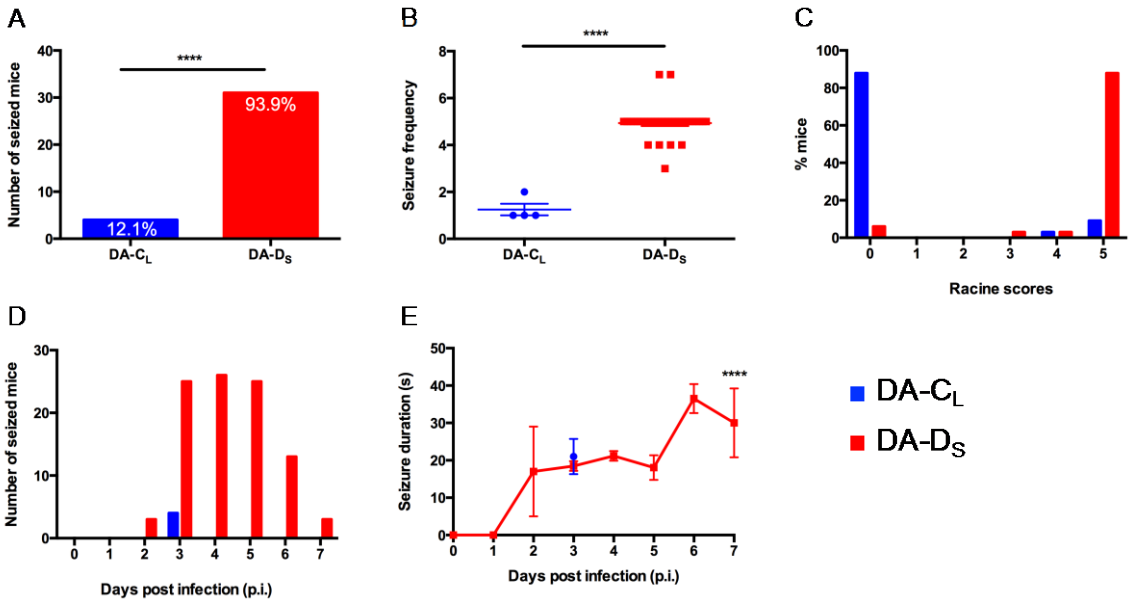

Figure 5 Seizures induced by infection with DA-D$_S$ were significantly more frequent and more severe than those induced by DA-C$_L$. (A) Significantly higher number of mice developed seizures following DA-D$_S$ infection. In contrast, the DA-C$_L$ plaque-variant failed to induce seizures in most of the infected mice (**** $p<0.0001$ by Fisher's exact test). The % of seized mice in each group was calculated as (number of seized mice/total number of infected mice) x 100. (B) The seizure frequency was significantly higher due to infection by DA-D$_S$ than DA-C$_L$ (**** $p<0.0001$ by unpaired t test with Welch's correction). The data are only from seized mice in DA-C$_L$ and DA-D$_S$ groups, N= 4 and 31, respectively. (C) In the DA-C$_L$ group, most of the mice (denoted as %) did not seize and hence, were given Racine score 0, while very few mice exhibited Racine stage 4 or 5 seizures. In comparison, in the DA-D$_S$ group the majority of mice (denoted as %) exhibited seizures of Racine stage 5, and few mice had seizures of Racine stage 3 and 4. (D) Seizures in DA-C$_L$ group were only seen on day 3 p.i., while seizures in DA-D$_S$ group began from day 2 p.i. and lasted till day 7 p.i. with most mice seizing on days 3, 4 and 5 p.i. (E) The duration of seizures that occurred on day 3 p.i. were not significantly different between the groups. However, the duration of seizures in the DA-D$_S$ group showed a significant linear trend over days p.i. (**** $p<0.0001$ by one-way ANOVA with post test for linear trend). Graphs (A, B, C and D) show pooled results from four separate experiments expressed as number/ percent/ mean ± SEM, N=33 per infected group. Graph (E) shows pooled results from three separate experiments expressed as mean ± SEM, N=23 per infected group.

Mice infected with DA-D$_S$ plaque variant displayed severe non-epileptic clinical signs in the acute phase.

We evaluated the effects of plaque-variant infection on non-epileptic clinical signs during the acute phase. Most mice developed hunched backs, ruffled fur, and/or ataxia post-infection. However, encephalitis-like signs were more prominent among DA-D$_S$-

infected mice compared to DA-C_L-infected mice. As shown in Figure 6, we found significant differences in clinical scores between the groups on days 1, 2, 5, 6 and 7 p.i. (Mann-Whitney rank sum test, p=0.0439 on day 1 p.i., p=0.0005 on day 2 p.i., p=0.1056 on day 3 p.i., p=0.0630 on day 4 p.i., p<0.0001 on days 5 and 6 p.i., and p=0.0028 on day 7 p.i.). Furthermore, four of the DA-D_S- and two of the DA-C_L-infected mice developed flaccid paralysis of hind limb(s) during the acute phase. DA-D_S-infected mice that developed flaccid paralysis also exhibited seizures.

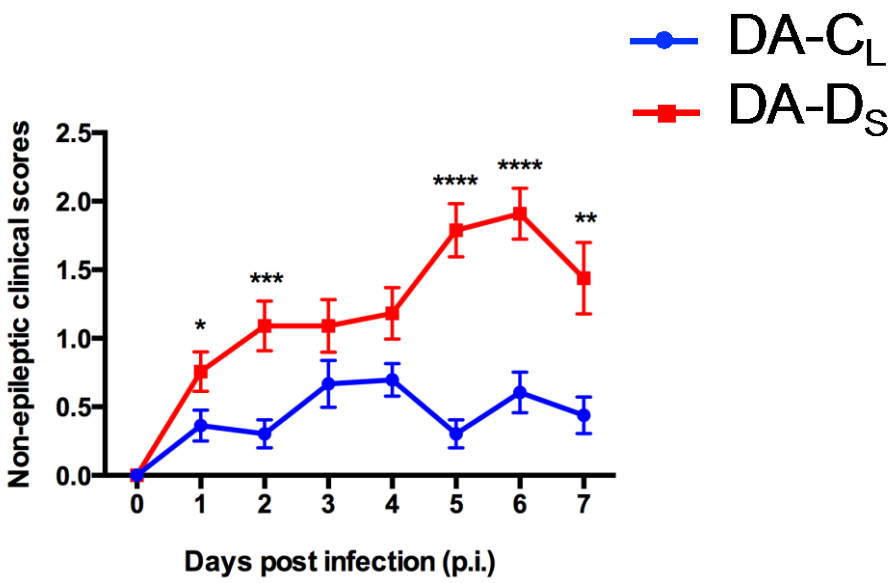

Figure 6 Mice infected with DA-D_S plaque variant displayed severe non-epileptic clinical signs in the acute phase. Mice were observed daily for signs of non-epileptic clinical disease during the acute phase. Both the virus infected groups showed clinical signs, but clinical scores were significantly higher in DA-D_S-infected group compared to that in DA-C_L-infected group (* p<0.05, ** p<0.01, *** p<0.001, **** p<0.0001 by Mann-Whitney rank sum test). The clinical scores lowered in DA-C_L group, but they remained persistently high in DA-D_S group. Graph shows pooled results from four separate experiments expressed as mean ± SEM, N=33 per infected group.

Mice infected with DA-D_S plaque variant had a significant delay in their recovery. Weight is one of the parameters used to monitor the health of mice. All mice lost weight following i.c. injection, but the weight loss was less marked in the control group and highest in the DA-D_S-infected group as illustrated in Figure 7A. Control mice gained weight after day 2 p.i., while mice in the infected groups continued to lose weight during the acute phase of infection. (Repeated Measures two-way ANOVA with Tukey's multiple comparisons test; for control vs. DA-C_L groups- $p<0.0001$ on days 1, 4, 5, 6, 7 p.i., $p=0.0002$ on day 2 p.i. and $p=0.0001$ on day 3 p.i.; for control vs. DA-D_S groups- $p<0.0001$ on days 1 till 7 p.i.; for DA-C_L vs. DA-D_S groups- $p=0.0030$ on day 1 p.i. and $p<0.0001$ on days 2 till 7 p.i.).

The mice in the DA-C_L-infected group began to gain weight during week 2 p.i., and were equal to the weights of control mice by week 3 p.i. The mice in DA-D_S-infected group started gaining weight during week 3 p.i., but their weights remained significantly lower than the other groups until week 4 p.i. (Figure 7B). (Repeated Measures two-way ANOVA with Tukey's multiple comparisons test; for control vs. DA-C_L groups- $p<0.0020$ on week 1 p.i., $p=0.0091$ on week 2 p.i., $p=0.8467$ on week 3 p.i., $p=0.5349$ on week 4 p.i., and $p=0.9892$ on week 5 p.i.; for control vs. DA-D_S groups- $p<0.0001$ on weeks 1 and 2 p.i., $p=0.0010$ on week 3 p.i., $p=0.0079$ on week 4 p.i., and $p=0.5601$ on week 5 p.i.; for DA-C_L vs. DA-D_S groups- $p=0.0004$ on week 1 p.i., $p<0.0001$ on weeks 2 and 3 p.i., $p=0.0132$ on week 4 p.i., and $p=0.2071$ on week 5 p.i.). Thus, compared to other groups, recovery in DA-D_S-infected group was significantly delayed.

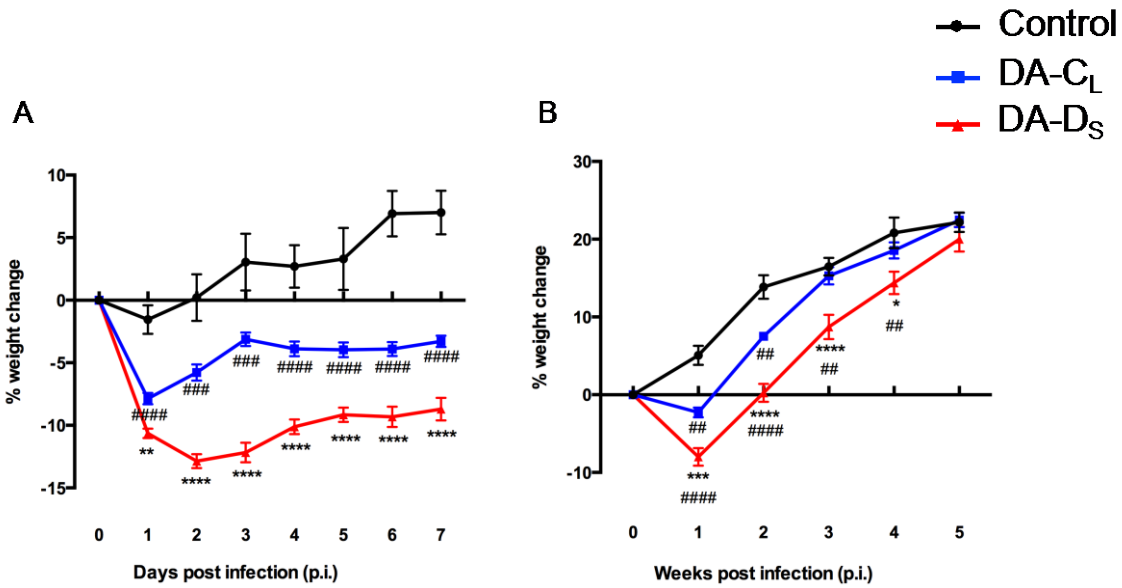

Figure 7 Mice infected with DA-D$_S$ plaque variant had a significant delay in their recovery. Mice from the control and infected groups were weighed daily until day 7 p.i. and then once weekly until week 5 p.i. (A) We found that the infected mice lost weight following infection during the acute phase, but the highest weight loss was found in the DA-D$_S$-infected group. (B) DA-C$_L$-infected mice recovered by week 3 p.i., while recovery among DA-D$_S$-infected mice was not seen until week 5 p.i. (* $p<0.05$, **/## $p<0.01$, ***/### $p<0.001$, ****/#### $p<0.0001$ by Repeated Measures two-way ANOVA with Tukey's multiple comparisons test). Graph A shows pooled results from four separate experiments expressed as mean ± SEM, N=4 in control group and N=32 per infected group. Graph B shows pooled results from two separate experiments expressed as mean ± SEM, N=4 in control group and N=13 per infected group.

DA-D$_S$ infection induced significant neuro-edema in mice.

To assess the impact of plaque-variants on neuro-edema, we compared wet brain weights from infected and control groups at day 7 p.i. As depicted in Figure 8, mouse brains from the DA-D$_S$ group weighed significantly more than the brains from control or DA-C$_L$ group. However, brain weights from DA-C$_L$ and control groups were not found statistically different (One-way ANOVA with Tukey's multiple comparisons test; control vs. DA-D$_S$ group-p=0.0003; control vs. DA-C$_L$ group-p=0.0838; DA-C$_L$ vs. DA-D$_S$ group-p=0.0007). Our results indicate that only DA-D$_S$ plaque variant was able to induce neuro-edema in mice.

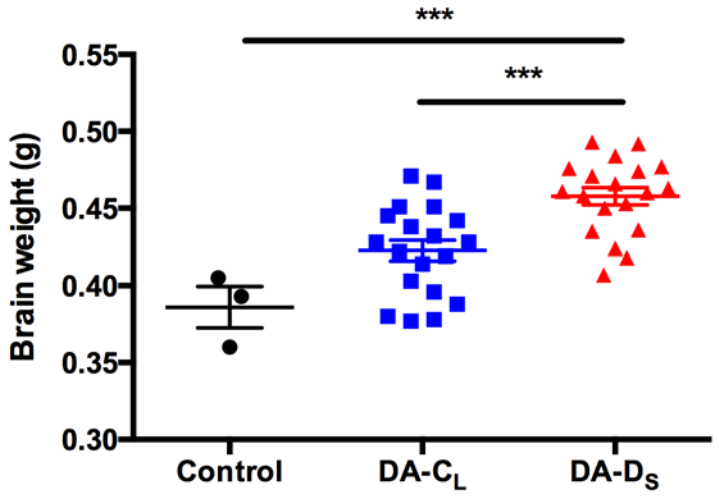

Figure 8 DA-D_S infection induced significant neuro-edema in mice. To determine the effects of plaque-variants on neuro-edema, brains from infected and control mice were collected and weighed at day 7 p.i. The brains from DA-D_S-infected group weighed significantly more compared to that from control or DA-C_L-infected group. (*** $p<0.001$ by One-way ANOVA with Tukey's multiple comparisons test). Graph shows pooled results from two separate experiments expressed as mean ± SEM, N=3 in control group and N=19 per infected group.

Increased viral burden in mice infected with DA-D_S plaque-variant.

We used brain and spinal cord homogenates from day 7 p.i. to assess viral burden in the infected groups. As shown in Figure 9, we found that viral titers in the brains from DA-D_S-infected mice were approximately five times higher than that in the brains from DA-C_L-infected mice (Unpaired t test with Welch's correction p=0.0010). However, viral titers in the spinal cords were found to be similar between the infected groups (Unpaired t test with Welch's correction p=0.8721).

We also found significant differences between the viral titers in brain vs. spinal cords from the DA-D_S-infected group (Unpaired t test with Welch's correction p=0.0004), while no such differences were found in the DA-C_L-infected group (Unpaired t test with

Welch's correction p=0.1964). Our plaque assay results from day 7 p.i. show that viral burden remained high in mice infected with DA-D_S plaque-variant.

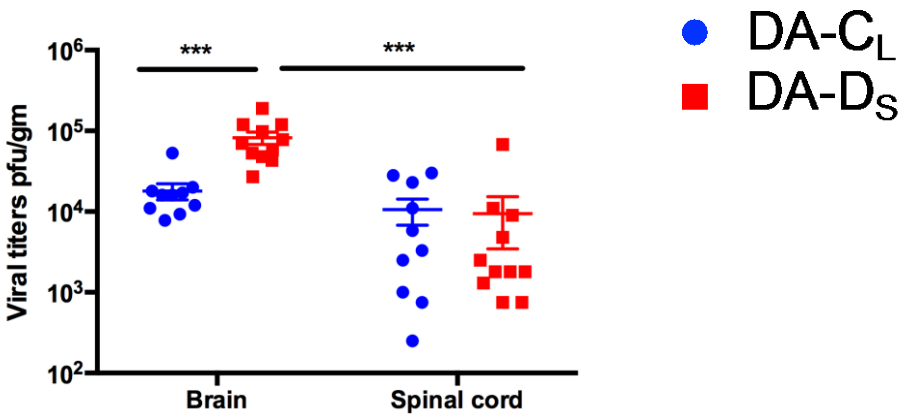

Figure 9 Increased viral burden in mice infected with DA-D_S plaque-variant. At day 7 p.i., brains from DA-D_S-infected mice had significantly higher viral titers than DA-C_L-infected mice. Viral load was also detected in their spinal cords at this time point, but no significant difference was observed between the groups. (*** $p<0.001$ by Unpaired t test with Welch's correction). Graph shows mean ± SEM, N=10 in DA-C_L group and N=11 in DA-D_S group.

Increased number of viral-antigen positive cells in the hippocampus of DA-D_S-infected mice.

We analyzed coronal sections of mouse brain from the infected groups for virus localization in the hippocampus. At day 7 p.i., viral-antigen was mainly found in the CA1 and CA2 pyramidal layers, while it was completely absent from the CA3 pyramidal layer and the granule cell layer of dentate gyrus (Figure 10A and B). We enumerated the number of virus-antigen positive cells in the hippocampi and found that there was a significantly higher number of virus-infected neurons in DA-D_S-infected mice compared to DA-C_L-infected mice (Figure 10C) (Unpaired t test with Welch's correction p=0.0033). In addition to virus-antigen positive cells in the hippocampus, viral infection

was noted in the cortex. But in both the infected groups, the virus-antigen spread was limited to the cortical area nearest to the CA1 and CA2 hippocampal regions.

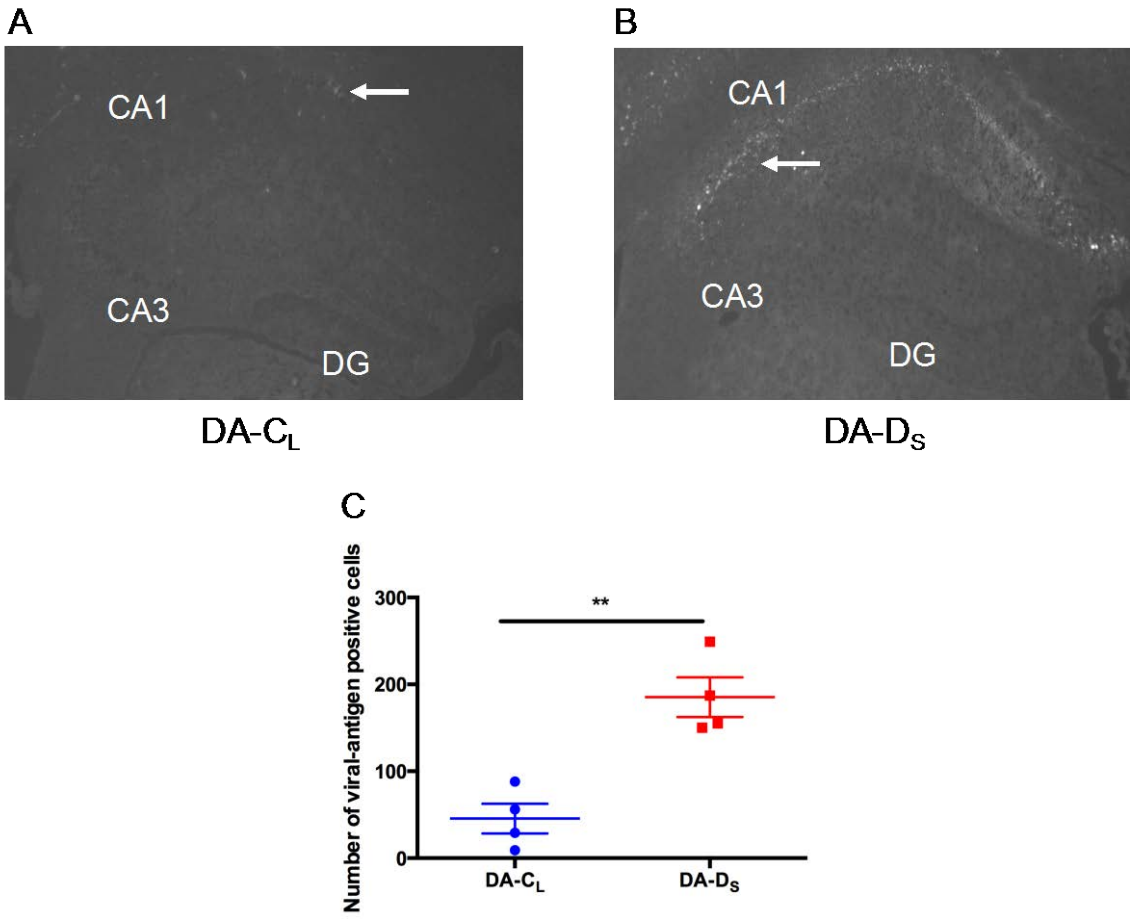

Figure 10 Increased number of viral-antigen positive cells in the hippocampus of DA-D$_S$-infected mice. At day 7 p.i., (A and B) viral-antigen was primarily detected in the CA1 and CA2 pyramidal layers (white arrows) of the hippocampus in both the infected groups. Some of the cortical neurons surrounding the CA1 and CA2 pyramidal layers also stained positive for viral-antigen. (C) The number of viral-antigen positive cells in the hippocampus was significantly higher in the DA-D$_S$-infected group than that in the DA-C$_L$-infected group. (** $p<0.01$ by Unpaired t test with Welch's correction). Graph shows mean ± SEM, N=4/infected group. Cornu ammonis1 (CA1), Cornu ammonis2 (CA2), Cornu ammonis3 (CA3), and dentate gyrus (DG).

Heterogeneous astroglial pathology among infected mice.

Astrogliosis is a characteristic finding in several neurological diseases including epilepsy [95,96]. At day 7 p.i., we examined brain sections from infected mice for the number and morphology of astrocytes in the hippocampus. In general, we found an increase in the number of astrocytes in DA-D_S-infected mice. However, the astrocyte count was not significantly different between the infected groups (Figure 11C) (Unpaired t test with Welch's correction p=0.1564). This could be because of the small sample size and/or pooled results from seized and non-seized mice in the DA-C_L-infected group. Interestingly, the non-seized mice in DA-C_L-infected group had less astrocytes compared to the seized mice in the DA-D_S and DA-C_L-infected groups.

In comparison to the non-reactive/ resting astrocytes, reactive astrocytes exhibit increased GFAP expression and hypertrophy of the cell body and cellular processes [96]. In our study, the astrocytes in the hippocampus showed variability in the extent of GFAP expression and hypertrophy between and within the infected groups. Most astrocytes from the DA-D_S-infected mice were found highly activated and hypertrophied, while the morphology of astrocytes varied from mildly activated to highly activated among the DA-C_L-infected mice. Apart from astrogliosis, we found loss of astrocytes in some of the infected mice in the CA1 and CA2 regions, except for the stratum lacunosum-moleculare area (SLM), of the hippocampus (Figure 11B). Although astrogliosis has previously been reported in hippocampus following TMEV infection [81], this is the first report of loss of astrocytes in this model.

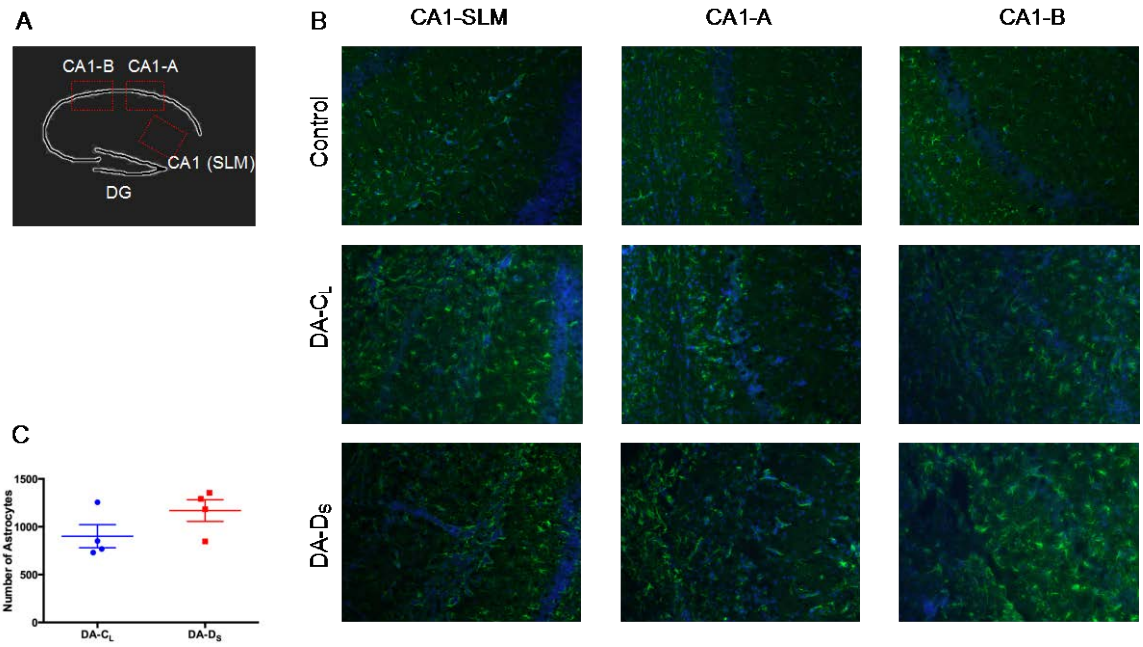

Figure 11 Heterogeneous astroglial pathology among infected mice. (A) Schematic diagram of the coronal section of hippocampus depicting different areas of CA1 field. (B) In comparison to the control mice that express resting/quiescent astrocytes, viral-infected mice exhibit reactive astrocytes that appear hypertrophied and have increased expression of GFAP protein. Among the infected mice, the CA1 region of the hippocampus showed varied astroglial pathology. In both the infected groups, activated astrocytes were found at the SLM area of CA1. The astrocytes were also found lining the PVCs at SLM. At the CA1-A area of the hippocampus, we found activated, but fewer astrocytes (possible astroglial degeneration) near the damaged CA1 pyramidal layer in both groups. At the CA1-B area, astrocytes were more reactive in the DA-D_S-infected group than that in the control or DA-C_L-infected group. Images were taken under 200x magnification. (C) The total astrocyte count within the hippocampus was not found to be significantly different between the infected groups (Unpaired t test with Welch's correction). Graph shows mean ± SEM, N=4/infected group. Cornu ammonis1 (CA1), dentate gyrus (DG) and stratum lacunosum-moleculare (SLM).

Extensive inflammation and neuronal damage in the hippocampus of mice infected with DA-D_S variant.

To evaluate the effects of DA plaque-variants on pathology in the hippocampus, we examined H&E stained coronal sections of brain for inflammation and neuronal damage at varying time points. The preliminary data from day 3 p.i. showed that when compared to controls (Figure 12A), infected mice developed inflammation at the alveus,

hippocampal fissure and stratum lacunosum-moleculare (SLM) area of CA1 and CA2 regions, while only the DA-D_S-infected mice showed neuronal loss at CA1 and CA2 pyramidal layers (Figure 12B and F). By day 7 p.i., the neuronal damage was also found in the DA-C_L-infected group along with the existent inflammation (Figure 12C). In contrast, there was a marked increment in the intensity of inflammation and CA1 and CA2 neuronal loss in the DA-D_S-infected group (Figure 12G). The extent of acute neuronal loss (Mann-Whitney test. Sum of ranks, p=0.0079) and inflammation (Unpaired t test with Welch's correction, p=0.0199) were significantly greater following DA-D_S-infection compared to DA-C_L-infection (Figure 12J and K). In the chronic phase, the inflammation mostly subsided and no further neuronal damage was found in the DA-C_L-infected mice (Figure 12D and E), while the inflammation was exacerbated in the DA-D_S-infected mice by week 5 p.i. (Figure 12H) and persisted at week 11p.i., which was the latest time-point at which histological analysis was performed (Figure 12I). Moreover, we did not find any damage to the dentate gyrus and CA3 neurons in either of the infected groups, which is consistent with other studies using the DA strain [81].

Our results show that both plaque variants are capable of inducing inflammation in the hippocampus, but the intensity of inflammation is much more severe following DA-D_S-infection compared to DA-C_L-infection. In the chronic phase, inflammation resolves following DA-C_L-infection, while it continues to increase following DA-D_S-infection. The DA-D_S variant also induces an early and severe onset of neuronal damage, as most mice lose almost all of their CA1 and CA2 neurons by day 7 p.i. On the contrary, the

DA-C_L variant causes minimal neuronal loss in the acute phase, which does not progress in the chronic phase.

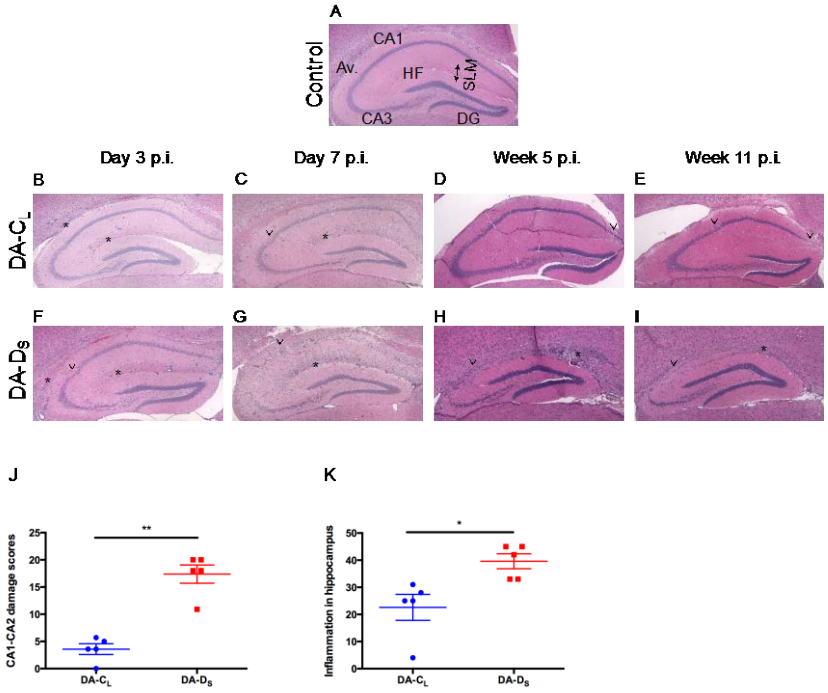

Figure 12 Extensive inflammation and neuronal damage in the hippocampus of mice infected with DA-D$_S$ variant. (A) H&E stained coronal section of hippocampus from control mice. Hippocampal regions from the infected groups were analyzed at days 3 (B and F) and 7 (C and G) and weeks 5 (D and H) and 11 (E and I) p.i. for histopathology. B-E are the representative images from DA-C_L-infected group and F-I are the representative images from DA-D_S-infected group. By day 3 p.i., both the infected groups (B and F) showed increase in cellularity and PVCs at alveus, hippocampal fissure and stratum lacunosum-moleculare area of CA1 and CA2 regions. However, the loss of CA1 and CA2 pyramidal neurons was found only in the DA-D_S-infected group at this time-point. At day 7 p.i., both the inflammation, and CA1 and CA2 neuronal loss, were extremely severe in the (G) DA-D_S-infected mice and greater than that in the (C) DA-C_L-infected mice. (C) A representative section of hippocampus from DA-C_L-infected group presenting CA1-CA2 damage score 2. (G) A representative section of hippocampus from DA-D_S-infected group presenting CA1-CA2 damage score 10. By week 5 p.i., the inflammation mostly resolved in the (D) DA-C_L-infected mice, while it remained high in the (H) DA-D_S-infected mice. At week 11 p.i., no inflammation was found in the (E) DA-C_L-infected group and the intensity of inflammation appeared to decrease in the (I) DA-D_S-infected group. The arrowheads depict neuronal loss and the asterisks depict inflammation in the images. All images were taken under 100X magnification. At day 7 p.i., (J) the damage to the CA1 and CA2 pyramidal layers (** $p<0.01$ by Mann-Whitney test. Sum of ranks) and (K) the intensity of inflammation (* $p<0.05$ by Unpaired t test with Welch's correction) were found to be significantly higher in the DA-D_S-infected group in comparison to that in the DA-C_L-infected group. Graphs show mean ± SEM, N=5 per infected group. Cornu ammonis1 (CA1), cornu ammonis2 (CA2), cornu ammonis3 (CA3), dentate gyrus (DG), alveus (Av.), hippocampal fissure (HF) and stratum lacunosum-moleculare (SLM).

Acute inflammation was more pronounced at the lumbar segment of spinal cord following DA-D_S-infection.

Unlike SJL mice, the DA infection fails to cause demyelinating lesions in the spinal cord of C57BL/6 mice [72]. To study the impact of DA plaque variants on spinal cord disease in C57BL/6 mice, we analyzed H&E stained spinal cord sections for damage at acute (days 3 and 7 p.i.) and chronic (weeks 5 and 11 p.i.) phases of infection.

At day 3 p.i., no significant lesions were observed in the spinal cords of any of the infected mice in comparison to control mice. By day 7 p.i., both the infected groups developed meningitis, PVC, inflammatory foci, and/or possible neuronal degeneration at the ventral and/or lateral horns of the gray matter of spinal cord. In some mice, inflammation even extended to the dorsal horn of the gray matter, and ventral and lateral columns of the white matter.

The magnitude of inflammation was similar at the cervical and thoracic segments between the infected groups, but the lumbar and sacral segments of the DA-D_S-infected group showed higher neuropathology than the DA-C_L-infected group. In the DA-D_S-infected group, lesions were found in 6/6 mice at the lumbar segment and 4/6 mice at the sacral segment, while in the DA-C_L-infected group, lesions were only found in 2/5 mice at the lumbar and sacral segments (Figure 13A-D).

Upon comparing the cumulative distribution of the scores, we found that DA-D_S plaque variant induced significantly more lesions at the lumbar segment in comparison to the DA-C_L plaque variant (Figure 13E) (Kolmogorov-Smirnov test; for cervical and thoracic segments-$p>0.9999$; for lumbar segment-$p=0.0390$; and for sacral region-$p=0.2424$).

By week 5 p.i., the inflammation subsided in both the infected groups. In addition, we did not find demyelinating lesions in any of the infected mice at week 5 or 11 p.i. Our results show that although DA-C_L-and DA-D_S plaque variants induce acute inflammation in the spinal cord, they fail to cause chronic demyelinating disease in C57BL/6 mice. Nonetheless, the deleterious effects of DA-D_S plaque variant were more prominent than that of DA-C_L plaque variant, specifically at the lumbar segment of the spinal cord.

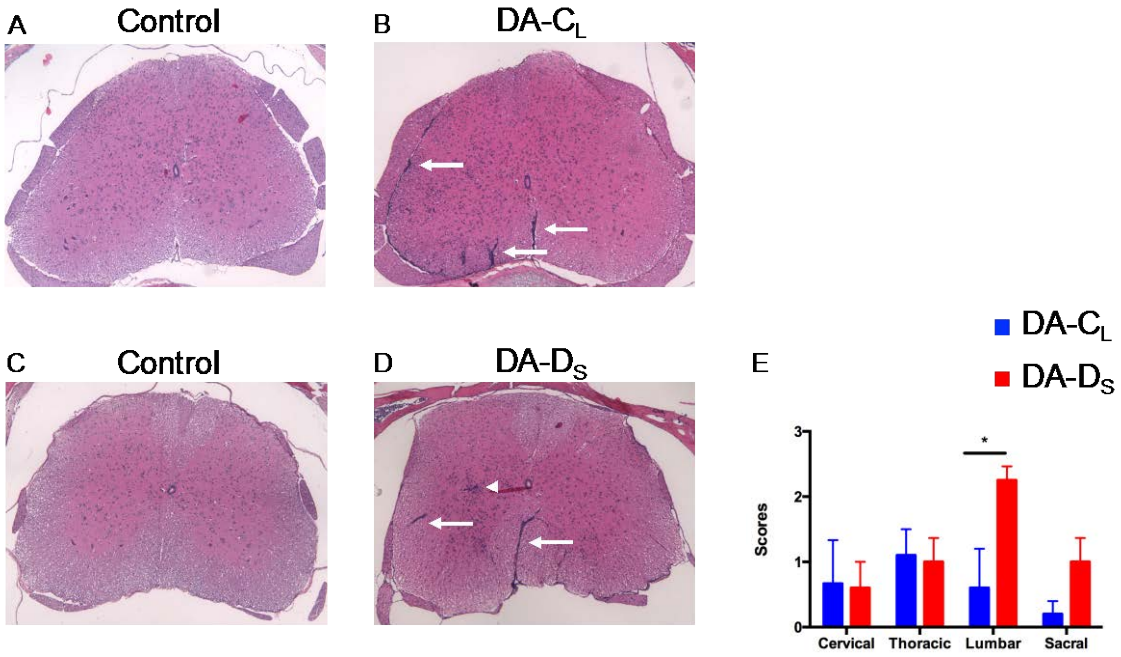

Figure 13 Acute inflammation was more pronounced at the lumbar segment of spinal cord following DA-D$_S$-infection. H&E stained lumbar segments from the (A and C) control group, (B) DA-C$_L$-infected group, and (D) DA-D$_S$-infected group. (A and C) No lesions were found in the control group. (B and D) The most affected lumbar segments showing meningitis, PVC, and inflammatory foci in the gray and white matter, and representing scores 3. (E) The degree of inflammation was similar at the cervical, thoracic and sacral segments, while the lumbar segments from the DA-D$_S$-infected group were found significantly more inflamed than that in the DA-C$_L$-infected group (* $p<0.05$ by Kolmogorov-Smirnov test). All images were taken under 100X magnification. Graph shows mean ± SEM, N=5 in DA-C$_L$ group and N=6 in DA-D$_S$ group. Arrowhead indicates possible neuronophagia and arrows indicate inflammation.

Increased immune cell infiltration into the CNS of mice following DA-D$_S$-infection.

TMEV infection stimulates the activation of resident immune cells and infiltration of peripheral immune cells into the CNS [21,81,97]. To immuno-phenotype leukocyte populations, we harvested brain leukocytes from control and infected mice at day 3 p.i., as seizures peak at this time point. We found a significant increase in the expression levels of CD45.2+ (which includes microglia, macrophages/monocytes, neutrophils, T cells, B cells, etc.) in the cells isolated from the CNS of the DA-Ds-infected group compared to control mice. However, the expression levels of CD45.2+ cells were not

found to be statistically different between the controls and DA-C_L groups, and between the DA-C_L and DA-D_S groups (Figure 14A) (One-way ANOVA with Tukey's multiple comparisons test; control vs. DA-D_S group-p=0.0246; control vs. DA-C_L group-p=0.3975; DA-C_L vs. DA-D_S group-p=0.1366).

Upon further analysis, we found that the expression levels of CD45.2intermediate (int) cells were similar in all groups (Figure 14B) (One-way ANOVA with Tukey's multiple comparisons test; control vs. DA-D_S group-p=0.8870; control vs. DA-C_L group-p=0.9958; DA-C_L vs. DA-D_S group-p=0.8668), but the expression levels of CD45.2high (hi) cells were DA- D_S > DA- C_L > control group (Figure 14C) (One-way ANOVA with Tukey's multiple comparisons test; control vs. DA-D_S group-p=0.0003; control vs. DA-C_L group-p=0.0425; DA-C_L vs. DA-D_S group-p=0.0385). To differentiate between microglia and macrophage/monocyte/granulocyte populations, we gated cells based on their CD45.2 and CD11b expression. As depicted in Figure 14D, we did not find any significant differences in the expression levels of CD45.2int CD11b+ cells (microglia) between the groups (One-way ANOVA with Tukey's multiple comparisons test; control vs. DA-D_S group-p=0.7105; control vs. DA-C_L group-p=0.9256; DA-C_L vs. DA-D_S group-p=0.8420). Interestingly, the expression levels of CD45.2hi CD11b+ cells (macrophage/monocyte/granulocyte) in the DA-D_S-infected group were found significantly higher than that in control or DA-C_L group, Figure 14E (One-way ANOVA with Tukey's multiple comparisons test; control vs. DA-D_S group-p=0.0014; control vs. DA-C_L group-p=0.1335; DA-C_L vs. DA-D_S group-p=0.0374). Figure 14F shows a

significant increase in the expression levels of CD45.2+ Gr1+ cells in the DA-D_S-infected group compared to the control group, but not the DA-C_L group (One-way ANOVA with Tukey's multiple comparisons test; control vs. DA-D_S group-p=0.0052; control vs. DA-C_L group-p=0.2092; DA-C_L vs. DA-D_S group-p=0.0775).

Our results indicate that DA-D_S plaque-variant had a significant impact on the infiltration of peripheral innate immune cells into the CNS. On one hand, the inflammatory response is crucial for protection against virus infection, but on the other hand, the dysregulated inflammation initiates widespread hippocampal damage, leading to seizure development.

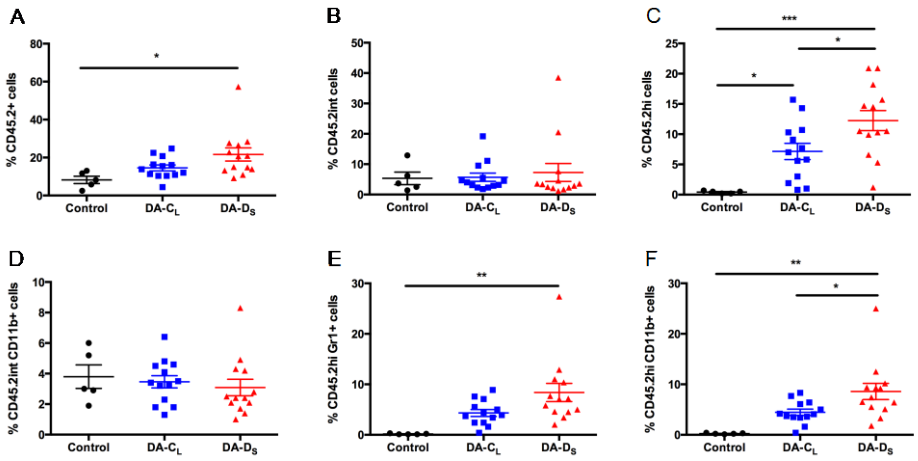

Figure 14 Increased immune cell infiltration into the CNS of mice following DA-D_S-infection. Brain leukocytes from control and infected mice were collected at day 3 p.i. and stained for cell specific markers. (A) Our results showed that DA-D_S infection significantly increased the expression levels of CD45.2+ in the brain. Upon further analysis, we found that (B and D) neither of the plaque-variants significantly altered CD45.2int and CD45.2int CD11b+ expression levels, while (C) the expression levels of CD45.2hi were DA-D_S > DA-C_L > control group, and (E and F) DA-D_S plaque variant significantly increased the expression levels of CD45.2hi CD11b+ and CD45.2hi Gr1+ in mice brains during the acute phase. Graphs show pooled results from five separate experiments expressed as mean ± SEM, N=5 in control group and N=13 per infected group. (* $p<0.05$, ** $p<0.01$, *** $p<0.001$ by One-way ANOVA with Tukey's multiple comparisons test).

Behavioral and cognitive tests

In addition to recurrent seizures, epilepsy is often associated with neuropsychological dysfunction, such as impaired memory and attention, depression, anxiety, etc. [98,99].

Mice with DA-D_S infection developed anxiety-like behavior in the chronic phase. We conducted EPMT to determine the effects of plaque-variants on the development of anxiety-like behavior in mice. This test is based upon the principle that mice have a natural disinclination for open and elevated spaces and preference for dark and enclosed spaces. However, mice also exhibit curiosity for novel environments. Hence, this test is truly a balance between both aspects of mouse behavior. The less curious mice would stay in the closed arms and have fewer visits to the open arms [90].

As shown in Figure 15A, we found no statistical differences in the number of closed arm entries between the groups suggesting similar locomotor activity among all mice. (One-way ANOVA with Tukey's multiple comparisons test; control vs. DA-C_L group-p=0.9602; control vs. DA-D_S group-p=0.9774; and DA-C_L vs. DA-D_S group-p=0.8312). However, we saw significantly fewer open arm entries in the DA-D_S-infected group compared to the DA-C_L-infected group (Figure 15B). The number of open arm entries was not statistically different between the controls and infected mice. This could be because of the smaller sample size of the control group. Our findings suggest that anxiety-like behavior was only induced among mice following DA-D_S infection (One-

way ANOVA with Tukey's multiple comparisons test; control vs. DA-C_L group-p=0.3403; control vs. DA-D_S group-p=0.7249; and DA-C_L vs. DA-D_S group-p=0.0370).

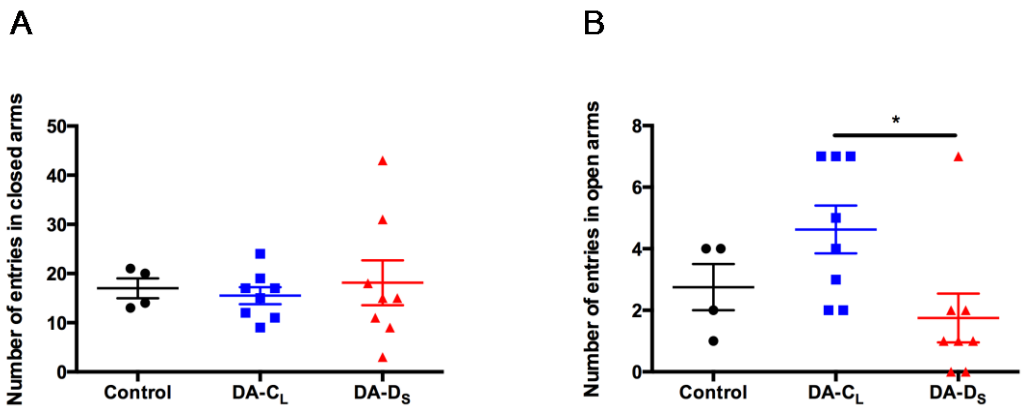

Figure 15 Mice with DA-D_S infection developed anxiety-like behavior in the chronic phase. (A) Neither of the plaque-variants affected locomotor activity, but (B) only DA-D_S plaque-variant induced anxiety-like symptoms as infected mice hesitated to enter open arms of the elevated plus maze. Graphs show results expressed as mean ± SEM, N=4 in control group and N=8 per infected group. (* $p<0.05$ by one-way ANOVA with Tukey's multiple comparisons test).

The two plaque-variants had no effect on the context-associated memory, but they significantly impaired spatial-associated memory in mice.

We conducted NORT and NOLT to examine whether plaque-variants had any effect on context and/or spatial-based memory in mice. NORT is based upon the inclination of mice to explore a novel object over a familiar object, while NOLT is based upon the inclination of mice to explore an object in a novel location (displaced) over an object in a familiar location (non-displaced) [100].

We started with NORT, and found that both the control and infected mice displayed an increase in the discrimination index (DI) in the test phase when compared to that in the

familiar phase (Figure 16A), but we did not find DI to be statistically different between and within the groups (Two-way ANOVA with Tukey's multiple comparisons test, control $_{fam}$ vs. DA-$C_{L\ fam}$ group-p=0.9991; control $_{fam}$ vs. DA-$D_{S\ fam}$ group-p>0.9999; DA-$C_{L\ fam}$ vs. DA-$D_{S\ fam}$ group-p=0.9995; control $_{test}$ vs. DA-$C_{L\ test}$ group-p=0.9723; control $_{test}$ vs. DA-$D_{S\ test}$ group-p=0.9978; DA-$C_{L\ test}$ vs. DA-$D_{S\ test}$ group-p=0.9986; control $_{fam}$ vs. control $_{test}$ group-p=0.5054; DA-$C_{L\ fam}$ vs. DA-$C_{L\ test}$ group-p=0.3670; and DA-$D_{S\ fam}$ vs. DA-$D_{S\ test}$ group-p=0.3247).

As shown in Figure 16B, we found no significant differences in the novel object exploration time among the groups (Two-way ANOVA with Tukey's multiple comparisons test, control $_{fam}$ vs. DA-$C_{L\ fam}$ group-p=0.9974; control $_{fam}$ vs. DA-$D_{S\ fam}$ group-p>0.9999; DA-$C_{L\ fam}$ vs. DA-$D_{S\ fam}$ group-p=0.9959; control $_{test}$ vs. DA-$C_{L\ test}$ group-p=0.2269; control $_{test}$ vs. DA-$D_{S\ test}$ group-p=0.4709; DA-$C_{L\ test}$ vs. DA-$D_{S\ test}$ group-p=0.9917; control $_{fam}$ vs. control $_{test}$ group-p=0.0664; DA-$C_{L\ fam}$ vs. DA-$C_{L\ test}$ group-p=0.4506; and DA-$D_{S\ fam}$ vs. DA-$D_{S\ test}$ group-p=0.4031). Our findings suggest that neither of the plaque-variants had any significant effect on the context-associated memory in mice.

Our results from NOLT experiments showed that both the control and infected mice displayed an increase in the discrimination index (DI) in the test phase when compared to that in the familiar phase (Figure 16C), although this difference was found to be the least in the DA-D_S-infected group. Moreover, we did not find the DI to be statistically

different between and within the groups (Two-way ANOVA with Tukey's multiple comparisons test, control $_{fam}$ vs. DA-$C_{L\ fam}$ group-p=0.9969; control $_{fam}$ vs. DA-$D_{S\ fam}$ group-p>0.9999; DA-$C_{L\ fam}$ vs. DA-$D_{S\ fam}$ group-p=0.9768; control $_{test}$ vs. DA-$C_{L\ test}$ group-p=0.9945 control $_{test}$ vs. DA-$D_{S\ test}$ group-p=0.8557; DA-$C_{L\ test}$ vs. DA-$D_{S\ test}$ group-p=0.9722; control $_{fam}$ vs. control $_{test}$ group-p=0.6261; DA-$C_{L\ fam}$ vs. DA-$C_{L\ test}$ group-p=0.2928; and DA-$D_{S\ fam}$ vs. DA-$D_{S\ test}$ group-p=0.9864).

However, (Figure 16D) we found that only the control mice preferred the displaced (novel location) object to the non-displaced (familiar location) object, and the exploration time for the displaced object was significantly lower among the infected groups than that among the control group (Two-way ANOVA with Tukey's multiple comparisons test, control $_{fam}$ vs. DA-$C_{L\ fam}$ group-p=0.6526; control $_{fam}$ vs. DA-$D_{S\ fam}$ group-p=0.5478; DA-$C_{L\ fam}$ vs. DA-$D_{S\ fam}$ group-p>0.9999; control $_{test}$ vs. DA-$C_{L\ test}$ group-p=0.0272; control $_{test}$ vs. DA-$D_{S\ test}$ group-p=0.0066; DA-$C_{L\ test}$ vs. DA-$D_{S\ test}$ group-p=0.9838; control $_{fam}$ vs. control $_{test}$ group-p=0.3566; DA-$C_{L\ fam}$ vs. DA-$C_{L\ test}$ group-p=0.9804; and DA-$D_{S\ fam}$ vs. DA-$D_{S\ test}$ group-p=0.9999). Our findings suggest that both the plaque-variants significantly impaired the spatial-associated memory in mice, but this effect was more pronounced following DA-D_S infection.

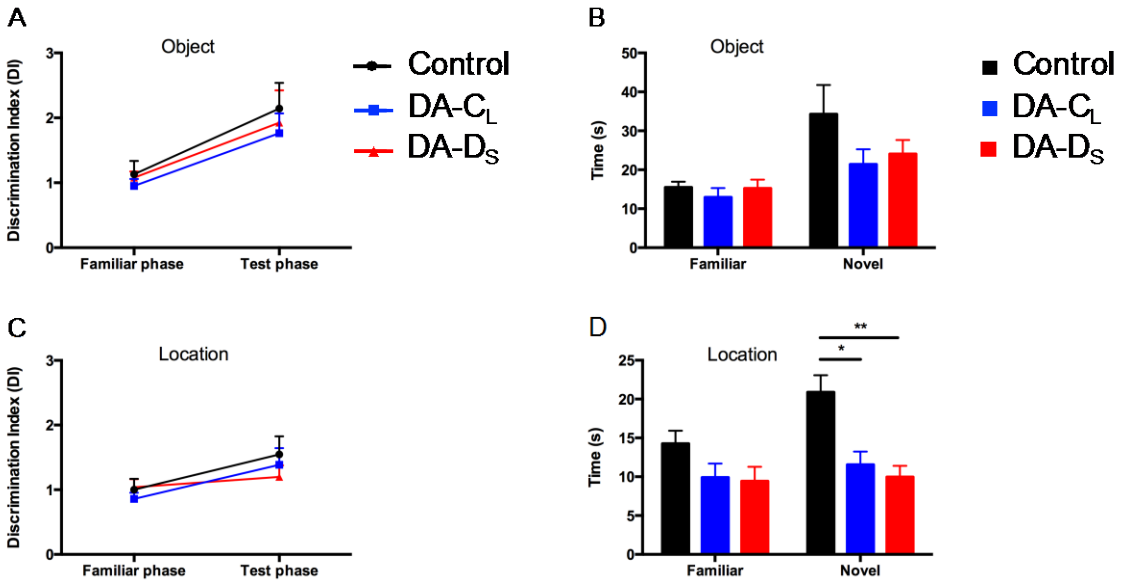

Figure 16 The two plaque-variants had no effect on the context-associated memory, but they significantly impaired spatial-associated memory in mice. The results from cognitive tests conducted in the chronic phase showed that (A and B) DI and exploration time (novel object) in NORT remained unaffected following viral infection. (C) DI in NOLT was relatively lower following DA-D$_S$-infection, but (D) both DA-C$_L$ and DA-D$_S$ plaque-variants significantly decreased exploration time of the displaced object in NOLT. Graphs show results expressed as mean ± SEM. N=4 in control group and N=8 per infected group. (* $p<0.05$, ** $p<0.01$ by Two-way ANOVA with Tukey's multiple comparisons test). Discrimination index (DI), novel object recognition test (NORT), and novel object location test (NOLT).

Genetic Differences between viral strains.

Total RNA was extracted from DA-C$_L$ and DA-D$_S$ infected L2 cells and cDNAs representing overlapping amplicons spanning nts 137-3'poly(A) tail (nt positions are all relative to Genbank Accession M20301 [83]) were synthesized by RT-PCR, purified by agarose gel electrophoresis and sequenced as described in Materials and Methods. A list of the overlapping amplicons can be found in Table 2. The nucleotide sequences of the DA-C$_L$ and DA-D$_S$ variants and the translated proteins were aligned and compared to each other and to the three other TMEV-DA complete genomes in Genbank (Genbank Accessions M20301, JX443418, and KF680264) [83] with Clustal Omega. Sequence

differences are summarized in Table 4. There are three nucleotide differences between DA-C_L and DA-D_S. The first is a T1244C change in DA-C_L compared to both DA-D_S and the three sequences for the DA strain of TMEV that are present in Genbank. This change results in a M60T amino acid change in the DA- C_L leader protein and a W56R change in the L* protein relative to both DA-D_S and the Roos lab strain of TMEV-DA. The second is in the coding sequence for the helicase domain of protein 2C, where DA-D_S contains a T5030C change relative to DA-C_L and the Genbank sequences. This produces a corresponding I133T mutation in the DA-D_S 2C protein relative to the 2C protein encoded in DA-C_L and the other three TMEV-DA sequences in Genbank. The third nucleotide difference between the DA-C_L and DA-D_S variants is coding silent at position 6054, where DA-D_S and the three other viruses we analyzed contain an A at this position and the DA-C_L virus contains a G.

There are three additional sites where the DA-C_L and DA-D_S sequences differ from all of the complete genomes in Genbank. In the 5' untranslated region (5'UTR) there is a C at position 475 in the DA-C_L and DA-D_S sequences and a T is present in all three TMEV genome sequences in Genbank. Nucleotide7813 is a G in both DA-C_L and DA-D_S whereas all three of the Genbank Accessions contain a C at this position. This difference results in an alanine at amino acid 410 in the DA-C_L and DA-D_S 3D proteins, whereas the other 3 viruses encode a proline at this position. A third difference is present at nucleotide 1929 where both DA-C_L and DA-D_S contain a C, whereas a T is present in Genbank Accession JX443418 and a G is present in Genbank Accessions M20301 and

KF680264. This nucleotide difference is coding silent relative to the translation of M20301 and KF680264 and is thus unlikely to be significant. There are approximately 40 other sites where the DA-C_L and DA-D_S sequences are discordant from one or two of the three complete TMEV-DA genome sequences but are identical to at least one TMEV-DA genome sequence in Genbank (not shown). The vast majority of these correspond to coding silent polymorphisms amongst the three TMEV genomes in Genbank.

Nucleotide Position	**DA-D_S**	**DA-D_S amino acid**	**DA- C_L**	**DA- C_L amino acid**	**Genbank M20301**	**Genbank M20301 amino acid**	**Genbank JX443418**	**Genbank JX443418 amino acid**	**Genbank KF680264**	**Genbank KF680264 amino acid**
475	C	NA	C	NA	T	NA	T	NA	T	NA
1244	T	L protein 60M L*protei n 56W	C	L protein 60T L*protei n 56R	T	L protein 60M L*protein 56W	T	L protein 60M L*protein 56W	T	L protein 60M L*protein 56W
1929	C	VP2 protein 141K	C	VP2 protein 141K	G	VP2 protein 141K	T	VP2 protein 141N	G	VP2 protein 141K
5030	C	2C protein 133T	T	2C protein 133I	T	2C protein 133I	T	2C protein 133I	T	2C protein 133I
6054	A	3C protein 40Q	G	3C protein 40Q	A	3C protein 40Q	A	3C protein 40Q	A	3C protein 40Q
7813	G	3D protein A410	G	3D protein A410	C	3D protein A410	C	3D protein A410	C	3D protein A410

Table 4 Summary of sequence differences between DA-C_L and DA-D_S and Genbank Accessions M20301, JX443418, and KF680264.

Discussion

Fujinami and co-workers were the first to characterize the TMEV-induced epilepsy model. They found that C57BL/6 mice infected with the DA strain of TMEV exhibit symptomatic seizures in the acute phase, recover from viral infection within a month, but after an unspecified latent phase develop unprovoked recurrent seizures (epilepsy). In this infection-driven model, the lesions are mainly concentrated in the CA1 and CA2 regions of the hippocampus. In the chronic phase, the neuronal loss and gliosis worsens to cause hippocampal atrophy and glial scarring, termed hippocampal sclerosis (HS) [34,38,101-103]. HS is also the hallmark neuropathology of mesial temporal lobe epilepsy (MTLE), the most prevalent form of human epilepsy [104] [105,106]. Since DA-infection shares similarities with MTLE, it serves as an excellent model to study epileptogenesis and epilepsy.

Our current work is an extension of the TMEV-induced epilepsy studies. Here, we investigated the independent roles of the large (DA-C_L) and small (DA-D_S) plaque-size variants of DA strain of TMEV in the development of seizures. The *in vivo* studies revealed a striking contrast between the phenotypes of the DA-C_L and DA-D_S plaque variants. We found that the percentage of seized mice was significantly higher following DA-D_S-infection (~94%) compared to DA-C_L-infection (~12%). We recorded repeated seizures in the DA-D_S-infected group that began on day 2 and ceased after day 7 p.i., whereas seizures in the DA-C_L-infected group were only observed on day 3 p.i.

Additionally, the frequency and severity (Racine stage 4 or 5) of seizures in the DA-D_S-infected group peaked on day 3 p.i. and remained high until day 5 p.i. The previous study, where similar titers (2.5×10^5 pfu) of the DA strain were used and mice were examined twice daily, showed acute seizures in ~57% of the infected C57BL/6 mice [107]. The phenotypic variability between the DA strain and the plaque variants indicate that the neuro-virulence is DA-D_S-plaque variant>DA strain>DA-C_L-plaque variant.

Furthermore, we monitored clinical illness including weight loss and non-epileptic clinical signs in mice following infection. Compared to DA-C_L, the DA-D_S plaque variant caused severe illness (ruffling, hunched back and ataxia) in mice during the acute phase. However, the severity of clinical illness was variable within the group. In addition, the acute weight loss was highest in the DA-D_S-infected mice, and their weights remained significantly lower than the control or DA-C_L-infected mice until one-month p.i. This implies that there was significant delay in the recovery among DA-D_S-infected mice.

The plaque assay studies at day 7 p.i. revealed that viral titers remained significantly higher in the brains of DA-D_S- infected mice compared to those of DA-C_L-infected mice. Similar to the DA infection [81], we also detected virus-antigen positive cells in the hippocampus at day 7 p.i. Within the hippocampus, the virus-antigen was localized in the CA1 and CA2 pyramidal neurons, but the neurons in dentate gyrus and CA3 region were not affected. The number of viral-antigen positive cells was significantly higher in

the DA-D_S-infected group compared to the DA-C_L-infected group. These findings confirm that the DA-D_S-, but not DA-C_L-, plaque variant could efficiently replicate *in vivo*.

Since viral-antigen positive cells were mainly confined to the CA1 and CA2 pyramidal layers of the hippocampus, we examined these regions for neuronal loss. By day 7 p.i., the DA-D_S-infected group had wide-spread loss of CA1 and CA2 neurons, and increased presence of PVCs and inflammatory foci in the hippocampal fissure and near CA1 and CA2 pyramidal layers. In contrast, neuronal loss in the DA-C_L-infected group was patchy, with significantly fewer PVCs and inflammatory foci. In the chronic phase, mice from the DA-D_S-infected group developed evident anatomical changes at CA1 and CA2 regions of hippocampus. The extensive loss of pyramidal neurons in the DA-D_S-infected group may have emanated from the high viral burden, inflammation, and/or seizures from the acute phase.

Moreover, we detected viral burden and inflammation in the spinal cords of infected mice at day 7 p.i. The magnitude of inflammatory lesions varied within the spinal cord segments of the same mouse and between the infected mice. However, the most marked lesions were found in the lumbar segment of the spinal cord among DA-D_S-infected mice. Mice also developed ataxia/ flaccid paralysis of the hind limb(s) during the first week, which was more pronounced following DA-D_S-infection. Therefore, we suggest that mice develop short-lived hind limb deficits, the intensity of which depends upon the

severity of spinal cord lesions. Nonetheless, the intensity and duration of inflammation and viral burden was much higher in the brains than the spinal cords of the infected mice.

TMEV-infection triggers a significant host immune response, including the activation of resident (glia) and the infiltration of peripheral immune cells into the CNS. The immune response is extremely crucial for protecting the CNS against viral infection, but also leads to massive neuronal destruction in the process. The neuronal damage (particularly CA1 and CA2 pyramidal neurons) and seizures begin very early following TMEV (DA strain)-infection (day 2-3 p.i.), the time-point at which the adaptive immune response is not significant, implying that these events are mainly mediated by the innate immune response [21,81,97,103]. Here, we found that at day 3 p.i, which is the peak time for seizures in our study, the expression levels of infiltrating innate immune cells (such as, monocytes, macrophages and granulocytes), but not resident immune cells (microglia), were significantly higher in the DA-D_S-infected group compared to the control and DA-C_L-infected groups. Our findings imply that the excessive levels of infiltrated innate immune cells are detrimental to the hippocampal neurons and result in seizures following DA-D_S-infection, while microglia may not be a critical factor here. These results align with the previous studies using DA-infected mice, where the hippocampal damage and seizure frequency were significantly reduced after blocking or depleting granulocytes and more specifically, inflammatory monocytes. However, the authors did not rule out the role of microglia in causing seizures [20,97].

Astrocytes play crucial and diverse roles in maintaining the healthy state of the CNS, while reactive astrocytes may be a direct cause of disease or may contribute to disease progression. Upon molecular, cellular and/or functional alterations, the reactive astrocytes can lose their normal functions or gain atypical functions. On the contrary, reactive astrocytes may have beneficial roles in the diseased state. For instance, the glial scarring by astrocytes may be a mechanism to limit the spread of infection, insult or inflammation [96]. Here, we found the dual and region-specific astroglial pathology in the hippocampus at day 7 following DA plaque variants infection. In general, infected mice displayed reactive astrocytes, and seized mice had higher number of astrocytes than the non-seized mice. In addition, we found the loss of astrocytes near CA1 and CA2 pyramidal layers in some of the infected mice. The missing astrocytes could be a consequence of glial degeneration mediated by viral infection, acute inflammation, or adjacent neuronal damage. The loss of astrocytes is also a characteristic finding in Rasmussen's encephalitis, a form of inflammation-induced human epilepsy [108]. Thus, the dysfunctional or lost astrocytes may cause excitotoxicity, neurotoxicity, seizures and epilepsy.

Neuropsychological issues, such as mood disorders, anxiety, depression, impaired cognition, etc. are common sequelae of epilepsy [98,99]. In fact, these deficits are more prevalent among people with epilepsy than the general population [109,110]. Therefore, we examined infected mice for behavioral and cognitive deficits at one-month p.i. Our results showed that mice developed anxiety-like symptoms following DA-D_S-infection,

but not DA-C_L-infection. The ventral hippocampus and amygdala are the two main regions of the brain involved in regulating emotional behavior. However, their roles are quite distinctive, as the amygdala affects fear-based situations, while ventral hippocampus contributes to anxiogenic situations [111,112]. This suggests that the DA-D_S plaque variant provoked anxiety-like symptoms in mice by causing functional alterations in the hippocampus. The anxiety-like symptoms are also seen among mice following DA-infection [38].

The results from memory tasks showed that both the infected groups had significant decline in spatial-based memory, and this deficit was more pronounced among DA-D_S-infected mice. However, context-based memory was spared in both the infected groups. In their review, Ciernia and Wood [100] discussed the roles of distinct regions of rodent brain in partaking different types of memory. They note that the hippocampus, in particular the dorsal CA1 region, is critical for spatial-based memory. Whereas, insular cortex, perirhinal cortex, ventromedial prefrontal cortex, and maybe the hippocampus are important for forming context-based memory. The previous study using DA-infected mice showed that the extent of hippocampal damage, but not cortical damage, regulates spatial-based memory in mice [102]. In our present study, we report that like the DA strain [38,102,103]; both plaque-variants could induce spatial-based memory deficits in mice probably due to CA1 neuronal damage. The infected mice in our study had intact context-based memory, though another group has reported context-based memory deficits using DA-infected mice [103]. These varied findings could be because of the

differences in the test setup (short vs. long delay phase) or in the neuro-virulence of the DA strain and plaque-variants.

Cardioviruses such as TMEV translate their genomes as a 7kb polyprotein precursor that subsequently undergoes autoproteolytic cleavage to yield 12 viral proteins, one of which is the 76 amino acid leader protein [113-116]. The demyelinating strains of TMEV such as TMEV-DA also express an 18-kDA L* protein from an alternate open reading frame [2] first identified by Kong and Roos [117]. The leader protein contains an N-terminal Zinc binding Cys-His-Cys-Cys (C-H-C-C) motif that is essential for this protein's ability to inhibit IFN-α/β production, allowing for viral persistence [118-122]. Part of the mechanism for this inhibition of interferon induction has been linked to leader protein binding to nucleoporins and blocking mRNA nuclear export [123,124]. The Leader protein also contains an acidic domain, a serine/threonine rich domain which in TMEV contains two phosphorylation sites, and a C-terminal TMEV-specific domain that plays a role in cellular localization and trafficking between the nucleus and cytoplasm [124,125]. L* is synthesized from an overlapping ORF 13 nucleotides downstream from the AUG start codon for the polyprotein [122,126] and has been shown to inhibit the interferon-inducible OAS/RNase L pathway allowing for the evasion of host innate immunity [121]. The ability to impair the innate host immune response in certain cell types by either Leader or L* contributes to viral evasion of the host immune response and viral persistence [118,123,124,126,127]. Mutations in leader result in significantly less neurovirulence as indicated by decreased viral persistence in the CNS [120]. Our data show that the thymine to cytosine

mutation at position 1244 in DA-C_L compared to both DA-D_S and the three TMEV Genbank sequences results in a methionine to threonine amino acid change at position 60 in the DA- C_L leader protein and a tryptophan to arginine change at position 56 for the L* protein. Interestingly, mutation of leader methionine 60 to valine, leucine, or isoleucine blocks binding to nucleoporins, RNA export from the nucleus, interferon induction *in vitro*, and viral persistence *in vivo* [122,124]. Thus, we postulate that these mutations in the leader and L* proteins of DA-C_L lead to the attenuating phenotype of the DA-C_L variant in the C57BL/6 mouse model of epilepsy. Compared to the DA-D_S variant, infection with the DA-C_L variant resulted in to less neuro-edema, less viral burden and less neuro-inflammatory burden in the hippocampus of our DA-C_L infected mice. The overall result was better recovery of mice infected with the DA-C_L variant versus the DA-D_S and significantly fewer and less severe episodes of seizure activity in DA-C_L infected mice. Our data are consistent with previous findings that mutations in the leader protein [118] and the L* protein [113,124] both reduce viral neurovirulence and virus persistence in macrophages *in vitro*, and in the brain and spinal cord in mice [113,127,128]. Experiments are ongoing to elucidate the relative importance of the mutation in leader versus L*, as current research has yielded somewhat controversial claims as to the importance of each protein in viral persistence [113,121]. The sequence differences between DA-C_L and DA-D_S at nucleotides 5030 and 6054, respectively, appear to be unlikely to contribute to the attenuation of DA-C_L. The first because the nucleotide at this position is identical to that in the other three TMEV stains in Genbank and identical to the DA-C_L sequence, and the latter because it is coding silent.

The H-2D MHC class I locus strongly influences the susceptibility of the inbred mouse strains to the demyelinating disease or epilepsy. C57BL/6 mouse strain (*H-2*^{b} haplotype) is resistant to the demyelinating disease but susceptible to epilepsy, whereas the SJL mouse strain (*H-2*^{s} haplotype) is susceptible to the demyelinating disease but do not develop epilepsy [82,129-131]. Our findings in C57BL/6 mice together with the previous study by Oleszak and group in SJL mice [80] corroborate that both the C57BL/6 and SJL mouse strains develop severe neuro-pathological lesions, clinical disease, and viral burden following DA-D_S-infection, while the magnitude of the clinical disease in both the mouse strains is minimal following DA-C_L-infection. Hence, the neuro-virulence of DA-D_S and DA-C_L plaque-variants is independent of the H-2D MHC class I locus in C57BL/6 and SJL mouse strains. This is in contrast to the recent paper published on two naturally occurring variants of the BeAn strain of TMEV, (BeAn-1 and BeAn-2). They found that BeAn-1 was neuro-virulent in only the SJL mouse strain causing demyelinating disease (MS), while BeAn-2 was neuro-virulent in only the C57BL/6 mouse strain causing acute seizures. Thus, the neuro-virulence of the BeAn variants, unlike the DA variants, depends upon the genotype of C57BL/6 and SJL mice. Although, they do not show if the BeAn variants formed different sized-plaques as the DA variants do *in vitro* [132].

To conclude, we found that the DA-D_S plaque variant was extremely neuro-virulent and caused marked structural and functional alterations in the hippocampus of C57BL/6 mice, while the DA-C_L plaque variant had attenuated neuro-virulence. The previous

study from SJL mice [80] along with our current study in C57BL/6 mice indicate that the neuro-virulence of DA-D_S plaque variant is significantly higher than the DA-C_L plaque variant in the viral-induced models of two distinct neurological diseases, MS and epilepsy.

CHAPTER III

THE *NLRC5* GENE IS CRITICAL FOR INNATE IMMUNITY AND SEIZURE DEVELOPMENT IN TMEV-INDUCED EPILEPSY MODEL

Introduction

Theiler's murine encephalomyelitis virus (TMEV) is a single stranded RNA virus that belongs to *Picornaviridae* family. TMEV-infected C57BL/6 mice develop an unregulated innate immune response (activation of microglia/monocytes, astrocytes, etc.) invoking seizures within a week post infection (p.i.), and adaptive immune response (mainly MHC class I-dependent cytotoxic T cell activation) mediating viral clearance within a month p.i. In addition, the development of "bystander" hippocampal damage makes infected mice susceptible to recurrent spontaneous seizures (epilepsy). Although, TMEV infection culminates in epilepsy in C57BL/6 mice [21,34,36], the T cell-mediated viral clearance prevents them from developing chronic demyelinating disease of the central nervous system (CNS) that resembles multiple sclerosis. TMEV infection-driven murine epilepsy recapitulates the attributes of medial temporal lobe epilepsy (mTLE); hence, serves as an efficient model to study acute inflammatory triggers and pathophysiology of seizures [34,43].

Nucleotide-binding oligomerization domain-like receptors (NLRs) form an essential part of the innate immune system. They are intracellular pattern recognition receptors (PRRs)

that recognize conserved microbial motifs called pathogen-associated molecular patterns (PAMPs) and/or endogenous danger signals called danger-associated molecular patterns (DAMPS). Among the PRRs, NLRs form the biggest family with 22 members in humans and 34 members in mice [133]. NLRs have recently gained immense attention due to their diverse immunological functions in numerous autoimmune disorders, neurological diseases, viral and bacterial infections (Reviewed by: Biswas and Kobayashi [134]; Coutermarsh-Ott et al. [135]; Kong et al. [136]).

The NLR family, caspase activation and recruitment (CARD) domain containing 5 (NLRC5), also named NOD27, or CLR16.1 [133], is the largest protein of the NLR family possessing the molecular mass of 204 kDa. It consists of a tripartite domain structure, which includes an atypical caspase activation and recruitment domain (CARD) located at the N-terminal, a nucleotide-binding domain (NBD) located at the center, and a leucine-rich repeat domain (LRR) located at the C-terminal [137]. NLRC5 is located on chromosome 16q13 in humans [133,137], and chromosome 8 in mice [133]. NLRC5 protein in humans and mice share 64% of the amino acid sequence, suggesting that it is biologically conserved [56].

NLRC5 has a well-established role as the transactivator of major histocompatibility complex (MHC) class I (*H2-D* and *H2-K*) gene and the genes involved in MHC class I antigen processing and presentation, such as β_2-microglobulin (*β_2m*), transporter associated with antigen processing 1 (*TAP1*), and large multifunctional proteases 2

(*LMP2*) [45,49,50]. Apart from regulating MHC class I expression, NLRC5 has also been reported to contribute to immune signaling pathways (nuclear factor kappa-light-chain-enhancer of activated B cells [NF-κB]- and interferon [IFN]-dependent responses) following viral infection. However, most of these studies are conducted in *in vitro* and *ex vivo* systems, and the results pertaining to the function of NLRC5 as positive or negative regulator of anti-viral immunity are still inconclusive [49,53,54,56-58,137,138]. Since, NLRC5 contributes to both innate (by recognizing PAMPs) and adaptive (by MHC class I-dependent activation of cytotoxic T cell) immune responses, it is a common mediator for both arms of the immune system.

The objective of our current study is two-fold. The first objective is to delineate the function of Nlrc5 in regulating immune responses and inducing seizures in TMEV-induced model of epilepsy. The second objective is to investigate whether Nlrc5-dependent MHC class I expression determines the resistance of C57BL/6 mice to demyelinating disease following TMEV infection. For this, *Nlrc5* deficient (*Nlrc5*$^{-/-}$) mice (on C57BL/6 background) and wild type C57BL/6 mice were infected with TMEV, examined for clinical signs of seizures and demyelinating disease, brain and spinal cord pathology, and inflammation. The acute phase (day 0-7 p.i.) results showed that *Nlrc5* deficiency caused a significant reduction in the frequency of seizures, and reduced hippocampal pathological condition among the infected mice. Besides, we found a significant decrease in the inducible expression of MHC class I and its related genes, and pro-inflammatory mediators in the brain due to *Nlrc5* deficiency. Additionally, *Nlrc5*$^{-/-}$

infected mice showed a significant decrease in the expression of Natural Killer cells (NK) in the brain, with variable expression of other leukocyte subtypes in comparison to wild type infected mice. We observed a significant decrease in astrocytes, specifically at the CA1 and dentate gyrus regions of the hippocampus in *Nlrc5*$^{-/-}$ infected mice. The chronic phase (day 8-52 p.i.) results showed no signs of demyelinating disease or spinal cord lesions in *Nlrc5*$^{-/-}$ and wild type mice. Taken together, our results show that *Nlrc5* gene promotes inflammation and seizures in C57BL/6 mice, without affecting their resistance to demyelinating disease following TMEV infection. To our knowledge, this is the first study to report *in vivo* functions of Nlrc5 as a promoter of epilepsy.

Materials and Methods

Mice

Four-to-six-week-old female *Nlrc5*$^{-/-}$ (*Nlrc5* deficient mice on C57BL/6 background) mice were generously provided by Dr. Koichi K. Kobayashi, Department of Microbial Pathogenesis and Immunology, Texas A&M University, TX. Age-matched female C57BL/6 wild type mice were purchased from Taconic (Germantown, NY). Upon arrival, mice were assigned to one of four experimental groups; *Nlrc5*$^{-/-}$ /sham-infected control, wild type/ sham-infected control, *Nlrc5*$^{-/-}$ virus-infected, and wild type virus-infected. Mice were placed in a pathogen-free facility, with 12 hours of light and dark cycle and controlled room temperature and humidity. They were given free access to food and water throughout the duration of the experiment. All animal experiments were

approved by the Institutional Animal Care and Use Committee (IACUC) of Comparative Medicine Program at Texas A&M University, TX.

Virus

The BeAn strain of TMEV (ATTC) was initially propagated in baby hamster kidney (BHK) cells. Culture supernatant containing virus particles was collected and stored at -80°C, and later used for infections [85].

Infection

Mice were habituated to the facility for a week prior to infection. Mice in the infected groups were injected intracerebrally (I.C.) with 5.0×10^4 plaque forming unit (PFU) of BeAn strain in 20µl of Dulbecco's modified eagle medium (DMEM) (Sigma, Life Science, St. Louis, MO), whereas mice in the control group were either sham-infected I.C. with 20µl of 1x Phosphate Buffered Saline (PBS) or remained untreated. All injections were performed under isoflurane (Isoflo, North Chicago, IL) anesthesia.

Body weight measurement

During the acute phase, mice (n=4/control and n=26/infected group) body weights were recorded daily until day 6 p.i. % weight loss was calculated as ([mouse weight on day n^{th} p.i.- mouse weight on day 0 p.i.]/mouse weight on day 0 pi) *100.

Clinical scores

During the acute phase, mice were examined twice daily between 9 AM to 6 PM for seizures (n=4/control group and n=30-37/infected group) and non-epileptic clinical signs (n=4/control group and n=41/infected group) until day 6 p.i. and once on day 7 p.i. For seizures, mice were scored on a Racine scoring scale: (1) Mouth and facial movements, (2) Head nodding, (3) Forelimb clonus, (4) Rearing, and (5) Rearing and falling progressing to tonic-clonic seizure [139]. For non-epileptic clinical signs, mice were scored based upon the severity of sickness, where score (0) indicated no clinical signs; score (1) indicated mild ruffling, hunched back, and/or ataxia; score (2) indicated moderate ruffling, hunched back, and/or ataxia; score (3) indicated severe ruffling, hunched back, and/or ataxia; score (4) indicated paralysis; and score (5) indicated moribund. One cage of mice (n=4/control group and n=5/infected group) from each group was examined once weekly during the chronic phase (day 8-52 p.i.) for clinical signs of seizures and demyelinating disease.

Tissue isolation

To obtain tissues, mice were euthanized with 150mg/kg beuthanasia-D special (Schering-Plough Animal Health Corp. Union, NJ) and perfused intracardially using 10 ml of 1x PBS. Brains collected on day 7 p.i. were split into right and left halves, and each half was either used for quantitative real time PCR (qRT-PCR) assay or immunohistochemistry (IHC). For qRT-PCR, brains were snap frozen and stored at -80°C until use. For IHC, brains were immediately placed in freshly prepared 4%

paraformaldehyde (PFA) solution for 24-48 h at 4°C. For histology, spinal cords were retrieved on day 52 p.i., brains were instantly placed in 4 % PFA for 24-48 hours at 4°C, and spinal cords in 10% formaldehyde for 5 days at room temperature. For flow cytometry, brains and cervical lymph nodes (CLNs) were collected on day 3 p.i. in ice-cold RPMI 1640 (Gibco, Life Technologies, Grand Island, NY), and individually processed to analyze leukocyte populations.

Flow cytometry

For collecting leukocytes from brain: The whole brains (n=3/ infected group) were gently homogenized using 70-micron (μm) FALCON cell strainer (21008-952; VWR, Sugarland, TX) and suspended in RPMI 1640 containing 5% fetal bovine serum (FBS). The cell suspensions containing brain homogenates were collected in individual 50 ml conical tubes, and centrifuged at 500 x g for 5 min at room temperature. After discarding the supernatant, each pellet was suspended in 10 ml of 30% Percoll (17-0891-01; GE healthcare, Uppsala, Sweden) in PBS. This solution was gently overlaid onto 2 ml of 70% Percoll in PBS, and centrifuged at 500 x g for 30 min at 18°C. The leukocytes were collected from the 30% and 70% Percoll interphase, suspended in PBS, and centrifuged at 500 x g for 7 min at 18°C. The supernatants were discarded, and pellets were re-suspended in 3 ml of ice-cold flow buffer containing 3% BSA and 0.1% sodium azide in PBS.

For collecting leukocytes from CLNs: The CLNs (n=3-4/infected group) were homogenized by gently grinding them with sterile microscopic slides. Then, the cell suspensions containing CLN homogenates were filtered using sterile, 70-µm nylon mesh. The filtrates containing leukocytes were collected in individual 15 ml conical tubes, and centrifuged at 350 x g for 5 min at 4°C. The supernatants were discarded, and each pellet was suspended in 2 ml of flow buffer containing 3% BSA and 0.1% sodium azide in PBS. The cells were washed, re-suspended in flow buffer and maintained at 4°C.

Staining procedure: Leukocytes from brain and CLNs were treated with anti-mouse CD16/CD32 (1:100, 14-0161-82; eBioscience, San Diego, CA) for 10 min at 4°C to prevent any non-specific binding. For phenotyping, cells were stained with the anti-mouse antibodies as indicated below for 30 min at 4°C, washed and fixed with 2% PFA prior to flow cytometric analysis on BD FACSAria II. Data was analyzed using FlowJo® software V10.0.8r1 (Mac OS X, FlowJo, LLC, Ashland, OR). Ly-6G (Gr-1) was detected with clone RB6-8C5 (1:500, 12-5931-82; eBioscience, San Diego, CA). CD11c was detected with clone N418 (1:250, 17-0114-81; eBioscience, San Diego, CA). NK1.1 was detected with clone PK136 (1:500, 12-5941-63; eBioscience, San Diego, CA). CD11b was detected with clone M1/70 (1:500, 101224; BioLegend, San Diego, CA). CD45.2 was detected with clone 104 (1:100, 109805; BioLegend, San Diego, CA). CD8a was detected with clone 53-6.7 (1:250, 100711; BioLegend, San Diego, CA). CD4 was detected with clone GK1.5 (1:500, 100428; BioLegend, San Diego, CA). B220 was

detected with clone RA3-6B2 (1:500, 17-0452-83; eBioscience, San Diego, CA). CD69 was detected with clone H1.2F3 (1:500, 12-0691-82; eBioscience, San Diego, CA). CD80 was detected with clone 16-10A1 (1:500, 12-0801-82; eBioscience, San Diego, CA) [89,140].

Immunohistochemistry

Post-fixation, brains (n=7-9/infected group) were cryopreserved in 30% sucrose at 4°C for 3 days. After which, brains were embedded in optimum cutting temperature (OCT) compound (Tissue-Tek 4583, Torrance, CA), and cut on a cryostat (Leica CM 1950) to obtain 10-micron (μm) coronal sections. The serial sections, comprising of dorsal hippocampus, starting -1.7 mm from bregma were collected on plus-charged coated microscopic slides (12-550-17; Fisherbrand, Fisher Scientific). For each marker, rostro-caudally matched cryosections were selected from the groups.

The cryosections were hydrated, then blocked for 1 hour with 5% goat serum (16210-064; Gibco, Life Technologies, Grand Island, NY) in PBS containing 0.1% Triton X-100 (9002-93-1; Sigma-Aldrich, St. Louis, MO) for surface and cellular markers and 0.3% Triton X-100 for viral-antigen markers. The sections were incubated overnight at 4°C in primary antibodies, rabbit anti-ionized calcium-binding adapter molecule1 (IBA1) [019-19741; Wako Chemicals USA, Inc., Richmond, VA, 1:200] for macrophages/microglia, rabbit anti-glial fibrillary acidic protein (GFAP) [180063; Invitrogen, Life Technologies, Eugene, OR, 1:200] for astrocytes, or mouse anti-TMEV [Welsh lab:1:50] for TMEV-

antigen positive cells. The following day, sections were incubated at room temperature for 1 hour with secondary antibodies (1:1000), Alexa-Fluor 488 goat anti-rabbit IgG (A11034; Invitrogen, Life Technologies, Eugene, OR) for IBA, Alexa-Fluor 594 goat anti-rabbit IgG (A11037; Invitrogen, Life Technologies, Eugene, OR) for GFAP, and Alexa-Fluor 594 goat anti-mouse IgG (A11032, Invitrogen, Life Technologies, Eugene, OR) for viral-antigen. Later, cryosections were washed, counterstained with Hoechst 33342, trihydrochloride, trihydrate [1:1000, H3570; Life Technologies, Eugene, OR] and mounted with Fluoromount-G (0100-01; SouthernBiotech, Birmingham, AL).

To enumerate IBA- and GFAP-positive cells in the hippocampus, two-matched, but non-overlapped areas (400x field/area) from CA1, CA3 and dentate gyrus (DG) each were selected from the infected groups. Average cell count/area was used for comparison between the infected groups. The TMEV-stained sections were analyzed for the presence and localization of viral-antigen positive cells in the hippocampus. All images were acquired using a HRD076-NIK camera attached to OLYMPUS VANOX AHBS3 microscope.

Histology: brain

To determine acute neuronal loss and lesions in the hippocampus, 10 μm cryosections (n=3/infected group) were hydrated, and then stained in 0.5% cresyl violet for 5 min. After being rinsed with water, the sections were dehydrated in increasing concentrations of ethanol (75%-90%-100%), cleared in xylene, and coverslipped on the slides. All

images were acquired using a HRD076-NIK camera attached to OLYMPUS VANOX AHBS3 microscope.

Histology: spinal cord

Four μm paraffin-embedded sections from the spinal cords (n=4/control and n=4/ infected group) were stained with H&E. At least one transverse section from each spinal cord segment was examined for the presence of inflammatory foci, axonal/neuronal degeneration, and/or meningitis. All images were acquired using a HRD076-NIK camera attached to OLYMPUS VANOX AHBS3 microscope.

Quantitative real-time PCR (qRT-PCR)

Mouse brains (n=1-4/control group and n=3-5/infected group) were gently homogenized using Kinematica Inc, HOMOGEN KINMATICA PT 1200E electronic homogenizer (05-400-261, Fisher Scientific). Total RNA was isolated from each brain homogenate using Trizol-chloroform reagents, and purified using the TURBO DNA-free kit (AM1907, Invitrogen, Life Technologies). For each sample, one microgram (μg) of total RNA was reverse transcribed to cDNA using the qScript Flex cDNA Synthesis kit (95049-025, Quanta Biosciences) and following manufacturer's instructions. RNA expression was quantified on the 7300 Real-Time PCR System (Applied Biosystems) using the PerfeCTa SYBR Green SuperMix with ROX (Quanta Bio- sciences). The following primers were used for amplification, and the expression of target genes was determined by ratio of the number of target mRNA to *β-actin* mRNA [49].

Gene name	Primer sequence
Nlrc5	5'- CTTCCCGCCTCTCCTTCCACAAT -3' (forward) 5'- CTCCACCTGCCCACATCCTACCA -3' (reverse)
TMEV	5'- TGACTAAGCAGGACTATGCCTTCC -3' (forward) 5'- CAACGAGCCACATATGCGGATTAC -3' (reverse)
Ifn-γ	5'- TGCATCTTGGCTTTGCAGCTCTTC -3' (forward) 5'- GGGTTGTTGACCTCAAACTTGGCA -3' (reverse)
Ifn-β	5'- CAGCTCCAAGAAAGGACGAAC -3' (forward) 5'- GGCAGTGTAACTCTTCTGCAT -3' (reverse)
H2-Kb	5'- GTGATCTCTGGCTGTGAAGT -3' (forward) 5'- GTCTCCACAAGCTCCATGTC -3' (reverse)
H2-Aα	5'- CAACCGTGACTATTCCTTCC -3' (forward) 5'- CCACAGTCTCTGTCAGCTC -3' (reverse)
Ciita	5'- CCCTGCGTGTGATGGATGTC -3' (forward) 5'- ATCTCAGACTGATCCTGGCAT -3' (reverse)
$\beta_2 m$	5'- CCCCACTGAGACTGATACATACG -3' (forward) 5'- CGATCCCAGTAGACGGTCTTG -3' (reverse)
Tap1	5'- GGACTTGCCTTGTTCCGAGAG -3' (forward) 5'- GCTGCCACATAACTGATAGCGA -3' (reverse)
Il-6	5'- CCAGAAACCGCTATGAAGTTCC -3' (forward) 5'- TTGTCACCAGCATCAGTCCC -3' (reverse)
Tnf-α	5'- ACAGAAAGCATGATCCGCG -3' (forward) 5'- GCCCCCCATCTTTTGGG -3' (reverse)
Il-1β	5'- AAGGAGAACCAAGCAACGACAAAA -3' (forward) 5'- TGGGGAACTCTGCAGACTCAAACT -3' (reverse)
Tgf-β	5'-TGCGCTTGCAGAGATTAAAA -3' (forward) 5'- CGTCAAAAGACAGCCACTCA -3' (reverse)
Mip-1	5'- GGCTAACTGACCTGGAAAGG -3' (forward) 5'- GCACATCAGGTACGATCCAG -3' (reverse)
Mcp-2	5'- TTAAGGCATCACAGTCCGAG -3' (forward) 5'- TGAATGTGAAGTTGACCCGT -3' (reverse)
Rantes	5'- GGAATTCCTGCCGCGGGTACCATGAAG -3' (forward) 5'- CATGCCATGGTACAGGGTCAGAATCAAG -3' (reverse)
β-Actin	5'- GCTGTGCTGTCCCTGTATGCCTCT -3' (forward) 5'- CTTCTCAGCTGTGGTGGTGAAGC -3' (reverse)

Table 5 Primer sequences for target genes.

Elevated Plus Maze Test (EPMT)

EPMT is one of the most common behavioral tests to determine anxiety-like symptoms in rodents. This test is based upon an intricate balance between two main characteristics of mice behavior, their natural aversion for open and elevated spaces and preference for dark and enclosed spaces, and their inherent curiosity for exploring novel environments.

We followed the standard protocol from Komada et al. [90] with few modifications. The elevated plus maze was made of black Plexiglass. It consisted of two perpendicularly placed open (25 x 5 x 0.5 cm^3) and closed (25 x 5 x 16 cm^3) arms, with a platform (5 x 5 x 0.5 cm^3) at the intersection of the arms. The maze was kept elevated at a height of 50 cm above the floor. EPMT was conducted at one-month p.i. in an isolated room with dim lightings to minimize environmental distractions. Prior to testing, mice were acclimated to the room for 30 min. The test does not require former training. Experiments were performed during the day between 8:00 AM and 6:00 PM.

To test for anxiety, each mouse (n=3-4/control group and n=5/infected group) was individually placed at the central platform with its head facing the same closed arm. Mice were given 5 min of test period to freely explore the maze. During this period, the number of entries in open and closed arms, and % time spent in open arms were recorded for each mouse. An arm entry was defined as the placement of all four paws of the mouse in that arm of the maze. The time spent on the central platform was included with the time spent in the closed arms. The percentage (%) of time spent in open arms was calculated as [(time spent in open arms/total test time) x 100]. The number of entries and % time spent in open arms were used as a measure of anxiety-like behavior. The number of closed arm entries was used to determine locomotor activity. The maze was cleaned with 70% (vol/vol) ethanol between the tests to remove any feces, urine or animal odor.

Statistical analysis

qRT-PCR results were analyzed using the two-way analysis of variance (ANOVA) with the Tukey's multiple comparisons test or unpaired t-test with the Welch's correction. For rest of the parametric analysis, one-way ANOVA with the Tukey's multiple comparisons test or the unpaired t-test with the Welch's correction was used. For non-parametric analysis, the unpaired Mann-Whitney rank sum test was used. For nominal data (presence or absence of seizures), the Fisher's exact test was used. For all cases, significance was determined when $p \leq 0.05$. Statistical analysis was done using GraphPad Prism version 6.0d (Mac OS X, GraphPad Software, La Jolla, CA).

Results

TMEV-induced acute seizures were significantly reduced due to Nlrc5 deficiency. During the acute phase, mice were monitored for seizures twice a day until day 6 p.i. and once on day 7 p.i. The results from daily examination of mice showed that approximately 75% (28/37) of mice seized in the wild type infected group, while only 30% (9/30) of mice seized in the *Nlrc5*$^{-/-}$ infected group (Figure 17A) (Fisher's exact test, $p<0.0001$). As expected, no seizures were found in any of the control groups.

Mice in the wild type infected group had seizures beginning on day 2 until day 6 p.i., with highest seizures recorded on day 3 p.i. Mice in the *Nlrc5*$^{-/-}$ infected group had a slight delay in seizure occurrence, as seizures in this group started on day 3 p.i. The daily

phenotypic comparison between the infected groups showed that significantly fewer mice seized in the *Nlrc5*$^{-/-}$ group than in the wild type group on days 2, 3, 4 and 5 p.i. The *Nlrc5*$^{-/-}$ infected mice showed an unexpected increase in seizures on day 6 p.i., nevertheless, the % seized mice were not significantly different between the infected groups (Figure 17B) (Fisher's exact test, $p=0.0140$ on day 2 p.i., $p<0.0001$ on day 3 p.i., $p=0.0052$ on day 4 p.i., $p=0.0447$ on days 5 p.i., and $p=0.4570$ on day 6 p.i.).

We also found that most seized mice, whether in the wild type or the *Nlrc5*$^{-/-}$ infected groups, developed tonic-clonic seizures, and so attained the highest Racine score (Figure 17C and D). Moreover, the seizure frequency (total number of seizures/mouse) (Unpaired t test with Welch's correction, $p=0.3817$) and duration of seizure (Unpaired t test with Welch's correction, $p=0.7227$ on day 3 p.i., $p=0.7091$ on day 5 p.i., $p=0.5923$ on day 6 p.i.) were not significantly different between the seized mice from the wild type and *Nlrc5*$^{-/-}$ infected groups (Figure 17E and F). During weekly examinations of mice during the chronic phase (day 8 till 52 p.i.), we did not observe seizures in any of the infected groups.

Thus, we found that knocking out *Nlrc5* gene significantly reduced the number of seized mice and delayed seizure occurrence following TMEV infection. Although, the affected mice from wild type and *Nlrc5*$^{-/-}$ infected groups did not show any differences in seizure intensity. Taken together our results show a critical role of *Nlrc5* gene in TMEV-induced seizures.

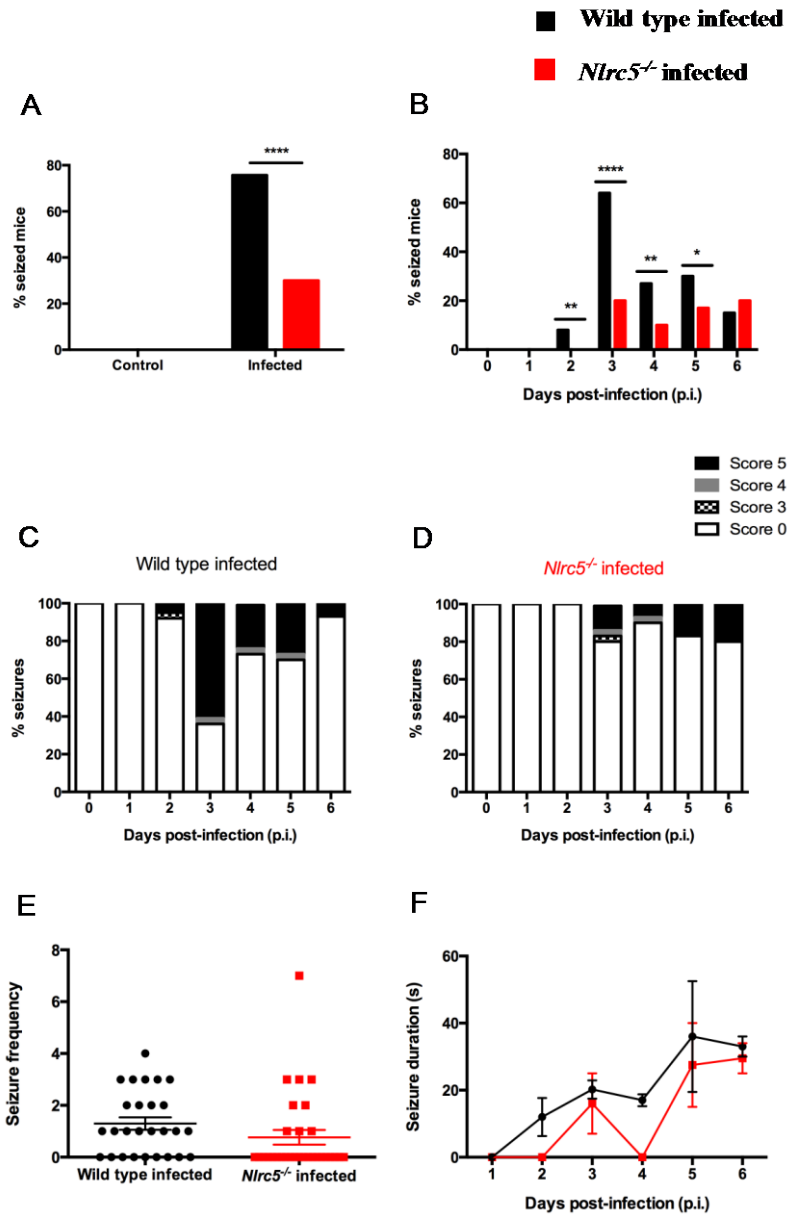

Figure 17 TMEV-induced acute seizures were significantly reduced due to Nlrc5 deficiency. (A) Acute phase results revealed a significant decrease in the proportion of *Nlrc5*$^{-/-}$ infected mice with seizures in comparison to wild type infected mice. The % seized mice in each group was calculated as (number of seized mice/total number of infected mice) x 100. No seizures were observed in the control groups. (B) Daily examinations of mice showed that *Nlrc5*$^{-/-}$ infected group had significantly fewer seizures than wild type infected group from days 2-5 p.i. The % seized mice per day was calculated as (number of seized mice in a day /total number of infected mice) x 100. (C and D) In both the infected groups, seizures were mostly of highest intensity, i.e. stage 5, while few mice had seizures of stage 3 and 4 on the Racine scale. (**** $p<0.0001$, ** $p<0.01$, * $p<0.05$ by Fisher's exact test). Graphs (A, B, C, D and E) show pooled results from six separate experiments expressed as percent or mean ± SEM, N=4 per control group and N=30-37 per infected group. Graph F shows pooled results from three separate experiments expressed as mean ± SEM, N=12 in wild type infected group and N=3 in *Nlrc5*$^{-/-}$ infected group.

Knocking out Nlrc5 gene alleviates non-epileptic clinical disease following TMEV infection.

Apart from seizures, mice were monitored for clinical signs of acute sickness, including ruffling, hunched back, and ataxia. Daily examination of mice showed that TMEV infection led to acute illness in mice. However, the mice deficient of *Nlrc5* gene exhibited lower clinical scores than the wild type mice in the acute phase. Significant differences were seen between the wild type and *Nlrc5*$^{-/-}$ infected groups on days 1, 2, 3, and 4 p.i. (Figure 18) (Mann-Whitney rank sum test, p=0.0324 on day 1 p.i., p=0.0009 on day 2 p.i., p=0.0002 on day 3 p.i., p=0.0347 on day 4 p.i., p=0.1976 on days 5 p.i., and p=0.1542 on day 6 p.i.). We did not find any sickness behavior among the control mice following PBS injection (data not shown).

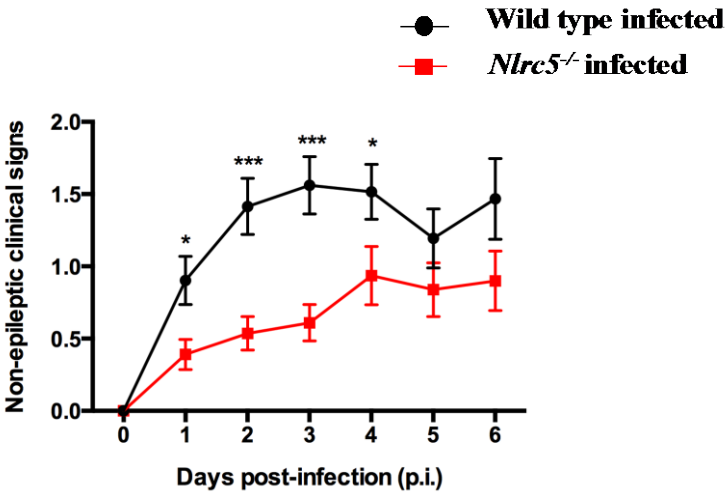

Figure 18 Knocking out *Nlrc5* gene alleviates non-epileptic clinical disease following TMEV infection. Mice were observed daily for signs of non-epileptic clinical disease during the acute phase. Both the wild type and *Nlrc5*$^{-/-}$ infected groups showed clinical signs of illness, but clinical scores were significantly lower in *Nlrc5*$^{-/-}$ infected group compared to that in wild type infected group (* $p<0.05$, *** $p<0.001$ by Mann-Whitney rank sum test). Graph shows pooled results from six separate experiments expressed as mean ± SEM, N=30-41 per infected group.

The Nlrc5 gene had a significant effect on body weight following infection.

In comparison to controls, we observed significant weight loss among TMEV-infected mice in both the wild type and *Nlrc5*$^{-/-}$ groups during the acute phase (wild type control vs. *Nlrc5*$^{-/-}$ control: Unpaired t test with Welch's correction, p=0.1674 on day 1 p.i., p=0.1450 on day 2 p.i., p=0.2523 on day 3 p.i., p=0.2693 on day 4 p.i., p=0.1902 on day 5 p.i., p=0.1194 on day 6 p.i.), (wild type control vs. wild type infected: Unpaired t test with Welch's correction, p<0.0001 from days 1 to 6 p.i.), (*Nlrc5*$^{-/-}$control vs. *Nlrc5*$^{-/-}$ infected: Unpaired t test with Welch's correction, p=0.0002 on day 1 p.i., p=0.0008 on day 2 p.i., p=0.0051 on day 3 p.i., p=0.0211 on day 4 p.i., p=0.0109 on day 5 p.i., p=0.0058 on day 6 p.i.). However, upon comparing the infected groups, *Nlrc5*$^{-/-}$ mice had significantly lower weight loss than the wild type mice on days 1, 2 and 3 p.i. (Figure 19) (Wild type infected vs. *Nlrc5*$^{-/-}$ infected: Unpaired t test with Welch's correction, p=0.0046 on day 1 p.i., p=0.0024 on day 2 p.i., p=0.0222 on day 3 p.i., p=0.9539 on day 4 p.i., p=0.8741 on day 5 p.i., p=0.8134 on day 6 p.i.). Hence, *Nlrc5* deficiency significantly reduced the extent of weight loss in TMEV-induced seizure model. Notably, the time-points for differences in weight loss correspond with the time-points for differences in seizure phenotype between the infected groups.

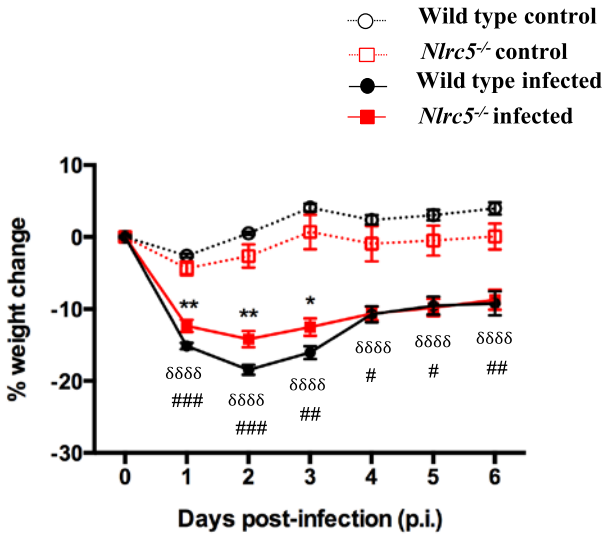

Figure 19 The *Nlrc5* gene had a significant effect on mice weights following infection. To determine recovery post infection, mice from the control and infected groups were weighed daily until day 6 p.i. Both the infected groups exhibited significant weight loss immediately following TMEV infection in comparison to their respective controls. However, the body weight comparisons between the infected groups showed that *Nlrc5*$^{-/-}$ mice weighed significantly more than the wild type mice at earlier time-points, indicating better recovery among *Nlrc5*$^{-/-}$ infected mice. (Between wild type control and infected groups: δδδδ $p<0.0001$; between *Nlrc5*$^{-/-}$ control and infected groups: $^{\#}p<0.05$, $^{\#\#}p<0.01$, $^{\#\#\#}p<0.001$; between wild type and *Nlrc5*$^{-/-}$ infected groups: * $p<0.05$, ** $p<0.01$ by Unpaired t test with Welch's correction). Graph shows pooled results from five separate experiments, expressed as mean ± SEM, N=4/control group and N=26/infected group.

The Nlrc5 gene had variable effects on different leukocyte populations in the brain and CLNs.

Since day 3 p.i. was the peak time for seizures, we chose this time-point to analyze different leukocyte populations in the brain and CLNs from infected mice. The results from the brains showed increased expression levels of innate immune cells compared to that of adaptive immune cells on day 3 p.i. Upon comparing the infected groups, we found a significant reduction in the expression levels of CD45.2 high(hi) NK1.1+ cells (natural killer [NK] cells), and a mild reduction in the expression of CD45.2 high CD11c+ cells (dendritic cells) in the *Nlrc5*$^{-/-}$ group compared to the wild type group.

However, we found an increasing, but insignificant trend in the expression levels of CD45.2 high CD11b+ cells (monocytes, macrophages, granulocytes, etc.) and CD45.2 high Gr1+ cells (granulocytes) in the *Nlrc5*$^{-/-}$ infected mice when compared with the wild type infected mice (Figure 20A). (Unpaired t test with Welch's correction, p=0.7153 for CD45.2 int CD11b+ cells, p=0.1206 for CD45.2 hi CD11b+ cells, p=0.1217 for CD45.2 hi Gr1+ cells, p=0.0144 for CD45.2 hi NK1.1+ cells, p=0.0649 for CD45.2 hi CD11c+ cells, p=0.6060 for CD45.2 hi CD8+ cells, p=0.4127 for CD45.2 hi CD4+ cells, and p=0.4912 for CD45.2 hi B220+ cells).

Previous studies have reported that *Nlrc5* deficient mice exhibit impaired in the activation of cytotoxic T cells upon intracellular bacterial infection [49,50], therefore we next analyzed the cytotoxic and helper T cells for their activation levels. Our results showed that there was a slight decrease in the levels of CD45.2 high CD4+ CD69+ cells (activated helper T cells) in the brains of *Nlrc5*$^{-/-}$ infected mice when compared with the wild type infected mice (Figure 20B), while the deficiency of *Nlrc5* gene did not affect the expression of CD45.2 intermediate(int) CD11b+ CD80+ cells (activated microglia) and CD45.2 high CD11b+ CD80+ cells (activated monocytes, macrophages, granulocytes, etc.) (Figure 20C). (Unpaired t test with Welch's correction, p=0.2047 for CD45.2 hi CD8+ CD69+ cells, p=0.0556 for CD45.2 hi CD4+ CD69+ cells, p=0.7486 for CD45.2 int CD11b+ CD80+ cells, and p=0.1428 for CD45.2 hi CD11b+ CD80+ cells). This suggests that *Nlrc5* gene has variable effects on the leukocyte populations in the brain.

In contrast to the leukocyte profile in the brain, we did not find any significant differences in the expression levels of leukocyte populations in the CLNs of *Nlrc5*$^{-/-}$ infected mice than wild type infected mice (Figure 20D and E) (Unpaired t test with Welch's correction, p=0.1206 for CD45.2 hi CD11b+ cells, p=0.6165 for CD45.2 hi Gr1+ cells, p=0.9743 for CD45.2 hi NK1.1+ cells, p=0.1159 for CD45.2 hi CD11c+ cells, p=0.0766 for CD45.2 hi CD8+ cells, p=0.2768 for CD45.2 hi CD4+ cells, p=0.5746 for CD45.2 hi B220+ cells, p=0.4708 for CD45.2 hi CD8+ CD69+ cells, and p=0.5756 for CD45.2 hi CD4+ CD69+ cells).

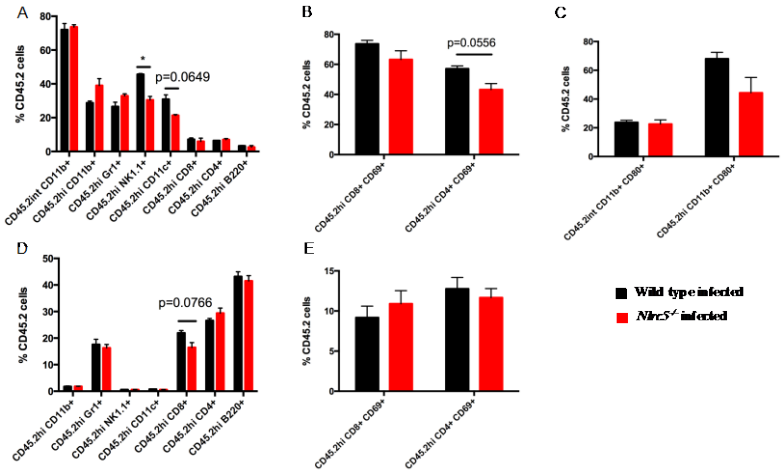

Figure 20 The *Nlrc5* gene had variable effects on different leukocyte populations in the brain and CLNs. To examine the extent of inflammation at the time of peak seizures, we analyzed the expression of leukocyte subsets in the brain and CLNs at day 3 p.i. In the brain, the deficiency of *Nlrc5* gene caused a significant reduction in the expression of CD45.2hi NK1.1+ (NK) cells, and mild reduction in the expression of CD45.2hi CD11c+ cells (dendritic cells) and CD45.2hi CD4+ CD69+ cells (activated T helper cells), while it led to a slight increase in the expression of CD45.2hi CD11b+ cells (monocytes/macrophages, granulocytes, etc.) and CD45.2hi Gr1+ cells (granulocytes). In the CLNs, the deficiency of *Nlrc5* gene only mildly downregulated the expression of CD45.2hi CD8+ cells (cytotoxic T cells). (* p<0.05 by Unpaired t test with Welch's correction). Graphs (A-E) show results expressed as mean ± SEM, N=3 per infected group.

Nlrc5 deficiency induced a significant reduction in the number of GFAP+ cells, but not IBA+ cells, following infection.

Acute immune response comprises of the activation and proliferation of both resident and infiltrated immune cells. Here, we enumerated the infiltrated and resident IBA+ cells (macrophage/microglia) and GFAP+ cells (astrocytes) in different regions of the hippocampus among the infected groups.

On day 7 p.i., we found activated astrocytes in the hippocampus of both infected groups, but the number of astrocytes was significantly decreased in the hippocampus from the *Nlrc5*$^{-/-}$ infected group compared to the wild type infected group. The proliferation of astrocytes was found to be region-specific, with significant differences recorded at CA1 and dentate gyrus regions of the hippocampus (Figure 21A-G) (Unpaired t test with Welch's correction, p=0.0065 for total cells, p=0.0245 for cells at CA1, p=0.3719 for cells at CA3, and p=0.0001 for cells at dentate gyrus [DG]). Moreover, we found an increase in the number of macrophages and microglia in the hippocampus from both infected groups. The activated cells adopted varying morphologies, such as rod-shape, and amoeboid-like shape. Within the hippocampus, the highest number of cells were found in the CA1 region and near the CA1-CA3 junction, while the dentate gyrus had least number of cells in both infected groups. However, the number of macrophages and microglia was not significantly different between infected groups (Figure 21H-N) (Unpaired t test with Welch's correction, p=0.3638 for total cells, p=0.2941 for cells at CA1, p=0.6764 for cells at CA3, and p=0.6225 for cells at dentate gyrus [DG]). Taken

together our results show that *Nlrc5* gene is a positive regulator of the activation and proliferation of astrocytes, while it may not have a critical role in macrophage and microglial proliferation at least on day 7 p.i.

In addition, we found TMEV-antigen positive cells in the hippocampus of both the infected groups at day 7 p.i. The virus mostly infected the CA1 and CA2 pyramidal neurons, while CA3 and dentate gyrus neurons were found uninfected (Figure 21O and P). This suggests that *Nlrc5* deficiency had no effect on viral replication during the acute phase of infection.

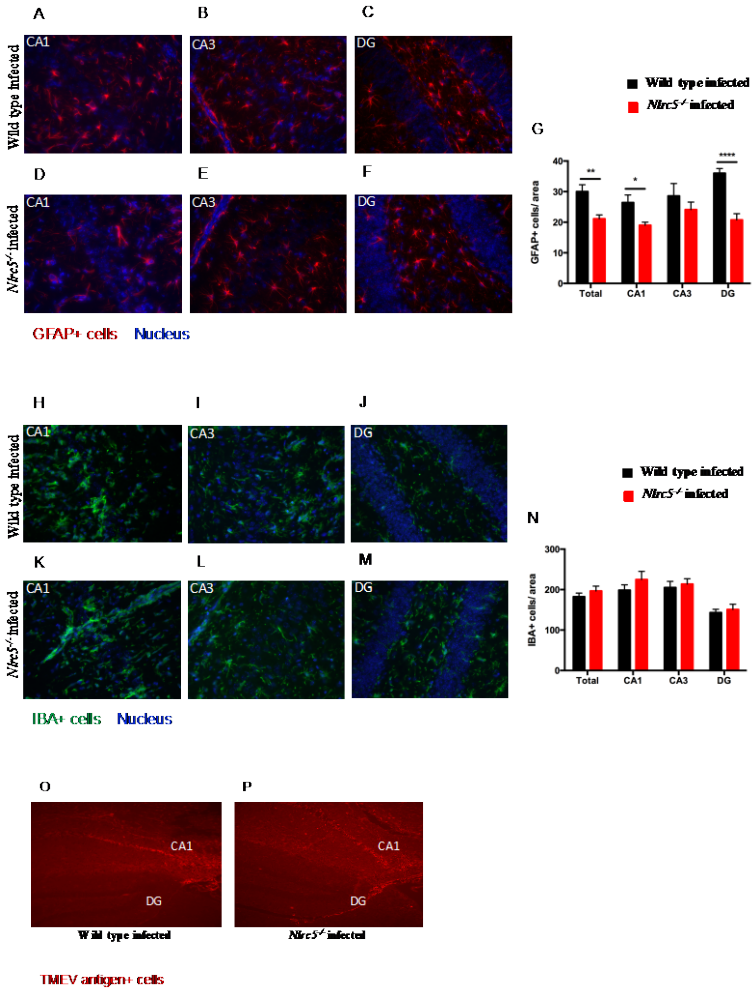

Figure 21 Nlrc5 deficiency induced a significant reduction in the number of GFAP+ cells, but not IBA+ cells, following infection. To assess the effect of Nlrc5 deficiency on the proliferation and activation of astrocytes, microglia/macrophages, and virus-infected cells in the hippocampus, we stained 10 µm coronal sections of fixed brain with antibody against GFAP, IBA, and TMEV-antigen, respectively. (A-F) are the representative images (400x) of CA1, CA3, and DG regions of hippocampus showing GFAP+ astrocytes. (G) The number of astrocytes was significantly reduced in the hippocampus, specifically in the CA1 and dentate gyrus regions, of *Nlrc5*$^{-/-}$ infected mice than wild type infected mice. (H-M) are the representative images (400x) of CA1, CA3, and DG regions of hippocampus showing IBA+ macrophages/microglia. (N) The infected groups had no significant differences in the number of macrophages and microglia in the hippocampus. (O and P) are the representative images (100x) from infected groups showing that TMEV-antigen positive cells were mainly localized in the CA1 and CA2 pyramidal neurons, while TMEV-antigen was not detected in the DG and CA3 neurons. (* $p<0.05$, ** $p<0.01$, **** $p<0.0001$ by Unpaired t test with Welch's correction). Graphs (G and N) show results expressed as mean ± SEM, N=7-9 per infected group. Cornu ammonis1 (CA1), cornu ammonis2 (CA2), and dentate gyrus (DG).

Nlrc5 deficiency mitigates hippocampal damage in TMEV-induced seizure model.

At day 7 p.i., we found marked inflammation near the hippocampal fissure, and neuronal damage in the CA1 region of hippocampus for both infected groups. Our preliminary data, showed a decrease in the extent of neuronal damage at CA1 region in *Nlrc5*$^{-/-}$ infected mice when compared to wild type infected mice. This suggests a detrimental role of *Nlrc5* gene in TMEV-induced seizure model (Figure 22A-C).

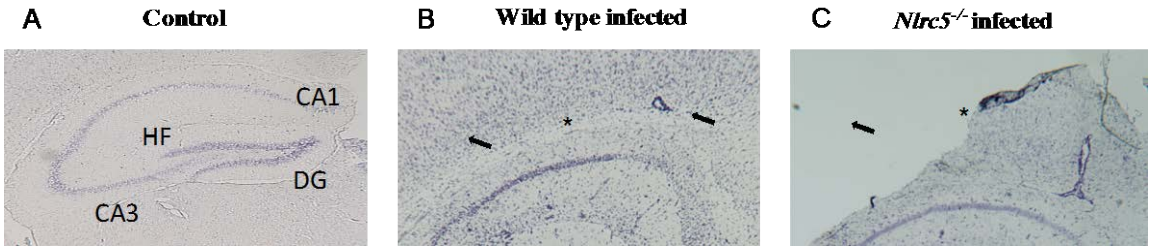

Figure 22 Nlrc5 deficiency mitigates hippocampal damage in TMEV-induced seizure model. To determine the effect of Nlrc5 on the extent of inflammation and damage in the hippocampus following infection, we compared the cresyl violet-stained 10 μm coronal sections of fixed brain. (A-C) are the representative images (20x) from wild type control, wild type infected and *Nlrc5*$^{-/-}$ infected group, respectively. The preliminary results indicate that TMEV-infection induced CA1 neuronal damage was less severe in *Nlrc5*$^{-/-}$ than that in wild type infected mice. Cornu ammonis1 (CA1), cornu ammonis2 (CA2), dentate gyrus (DG), and hippocampal fissure (HF).

Knocking out Nlrc5 gene did not alter the resistance to TMEV-induced demyelinating disease.

SJL mice are susceptible to TMEV-induced demyelinating disease and develop white matter lesions in their spinal cord within a month or two p.i. [31,42]. In contrast to SJL mice, none of the infected C57BL/6 and *Nlrc5*$^{-/-}$ mice in the current study exhibited meningitis, inflammatory foci, or demyelinating lesions in their spinal cords. Our results indicate that the impairment of Nlrc5-mediated MHC class I expression does not affect

the resistance of C57BL/6 mouse strain to TMEV-induced demyelinating disease (Figure 23A-D).

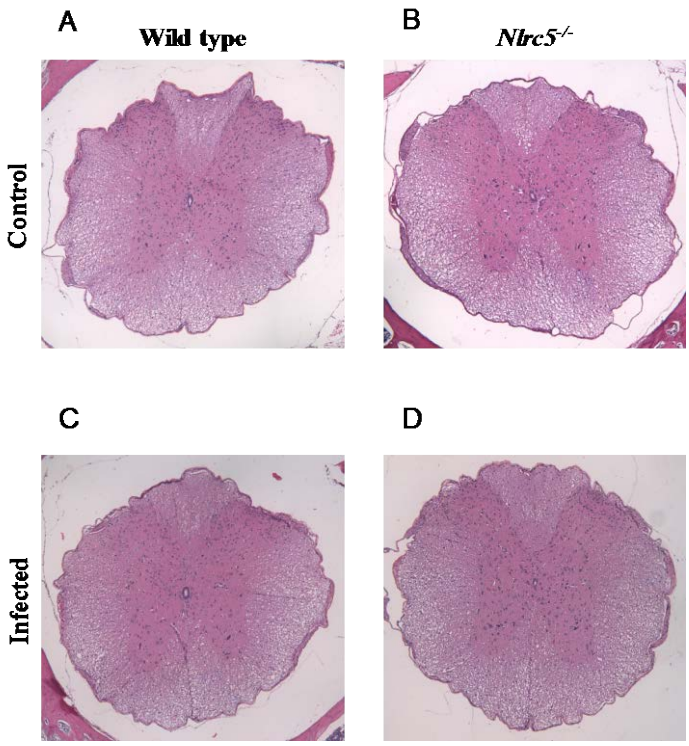

Figure 23 Knocking out *Nlrc5* gene did not alter the resistance to TMEV-induced demyelinating disease. To investigate whether Nlrc5 gene affects the resistance of C57BL/6 mice to TMEV-induced demyelinating disease, we compared the H&E-stained four μm transverse sections from cervical, thoracic, lumbar and sacral segments of spinal cords from infected mice and compared the histological condition with their respective controls. At day 52 p.i., we did not find active inflammation or demyelinating lesions in the spinal cords from any of the infected mice. (A-D) are the representative images (100x) from thoracic segment of the spinal cord from wild type control, *Nlrc5*$^{-/-}$ control, wild type infected and *Nlrc5*$^{-/-}$ infected groups.

Expression of target genes in the brain following TMEV infection:

a) TMEV-infected wild type mice showed an increase in the mRNA expression of Nlrc5.

It has been established previously that *Nlrc5*$^{-/-}$ mice exhibit significantly lower or minimal levels for Nlrc5 mRNA in splenocytes in response to intracellular infection [49]. Here, we found baseline expression of *Nlrc5* gene in the brains of wild type control mice, while there was a significant increase in the expression of *Nlrc5* gene in wild type infected mice at day 7 p.i., implying that TMEV infection effectively upregulates *Nlrc5* gene expression in the brain (Figure 24A) (Unpaired t test with Welch's correction, p=0.0036).

b) Comparative expression of TMEV mRNA in the brain.

At day 7 p.i., we found a slight, but insignificant decrease in the *TMEV* mRNA expression in *Nlrc5*$^{-/-}$ infected mice than the wild type infected mice. This denotes that *Nlrc5* deficiency has no significant effect on viral replication at least during the acute phase (Figure 24B) (Unpaired t test with Welch's correction, p=0.4010).

c) Nlrc5 exclusively affects MHC Class I-antigen processing and presentation machinery in the brain.

As expected, virus infection significantly upregulated expression of MHC class I (*H2-Kb*) mRNA in the brains of wild type mice. However, *Nlrc5* deficiency abrogated this effect, as expression of *H2-Kb* was significantly lower in *Nlrc5*$^{-/-}$ infected mice

compared to wild type infected mice (Figure 24C). Similar findings were noted in β_2m and *Tap1* expression (Figure 24D and E). In case of the genes involved in MHC class II pathway, virus infection significantly upregulated the expression of MHC class II (*H2-Aa)* (Figure 24F) and MHC class II transactivator (*Ciita*) (Figure 24G) in both wild type and *Nlrc5*$^{-/-}$ mice. Our results corroborate past studies showing that NLRC5 upregulates the expression of MHC class I and its associated genes, and has no effect on the expression of MHC class II genes (*H2-Kb*: Two-way ANOVA with Tukey's multiple comparisons test, p>0.9999 for wild type control vs. *Nlrc5*$^{-/-}$ control, p<0.0001 for wild type control vs. wild type infected, p=0.7620 for *Nlrc5*$^{-/-}$ control vs. *Nlrc5*$^{-/-}$ infected, p<0.0001 for wild type infected vs. *Nlrc5*$^{-/-}$ infected) (β_2m: Two-way ANOVA with Tukey's multiple comparisons test, p>0.9999 for wild type control vs. *Nlrc5*$^{-/-}$ control, p<0.0001 for wild type control vs. wild type infected, p=0.0760 for *Nlrc5*$^{-/-}$ control vs. *Nlrc5*$^{-/-}$ infected, p=0.0004 for wild type infected vs. *Nlrc5*$^{-/-}$ infected) (*Tap1*: Two-way ANOVA with Tukey's multiple comparisons test, p>0.9999 for wild type control vs. *Nlrc5*$^{-/-}$ control, p=0.0031 for wild type control vs. wild type infected, p=0.6848 for *Nlrc5*$^{-/-}$ control vs. *Nlrc5*$^{-/-}$ infected, p=0.0446 for wild type infected vs. *Nlrc5*$^{-/-}$ infected) (*H2-Aa*: Two-way ANOVA with Tukey's multiple comparisons test, p>0.9999 for wild type control vs. *Nlrc5*$^{-/-}$ control, p=0.0106 for wild type control vs. wild type infected, p=0.0017 for *Nlrc5*$^{-/-}$ control vs. *Nlrc5*$^{-/-}$ infected, p=0.5935 for wild type infected vs. *Nlrc5*$^{-/-}$ infected) (*Ciita*: Two-way ANOVA with Tukey's multiple comparisons test, p=0.9664 for wild type control vs. *Nlrc5*$^{-/-}$ control, p=0.0025 for wild type control vs.

wild type infected, p=0.0112 for *Nlrc5*$^{-/-}$ control vs. *Nlrc5*$^{-/-}$ infected, p=0.8203 for wild type infected vs. *Nlrc5*$^{-/-}$ infected).

d) Virus-induced type I interferon expression was significantly reduced in the brains due to Nlrc5 deficiency.

Virus infection increased mRNA levels for *Ifn-β* in wild type mice, but significantly lower mRNA levels of it were evident in *Nlrc5*$^{-/-}$ mice (Figure 24H). In contrast, *Nlrc5* deficiency did not affect the virus-induced expression of type II interferon (*Ifn-γ*) (Figure 24I). (*Ifn-β*: Two-way ANOVA with Tukey's multiple comparisons test, p=0.9832 for wild type control vs. *Nlrc5*$^{-/-}$ control, p=0.0691 for wild type control vs. wild type infected, p=0.9758 for *Nlrc5*$^{-/-}$ control vs. *Nlrc5*$^{-/-}$ infected, p=0.0479 for wild type infected vs. *Nlrc5*$^{-/-}$ infected) (*Ifn-γ*: Unpaired t test with Welch's correction, p=0.3862 for wild type infected vs. *Nlrc5*$^{-/-}$ infected)

e) Nlrc5 deficiency resulted in a significant decrease in the inducible expression of pro-inflammatory mediators.

In wild type mice, virus infection induced a significant increase in the mRNA expression levels of pro-inflammatory cytokines, such as interleukin *(Il)-1β*, *Il-6* and tumor necrosis factor *(Tnf)-α*. In contrast, *Nlrc5* deficiency significantly abated the increase in the mRNA levels for *Il-1β*, and to an extent for *Il-6*, while *Tnf-α* expression remained unaffected among the infected mice (Figure 24J-L). The mRNA expression level for the anti-inflammatory cytokine, tumor growth factor *(Tgf)-β*, was only slightly elevated in

wild type mice, but it was significantly increased in *Nlrc5*$^{-/-}$ mice following infection (Figure 24M). In case of the chemokines, TMEV-infected wild type mice showed a significant increase in the mRNA levels for monocyte chemoattractant protein-1 (*Mcp-1*), and regulated upon activation, normally T-expressed, and presumably secreted (*Rantes*); and had very high expression levels for macrophage inflammatory protein 2 (*Mip-2*) following infection. *Nlrc5* deficiency showed no effect on the mRNA levels for *Rantes*, and only slighted decreased the expression of *Mcp-1* and *Mip-2* in the infected group (Figure 24N-P). In addition, the expression levels for inducible nitric oxide synthase (*iNOS*) mRNA levels were significantly increased with infection in wild type group, but lower levels were noted in *Nlrc5*$^{-/-}$ group (Figure 24Q). (*Il-1β*: Two-way ANOVA with Tukey's multiple comparisons test, p>0.9999 for wild type control vs. *Nlrc5*$^{-/-}$ control, p=0.0026 for wild type control vs. wild type infected, p=0.9122 for *Nlrc5*$^{-/-}$ control vs. *Nlrc5*$^{-/-}$ infected, p=0.0082 for wild type infected vs. *Nlrc5*$^{-/-}$ infected) (*Il-6*: Two-way ANOVA with Tukey's multiple comparisons test, p=0.9924 for wild type control vs. *Nlrc5*$^{-/-}$ control, p=0.0443 for wild type control vs. wild type infected, p=0.9365 for *Nlrc5*$^{-/-}$ control vs. *Nlrc5*$^{-/-}$ infected, p=0.1936 for wild type infected vs. *Nlrc5*$^{-/-}$ infected) (*Tnf-α*: Two-way ANOVA with Tukey's multiple comparisons test, p=0.9246 for wild type control vs. *Nlrc5*$^{-/-}$ control, p<0.0001 for wild type control vs. wild type infected, p=0.0006 for *Nlrc5*$^{-/-}$ control vs. *Nlrc5*$^{-/-}$ infected, p=0.3736 for wild type infected vs. *Nlrc5*$^{-/-}$ infected) (*Tgf-β*: Two-way ANOVA with Tukey's multiple comparisons test, p=0.9974 for wild type control vs. *Nlrc5*$^{-/-}$ control, p=0.0696 for wild type control vs. wild type infected, p=0.0024 for *Nlrc5*$^{-/-}$ control vs. *Nlrc5*$^{-/-}$ infected,

p=0.1480 for wild type infected vs. *Nlrc5*$^{-/-}$ infected) (*Mcp-1*: Two-way ANOVA with Tukey's multiple comparisons test, p>0.9999 for wild type control vs. *Nlrc5*$^{-/-}$ control, p=0.0188 for wild type control vs. wild type infected, p=0.7924 for *Nlrc5*$^{-/-}$ control vs. *Nlrc5*$^{-/-}$ infected, p=0.1143 for wild type infected vs. *Nlrc5*$^{-/-}$ infected) (*Rantes*: Two-way ANOVA with Tukey's multiple comparisons test, p>0.9999 for wild type control vs. *Nlrc5*$^{-/-}$ control, p=0.0003 for wild type control vs. wild type infected, p=0.0009 for *Nlrc5*$^{-/-}$ control vs. *Nlrc5*$^{-/-}$ infected, p=0.9998 for wild type infected vs. *Nlrc5*$^{-/-}$ infected) (*Mip-2*: Two-way ANOVA with Tukey's multiple comparisons test, p>0.9999 for wild type control vs. *Nlrc5*$^{-/-}$ control, p=0.1626 for wild type control vs. wild type infected, p>0.9999 for *Nlrc5*$^{-/-}$ control vs. *Nlrc5*$^{-/-}$ infected, p=0.1651for wild type infected vs. *Nlrc5*$^{-/-}$ infected) (*iNos*: Two-way ANOVA with Tukey's multiple comparisons test, p=0.9895 for wild type control vs. *Nlrc5*$^{-/-}$ control, p=0.0054 for wild type control vs. wild type infected, p=0.1346 for *Nlrc5*$^{-/-}$ control vs. *Nlrc5*$^{-/-}$ infected, p=0.4004 for wild type infected vs. *Nlrc5*$^{-/-}$ infected).

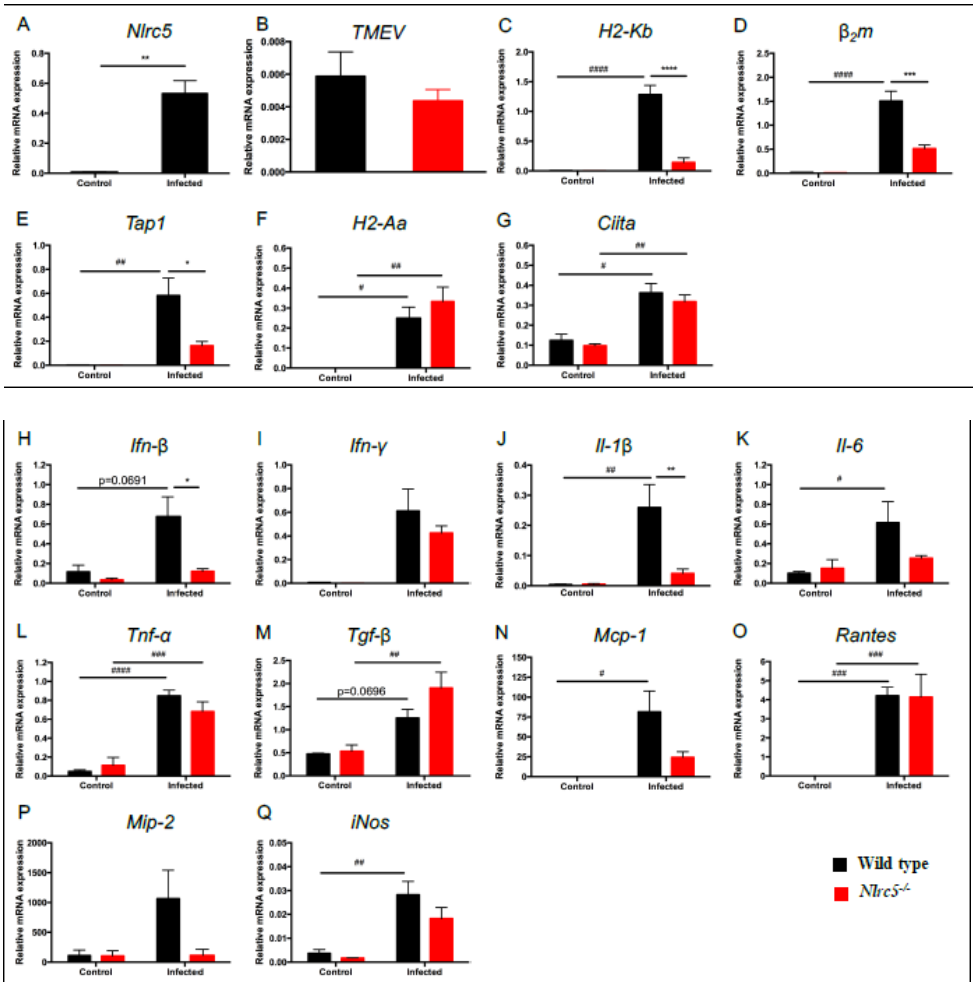

Figure 24 Expression of target genes in the brain following TMEV infection: To assess the effects of Nlrc5 deficiency on the expression of virus and inflammatory mediators, we compared the mRNA levels of target genes from the brains of infected mice at day 7 p.i. The comparisons between control and infected groups, and between wild type and *Nlrc5*$^{-/-}$ infected groups showed that (A) TMEV infection caused a significant increase in the expression of *Nlrc5* in wild type mice. (B) The mRNA levels for virus were similar between the infected groups. (C-E) Nlrc5 deficiency caused a significant reduction in the expression of MHC class I and its associated genes, (F-G) while it did not affect the expression of MHC class II and its related genes following TMEV infection. Nlrc5 deficiency significantly downregulated the expression of pro-inflammatory cytokines, (H) *Ifn-β*, (J) *Ifn-β*, but had minimal or no effects on the expression of (I) *Ifn-γ*, (K) *Il-6*, and (L) *Tnf-α*. (M) The expression of anti-inflammatory cytokine, *Tgf-β* was only mildly increased in wild type infected mice, but Nlrc5 deficiency significantly upregulated its expression following infection. The mRNA levels of chemokines, (N) *Mcp-1*, (O) *Rantes*, and (P) *Mip-2*, were highly upregulated in wild type infected mice, but Nlrc5 deficiency only slightly decreased the expression of *Mcp-1* and *Mip-2* following infection. (Q) When compared to the controls, the expression of *iNos* was significantly increased in wild type infected mice, but not in *Nlrc5*$^{-/-}$ infected mice. (Between control and infected groups: $^{\#}$ p<0.05, $^{\#\#}$ p<0.01, $^{\#\#\#}$ p<0.001, $^{\#\#\#\#}$ p<0.0001; between wild type and *Nlrc5*$^{-/-}$ infected groups: * p<0.05, ** p<0.01, *** p<0.001, **** p<0.0001 by Unpaired t test with Welch's correction or Two-way ANOVA with Tukey's multiple comparisons test). Graphs (A-Q) show results expressed as mean ± SEM, n=1-4/control group and n=3-5/infected group.

Mice did not exhibit anxiety-like symptoms following infection.

We did not find any significant differences in the number of entries in open and closed arms, and % time spent in open arms between the control and infected groups or between the wild type and *Nlrc5*$^{-/-}$ infected groups (Number of entries in open arms: One-way ANOVA with Tukey's multiple comparison test, p=0.9569 for wild type control vs. *Nlrc5*$^{-/-}$ control, p=0.6622 for wild type control vs. wild type infected, p=0.9854 for *Nlrc5*$^{-/-}$ control vs. *Nlrc5*$^{-/-}$ infected, p=0.4223 for wild type infected vs. *Nlrc5*$^{-/-}$ infected) (Number of entries in closed arms: One-way ANOVA with Tukey's multiple comparison test, p=0.4609 for wild type control vs. *Nlrc5*$^{-/-}$ control, p=0.9955 for wild type control vs. wild type infected, p=0.5544 for *Nlrc5*$^{-/-}$ control vs. *Nlrc5*$^{-/-}$ infected, p=0.9991 for wild type infected vs. *Nlrc5*$^{-/-}$ infected) (% time spent in open arms: One-way ANOVA with Tukey's multiple comparison test, p=0.8342 for wild type control vs. *Nlrc5*$^{-/-}$ control, p=0.8231 for wild type control vs. wild type infected, p=0.9926 for *Nlrc5*$^{-/-}$ control vs. *Nlrc5*$^{-/-}$ infected, p=0.3508 for wild type infected vs. *Nlrc5*$^{-/-}$ infected). However, one of the wild type infected mice explored the open arms more than the other mice, suggesting the development of aberrant emotional behavior (Figure 25A-C).

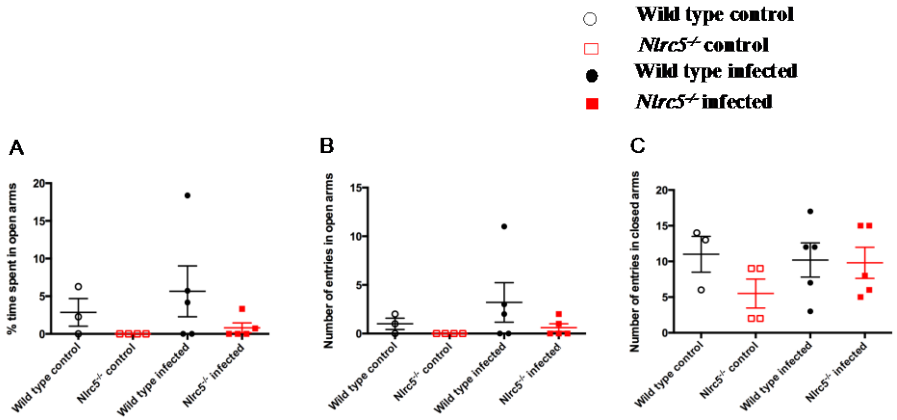

Figure 25 Mice did not exhibit anxiety-like symptoms following infection. To determine the effects of neuronal damage and *Nlrc5* gene on the development of anxiety-like symptoms in mice, we conducted EPMT at one-month p.i. (A) % time spent in open arms, (B) number of entries in open arms, and (C) number of entries in closed were similar among the groups, suggesting that the infected mice did not show any behavioral or locomotor abnormality, with the exception of one wild type infected mouse. The % time spent in open arms was calculated as (time spent in open arms/time spent in open and closed arms) x 100. The number of entries in open and closed arms was recorded manually at the time of the experiment. (One-way ANOVA with Tukey's multiple comparisons test). Graphs (A-C) show results expressed as mean ± SEM, N=3-4 per control group and N=5 per infected group.

Discussion

NLRC5 is a unique member of the NLR family, as it has the ability to shuttle between the cytoplasm and nucleus in a cell. The expression of NLRC5 varies based upon the tissue, cell type, and inflammatory condition [54]. It is highly expressed by immune-related tissues, such as spleen, thymus, lymph nodes, bone marrow, and tonsils; and immune cells, such as T cells, B cells, monocytes/ macrophages, and dendritic cells [54,137,141]. Its expression has also been reported in brain [52,55] and more specifically in cells that form the blood-brain barrier, such as pericytes [142], and cerebral endothelial cells (CECs) [143]. Moreover, it can be induced in response to various PAMPs, such as type I IFN (IFN-β) and type II IFN (IFN-γ) [45,55,137], lipopolysaccharide (LPS) [56,58,137],

polyinosinic:polycytidylic (poly [I:C]) [54,56,58,137], viruses (Newcastle disease virus [NDV] [58], respiratory syncytial virus [RSV] [144], vesicular stomatitis virus [VSV] [57], human rhinovirus [HRV] [138], etc.), and bacteria (*Listeria monocytogenes* [49,50,58]).

NLRC5 is a well-known transactivator of MHC class I and its associated genes, while it has been shown to have no effect on the transcription of MHC class II genes. The NLRC5-dependent MHC class I expression is more pronounced in T cells, NK cells and Natural Killer T (NKT) cells than in B cells, macrophages, and dendritic cells (antigen presenting cells) [49,51,57,141]. Since MHC class I presenting cytosolic peptide complex is essential for the activation of cytotoxic T cells, previous studies have shown that NLRC5, in extension, can also regulate the activation, proliferation and cytotoxicity of cytotoxic T cells in response to *Listeria monocytogenes* infection [49,50].

In addition, the function of NLRC5 in anti-viral immunity has been extensively studied in *in vitro* and *ex vivo* systems. The activated NLRC5 may respond to viral infection by regulating the expression of signaling pathways (NF-κB-, IFN-dependent pathways) [55,56,58], by interacting with other PRRs (such as retinoic acid inducible gene I [RIG-I] [144], NLRP3 [59,138]) , and/or by forming multi-protein complex called inflammasome [59,138]. Nonetheless, these studies have failed to reach a consensus regarding the positive, negative, or dispensable effects of NLRC5 in viral-induced inflammation. The conflicting results from previous studies are suggested to be a result of the use of different cell lines, variable expression levels of NLRC5 in different cell types, cell type-

specific signaling pathways, different treatments, and/or different *Nlrc5* gene deletion strategies.

To resolve the discrepancies about the role of NLRC5 in viral infection and to delineate its effect in epilepsy, we infected *Nlrc5*$^{-/-}$ mice with TMEV and compared the disease pathogenesis with wild type mice *in vivo*. Our acute phase results showed that *Nlrc5* ablation significantly decreased seizures, non-epileptic clinical disease, weight loss, and reduced the extent of hippocampal damage among the infected mice. In accordance with earlier studies [41], we found that TMEV infection significantly upregulates MHC class I expression in the brains of wild type mice. In contrast to wild type, *Nlrc5*$^{-/-}$ infected mice had significant reduction in the inducible expression of MHC class I, $\beta_2 m$ and *Tap1*. Past studies show that $\beta_2 m$ deficiency results in impaired MHC class-I-mediated cytotoxic T cell responses upon TMEV infection. $\beta_2 m$ deficient mice (on predominantly C57BL/6 background) develop demyelinating lesions in spinal cords and show compensatory increase in T helper cell-mediated viral clearance, however they do not exhibit clinical signs of demyelinating disease (waddling gait, spastic paralysis) [42]. This is partly in agreement with our study, where infected *Nlrc5* deficient mice, with impaired expression of MHC class I and $\beta_2 m$, neither presented clinical signs of demyelinating disease nor developed demyelinating lesions in spinal cord.

We also documented a significant but variable effect of *Nlrc5* deficiency on the expression of different immune cells in the brain and CLNs following infection. In the

brain, *Nlrc5* deficiency induced a significant decrease in CD45.2 high NK1.1+ cells (NK cells), and mild increase in CD45.2hi CD11c+ cells, while it led to no significant changes in CD45.2 high CD11b+ cells (monocytes, macrophages, granulocytes, etc.) and CD45.2 high Gr1+ cells (granulocytes) expression levels. In the CLNs, *Nlrc5* deficiency induced a mild decrease in CD45.2 high CD8+ cells (cytotoxic T cells). Furthermore, we found significantly reduced astrocyte numbers in the hippocampus of *Nlrc5*$^{-/-}$ infected mice than that in wild type infected mice. The Nlrc5-mediated differences in TMEV-induced activation of immune cell types may be due to differential expression of Nlrc5 in different cell types, or cell type-specific regulatory effects of Nlrc5.

The gene expression studies revealed that TMEV infection could effectively induce *Nlrc5* expression *in vivo*. Besides, we found that *Nlrc5* deficiency significantly downregulated the expression levels for *Ifn-β*, and *Il-β*; but had minimal or no effect on the expression levels for *Ifn-γ*, *Il-6*, *Tnf-α*, *Mcp-1*, *Mip-2*, *Rantes*, and *iNOS* upon TMEV infection. The gene expression studies were conducted at day 7 p.i. (the time-point when seizures generally cease), so future studies from day 3 p.i. (peak time for seizures) would better depict the contribution of pro-inflammatory mediators in TMEV-induced seizures. Nevertheless, we saw a significant role of Nlrc5 as the positive regulator of IFN-β and IL-β following viral infection. In contrast to our results, previous study showed that *Nlrc5*$^{-/-}$ mice develop increased amounts of IFN-β in their sera, without significantly affecting the viral titers and mice survival rates following VSV infection. Such

differences could be a result of different gene deletion techniques, or different virus treatments used [57].

The behavioral test to determine anxiety-like symptoms in mice did not show any significant difference due to *Nlrc5* deficiency. However, we found that one of the infected wild type mice displayed an aberrant behavior (anxiolytic) after a month p.i., which could be due to pronounced hippocampal pathology.

The other members of the NLR family, such as NLR family pyrin domain containing 1 (NLRP1) have previously been implicated in epilepsy. Increased expression of NLRP1 was found in resected hippocampus from patients with mTLE. NLRP1 was also found to contribute in neuronal death and chronic seizure activity in amygdala kindling-induced rat model of epilepsy. However, silencing of NLRP1 inflammasome did not lower acute seizures in rats, implying that NLRP1 has a role in late phase of the disease [145]. Since NLRC5 can interact with other NLRs (NLRP3), and form inflammasome [59,138], the TMEV-induced inflammation and seizures could be a collaborative effect of Nlrc5 and other inflammasome forming NLRs. Future studies are required to investigate the interactions between Nlrc5 and inflammasome forming NLRs in this model.

Although, inflammation is crucial for viral clearance, excessive and unregulated inflammation contributes to hippocampal pathology and seizures in TMEV-induced epilepsy model. Therefore, treatments limiting neuroinflammation would be beneficial to prevent seizure development and neuronal loss following infection. From our current

study, we found that *Nlrc5* deficiency alleviates immune-mediated seizures in C57BL/6 mice upon TMEV infection, signifying that Nlrc5 intensifies inflammation, positively regulates anti-viral immunity, and contributes to seizure development. Therefore, inhibiting the acute elevation of NLRC5 or its downstream signaling molecules (such as IL-1β) could prove to be promising therapeutic targets for treating epilepsy.

CHAPTER IV

NLRC3: A NOVEL DOWNREGULATOR INVOLVED IN TMEV-INDUCED EPILEPSY MODEL

Introduction

Epilepsy is one of the most common diseases of the central nervous system (CNS). It is characterized by two or more unprovoked seizures occurring more than 24 hours apart, a single unprovoked seizure with high risks of subsequent seizures in the future, or diagnosis of an epilepsy syndrome [2]. Currently, 70 million people worldwide are diagnosed with epilepsy [5], and one-third of the affected population is refractory to drugs. Moreover, there is no existent cure for epilepsy and the available anti-epileptic drugs provide symptomatic treatment only. Therefore, identifying novel therapeutic strategies to extenuate epilepsy is much needed [14].

Intracerebral (I.C.) infection of Theiler's murine encephalomyelitis virus (TMEV) triggers an overzealous innate immune response, seizures and neuronal damage within a week post infection (p.i.), subsequently leading to epilepsy in C57BL/6 mice. Hence, the TMEV-induced model of epilepsy proves to be beneficial in understanding the pathophysiology of both acute and chronic forms of seizures. The dysregulated innate immune response is the key attribute of this experimental model, and previous researchers have primarily focused on the pro-inflammatory part of the immune system.

However, we are left with the partial picture of the disease mechanism without investigating the role of the adaptive immune response or anti-inflammatory aspects. [21,34,36].

Nucleotide-binding oligomerization domain-like receptors (NLRs) are an integral part of the innate immune system. They are important in both infection and injury by recognizing conserved microbial motifs, pathogen-associated molecular patterns (PAMPs) such as nucleic acid, and/or danger-associated molecular patterns (DAMPs) which are endogenous danger signals released from necrotic cells, such as adenosine triphosphate (ATP). There are 22 identified NLRs in humans and 34 in mice. The NLRs are multi-faceted and they contribute to innate immunity by acting as either pro- or anti-inflammatory mediators, thereby aiding in microbial clearance and wound healing [135].

The NLR family, caspase activation and recruitment (CARD) domain containing 3 (NLRC3), alternatively named as NOD3 or CLR16.2, is an under researched member of the NLR family. Similar to other NLRs, it has a tripartite domain; which includes a less well-defined CARD domain at the N-terminal, a nucleotide-binding domain (NBD) at the center, and a leucine-rich repeat domain (LRR) at the C-terminal. The *NLRC3* gene is located on chromosome 16, and the protein encoded by this gene is localized in the cell cytoplasm. NLRC3 is mainly expressed by cells and tissues of the immune system, with highest expression reported in T lymphocytes, in both humans and in mice. It is

also highly expressed in natural killer cells (NK) and moderately expressed in B lymphocytes in humans [61, 60].

The limited studies focused on NLRC3 describe its role in negatively regulating inflammation under pathological conditions and maintaining homeostasis in absence of immune challenge. NLRC3 has been reported to constitute a negative-feedback mechanism to monitor immune responses and cellular proliferation by attenuating T cell- [61], Toll-like receptor 4 (TLR4)- [66], stimulator of interferon genes (STING)- [67], and mechanistic target of Rapamycin (mTOR)- [68] dependent signaling pathways. This consequently suppresses the activation and signaling by downstream transcriptional factors (e.g. nuclear factor kappa-light-chain-enhancer of activated B cells [NF-κB] and interferon regulatory factor 3 [IRF3]), and production of interferon (IFN) and pro-inflammatory cytokines (such as tumor necrosis factor [TNF], interleukin-6 [IL-6]). Furthermore, NLRC3 may inhibit the formation of inflammasomes, multi-protein complexes that mediate caspase-1 activation and IL-1β and IL-18 production, by other NLR members (e.g. NLR family, pyrin domain containing 3 [NLRP3], NLR family, CARD domain containing 4 [NLRC4]) [60, 146].

In our current study, we investigated the effect of Nlrc3 in the TMEV-induced murine model of epilepsy. For this, *Nlrc3* deficient (*Nlrc3*$^{-/-}$) mice (on C57BL/6 background) and wild type C57BL/6 mice were infected with TMEV, and examined for clinical signs of acute and chronic seizures, weight loss, seizures-associated behavioral abnormality,

leukocyte infiltration in the brain and cervical lymph nodes (CLNs), and demyelinating lesions in the spinal cord. The clinical examination of mice showed that the absence of *Nlrc3* gene increased the susceptibility of infected mice to acute seizures (day 3-7 p.i.), and chronic seizures (day 8-week 30 p.i.). We further established that the increase in the occurrence of epileptic seizures in *Nlrc3*$^{-/-}$ group was not mediated by the infiltration of peripheral immune cells in the brain during chronic phase. We also found that the *Nlrc3* gene did not affect the resistance of C57BL/6 mice to TMEV-induced demyelinating disease as none of the infected *Nlrc3*$^{-/-}$ mice developed spinal cord lesions or exhibited clinical signs of the demyelinating disease in the chronic phase. In addition, we found that *Nlrc3* deficiency led to significantly increased mobility and excitability (signs of behavioral abnormalities), but slightly faster recovery among mice following infection, while no behavioral abnormalities were detected in control mice due to *Nlrc*3 deficiency. Taken together, our results show that the *Nlrc3* gene contributes in attenuating acute seizures and epilepsy in C57BL/6 mice following TMEV infection, but may require the involvement of other gene(s) to completely inhibit seizure activity.

Materials and Methods

Mice

Six-to-nine-week-old female *Nlrc3*$^{-/-}$ mice were generously provided by Dr. Koichi K. Kobayashi, Department of Microbial Pathogenesis and Immunology, Texas A&M University, TX. Age-matched female C57BL/6 wild type mice were purchased from

Taconic (Germantown, NY). Upon arrival, mice were assigned to one of four experimental groups, *Nlrc3*$^{-/-}$ sham-infected control, wild type sham-infected control, *Nlrc3*$^{-/-}$ virus-infected, and wild type virus-infected. Mice were placed in a pathogen-free facility, with 12 hours of light and dark cycle and controlled room temperature and humidity. Mice were provided with *ad libitum* food and water throughout the duration of the experiment. All animal experiments were approved by the Institutional Animal Care and Use Committee (IACUC) of Comparative Medicine Program at Texas A&M University, TX.

Virus

The BeAn strain of TMEV (ATCC) was initially propagated in baby hamster kidney (BHK) cells. Culture supernatant containing virus particles was collected and stored at -80°C, and later used for infection [85].

Infection

After a week of acclimatization, mice in the infected groups were injected intracerebrally (I.C.) with 5.0 x 10^4 plaque forming unit (PFU) of BeAn strain in 20µl of Dulbecco's modified eagle medium (DMEM) (Sigma, Life Science, St. Louis, MO). Mice in the control groups were injected I.C. with 20µl of 1x phosphate buffer saline (PBS). All injections were performed under isoflurane (Isoflo, North Chicago, IL) anesthesia.

Clinical scores

During the acute phase, mice (n=4/control group and n=23-24/infected group) were examined for seizures twice daily between 9 AM to 6 PM until day 6 p.i. and the once on day 7 p.i. For epileptic seizures, control mice (n=4/group) and infected mice (n=12/group) were examined once weekly during the chronic phase (day 8 till week 30 p.i.). Mice were scored on a Racine scoring scale: (1) Mouth and facial movements, (2) Head nodding, (3) Forelimb clonus, (4) Rearing, and (5) Rearing and falling progressing to tonic-clonic seizure [139].

Body weight measurement

During the acute phase, mice (n=4/control group and n=22-23/infected group) body weights were recorded daily until day 6 p.i. % weight loss was calculated as ([mouse weight on day n^{th} p.i.- mouse weight on day 0 p.i.]/mouse weight on day 0 p.i.) *100.

Elevated Plus Maze Test (EPMT)

EPMT is one of the most common behavioral tests to determine behavioral anomalies such as anxiety-like symptoms in rodents. We followed the standard protocol from Komada et al. [90] with few modifications. The elevated plus maze was made of black Plexiglass. It consisted of two perpendicularly placed open (25 x 5 x 0.5 cm^3) and closed (25 x 5 x 16 cm^3) arms, with a platform (5 x 5 x 0.5 cm^3) at the intersection of the arms. The maze was kept elevated at a height of 50 cm above the floor.

To determine the effects of mouse genotype, seizures, and time-interval p.i., EPMT was conducted at two different time-points, day 17 and day 34 p.i. The experiments were performed in two different isolated rooms to maintain novel environmental conditions. Mice were given 30 min to acclimate to the room prior to any testing. Experiments were performed during the day between 8:00 AM and 6:00 PM.

To test for anxiety, each mouse (n=4/control group and n=5/infected group) was individually placed at the central platform with its head facing the same closed arm. Mice were given 5 min of test period to freely explore the maze. During this period, the number of entries in open and closed arms, and percentage (%) time spent in open arms were recorded for each mouse. An arm entry was defined as the placement of half of the mouse body mass in that arm of the maze. The % of time spent in open arms was calculated as [(time spent in open arms/total test time) x 100]. The number of entries and % time spent in open arms were used as a measure of anxiety-like behavior. The number of closed arm entries was used to determine locomotor activity. The maze was cleaned with 70% (vol/vol) ethanol between the tests to remove any feces, urine or animal odor.

Tissue isolation

To obtain tissues, mice were euthanized with 150mg/kg beuthanasia-D special (Schering-Plough Animal Health Corp. Union, NJ) and perfused intracardially using 10 ml of 1x phosphate buffered saline (PBS). For histology, spinal cords were retrieved at week 30 p.i., and fixed in 10% formaldehyde for 5 days at room temperature. For flow

cytometry, brains and cervical lymph nodes (CLNs) were collected at week 30 p.i. in ice-cold RPMI 1640 (Gibco, Life Technologies, Grand Island, NY), and individually processed to analyze leukocyte populations.

Flow cytometry

To collect leukocytes from the brain, whole brains (n=3/ infected group) were gently homogenized using 70-micron (μm) FALCON cell strainer (21008-952; VWR, Sugarland, TX) and suspended in RPMI 1640 containing 5% fetal bovine serum (FBS). The cell suspensions containing brain homogenates were collected in individual 50 ml conical tubes, and centrifuged at 500 x g for 5 min at room temperature. After discarding the supernatant, each pellet was suspended in 10 ml of 30% Percoll (17-0891-01; GE healthcare, Uppsala, Sweden) in PBS. This solution was gently overlaid onto 2 ml of 70% Percoll in PBS, and centrifuged at 500 x g for 30 min at 18°C. The leukocytes were collected from the 30% and 70% Percoll interphase, suspended in PBS, and centrifuged at 500 x g for 7 min at 18°C. The supernatants were discarded, and pellets were re-suspended in 3 ml of ice-cold flow buffer containing 3% BSA and 0.1% sodium azide in PBS.

To collect leukocytes from CLNs, the CLNs (n=3/infected group) were homogenized by gently grinding them with sterile microscopic slides. Then, the cell suspensions containing CLN homogenates were filtered using sterile, 70-μm nylon mesh. The filtrates containing leukocytes were collected in individual 15 ml conical tubes, and

centrifuged at 350 x g for 5 min at 4°C. The supernatants were discarded, and each pellet was suspended in 2 ml of flow buffer containing 3% BSA and 0.1% sodium azide in PBS. The cells were washed, re-suspended in flow buffer and maintained at 4°C.

Staining procedure: Leukocytes from brain and CLNs were treated with Anti-Mouse CD16/CD32 (1:100, 14-0161-82; eBioscience, San Diego, CA) for 10 min at 4°C to prevent any non-specific binding. For phenotyping, cells were stained with the anti-mouse antibodies as indicated below for 30 min at 4°C, washed and fixed with 2% PFA prior to flow cytometric analysis on BD FACSAria II. Data was analyzed using FlowJo® software V10.0.8r1 (Mac OS X, FlowJo, LLC, Ashland, OR). Ly-6G (Gr-1) was detected with clone RB6-8C5 (1:500, 12-5931-82; eBioscience, San Diego, CA). CD11c was detected with clone N418 (1:250, 17-0114-81; eBioscience, San Diego, CA). NK1.1 was detected with clone PK136 (1:500, 12-5941-63; eBioscience, San Diego, CA). CD11b was detected with clone M1/70 (1:500, 101224; BioLegend, San Diego, CA). CD45.2 was detected with clone 104 (1:100, 109805; BioLegend, San Diego, CA). CD8a was detected with clone 53-6.7 (1:250, 100711; BioLegend, San Diego, CA). CD4 was detected with clone GK1.5 (1:500, 100428; BioLegend, San Diego, CA). B220 was detected with clone RA3-6B2 (1:500, 17-0452-83; eBioscience, San Diego, CA) [89,140].

Histology: spinal cord

Four μm paraffin-embedded sections from the spinal cords (n=7/ infected group) were stained with H&E. At least one transverse section from each spinal cord segment was

examined for the presence of inflammatory foci, axonal/neuronal degeneration, and/or meningitis. All images were acquired using a HRD076-NIK camera attached to OLYMPUS VANOX AHBS3 microscope.

Statistical analysis

For parametric analysis, one-way analysis of variance (ANOVA) with the Tukey's multiple comparisons test or the unpaired t-test with the Welch's correction was used. Body weights were analyzed using repeated measures two-way ANOVA with the Tukey's multiple comparisons test. For nominal data (presence or absence of seizures), the Fisher's exact test was used. For all cases, significance was determined when $p \leq 0.05$. Statistical analysis was done using GraphPad Prism version 6.0d (Mac OS X, GraphPad Software, La Jolla, CA).

Results

Nlrc3 deficiency aggravated susceptibility to TMEV-induced epilepsy.

Corroborating previous studies, our acute phase results showed that TMEV infection resulted in ~71% (17/24) of wild type mice exhibiting seizures. In contrast to wild type mice, 100% (23/23) of *Nlrc3*$^{-/-}$ mice succumbed to acute seizures following infection (Fisher's exact test, $p<0.0001$) (Figure 26A). Clinical examinations, conducted twice daily, showed that in wild type infected group, seizures began on day 3 p.i. and ceased after day 6 p.i., with highest number of seizures recorded on day 4 p.i. In the case of

Nlrc3$^{-/-}$ infected mice, a similar pattern of acute seizures was noted but seizures in this group lasted a day longer than the wild type infected group (until day 7 p.i.). We also found an increase in the number of seizures recorded per day in *Nlrc3*$^{-/-}$ group in comparison to the wild type group, with significant differences observed on days 3, 4 and 7 p.i. (Fisher's exact test, day 3: $p=0.0009$; day 4: $p=0.0005$; day 5: $p=0.4665$; day 6: $p=0.8868$; and day 7: $p=0.0015$) (Figure 26B). In both infected groups, the majority of seizures were of the highest intensity depicting tonic-clonic seizures, hence were given a score of 5 on the Racine scale (Figure 26C and D). As expected, no seizures were observed in any of the control groups.

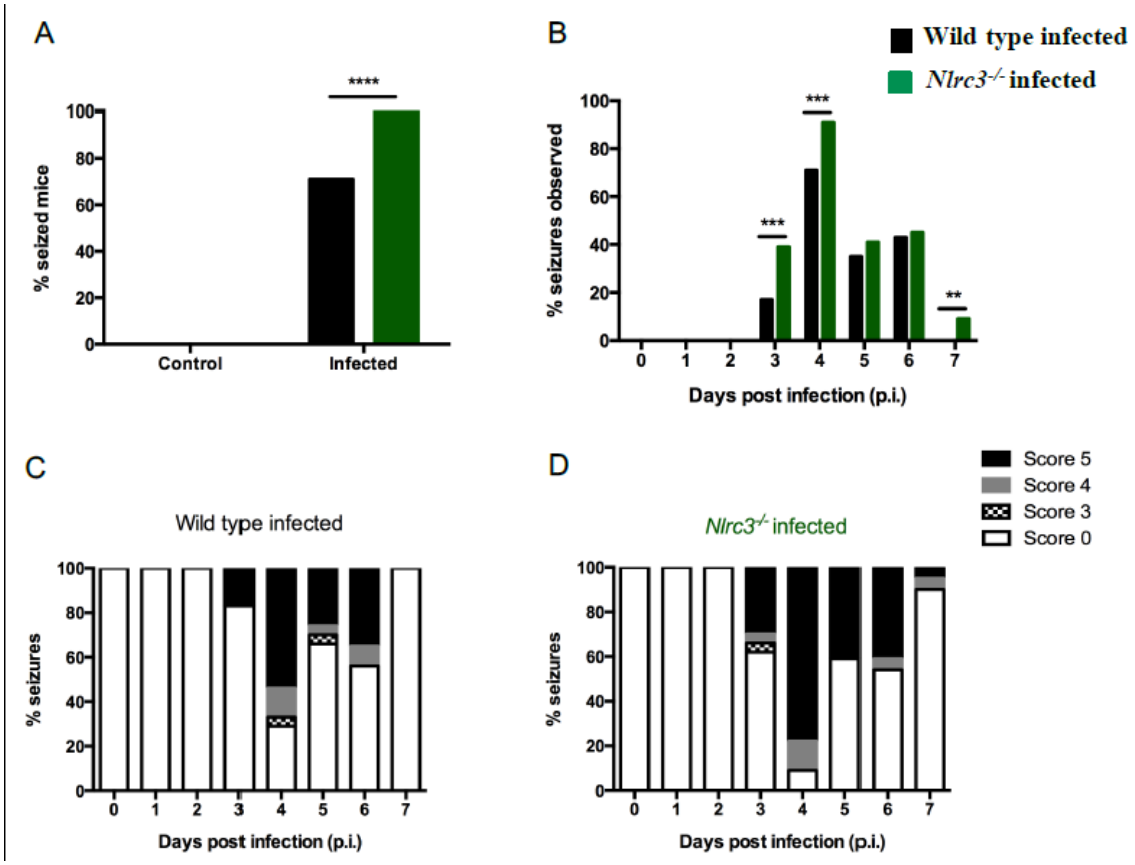

Figure 26 Nlrc3 deficiency increased the susceptibility of mice for TMEV-induced seizures. (A) Acute phase results revealed a significant increase in the proportion of *Nlrc3*$^{-/-}$ infected mice with seizures in comparison to wild type infected mice. The % seized mice in each group was calculated as (number of seized mice/total number of infected mice) x 100. No seizures were observed in the control groups. (B) Daily examinations of mice showed that *Nlrc3*$^{-/-}$ infected group had significantly more seizures that lasted a day longer than wild type infected group. The % seizures per day was calculated as (number of seizures in a day /total number of infected mice) x 100. (C and D) In both the infected groups, seizures were mostly of highest intensity, i.e. stage 5, while few mice had seizures of stage 3 and 4 on the Racine scale. (**** $p<0.0001$, *** $p<0.001$, ** $p<0.01$ by Fisher's exact test). Graphs (A, B, C, and D) show pooled results from four separate experiments expressed as percent, N=4 per control group and N=23-24 per infected group.

During the weekly examination of the mice in the chronic phase, we observed two unprovoked behavioral seizures in ~8 % (1/12) of the wild type infected mice on week 28 p.i. In comparison to the wild type group, ~42% (5/12) of *Nlrc3*$^{-/-}$ infected mice experienced behavioral seizures in the chronic phase. In the *Nlrc3*$^{-/-}$ infected group,

epileptic seizures occurred randomly. Seizures were documented as early as week 3 p.i. and were recorded until the day of termination (Figure 27). Moreover, the epileptic seizures observed per mouse varied from one to six in *Nlrc3*$^{-/-}$ group during the chronic phase. As expected, no seizures were observed in any of the control groups during either the acute or chronic phase. Collectively, our results show that knocking out *Nlrc3* gene exacerbated TMEV-induced epilepsy. Conversely, the *Nlrc3* gene moderately protected mice from developing acute seizures and epilepsy following CNS infection.

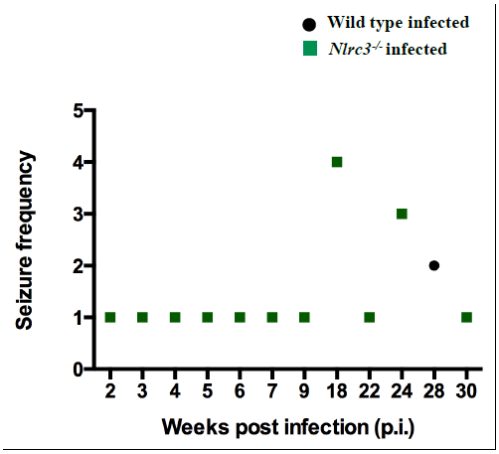

Figure 27 *Nlrc3*$^{-/-}$ infected mice had increased susceptibility to TMEV-induced epilepsy compared to wild type infected mice. Weekly examinations of the mice showed that chronic seizures in *Nlrc3*$^{-/-}$ infected group started as early as week 2 p.i. and were recorded until the termination of mice, i.e. week 30 p.i. In contrast to *Nlrc3*$^{-/-}$ mice, chronic seizures were only documented at week 28 p.i. in the wild type infected group. The seizure frequency in each group was calculated as number of seizures per week during chronic phase. Graph shows pooled results from two separate experiments expressed as seizure frequency, N=12 per infected group.

Infected Nlrc3$^{-/-}$ *mice showed faster recovery than infected wild type mice.*

To assess the effects of virus infection and genotype, mice from all four groups were weighed daily during the acute phase and once per week during the chronic phase. Changes in the weights of mice were similar between control groups, which indicates

that *Nlrc3*$^{-/-}$ mice do not show any growth abnormalities (Repeated measures two-way ANOVA with Tukey's multiple comparisons test, day 0: p>0.9999; day 1: p=0.9976; day 2: p=0.9993; day 3: p=0.9372; day 4: p=0.8891; day 5: p=0.9890; and day 6: p=0.9925). Significant weight loss was evident in both infected wild type and *Nlrc3*$^{-/-}$ mice compared to their respective controls during the acute phase. Although, the weight change was not significantly different between the infected *Nlrc3*$^{-/-}$ group and the control *Nlrc3*$^{-/-}$ group on day 6 p.i., implying that infected *Nlrc3*$^{-/-}$ mice started to regain weight at this time-point (Repeated measures two-way ANOVA with Tukey's multiple comparisons test between wild type control vs. wild type infected, day 0: p>0.9999; day 1: p=0.0061; day 2 till day 6: p<0.0001; between *Nlrc3*$^{-/-}$control and *Nlrc3*$^{-/-}$ infected, day 0: p>0.9999; day 1: p=0.0058; day 2 till day 4: p=<0.0001; day 5: p=0.0054; and day 6: p=0.1225). Both infected groups began to regain weight at day 3 p.i. and completely recovered by day 21 p.i., but the weight gain was significantly higher in *Nlrc3*$^{-/-}$ mice than wild type mice on days 5 and 6 p.i. (Repeated measures two-way ANOVA with Tukey's multiple comparisons test, day 0: p>0.9999; day 1: p=0.9791; day 2: p=0.5336; day 3: p=0.2822; day 4: p=0.4155; day 5: p=0.0350; and day 6: p<0.0001 chronic phase) (Figure 28). Our results signify that although *Nlrc3*$^{-/-}$ mice experienced more seizures, they showed better recovery than wild type mice in terms of improvement in weight.

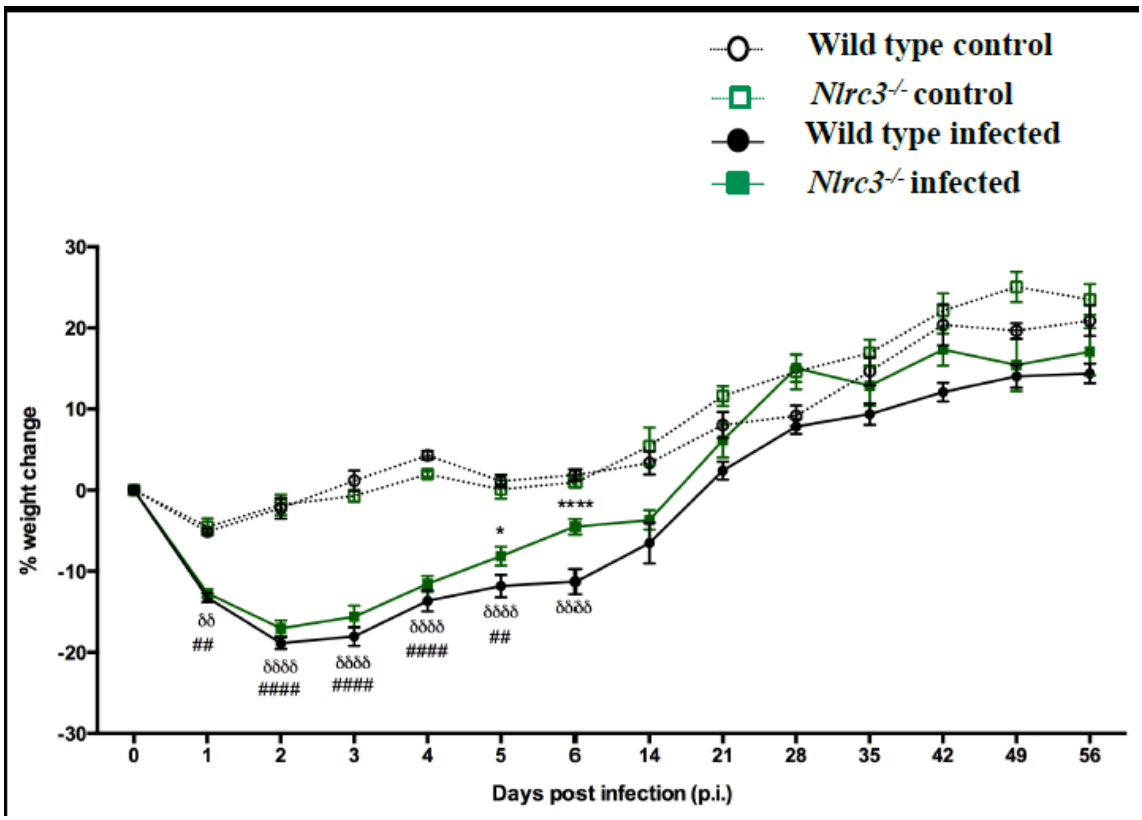

Figure 28 *Nlrc3*$^{-/-}$ infected mice showed better recovery than wild type infected mice. Mice from the control and infected groups were weighed daily until day 6 p.i. and then once weekly until day 56 p.i. Both the infected groups exhibited significant weight loss immediately following TMEV infection in comparison to their respective controls. However, *Nlrc3*$^{-/-}$ infected mice started to regain weight earlier than wild type infected group, indicating faster recovery in *Nlrc3*$^{-/-}$ infected group. Both the infected groups showed complete recovery by day 21 p.i., when their weights matched with those of their respective controls. (Between wild type control and infected groups: δδ $p<0.01$, δδδδ $p<0.0001$; between *Nlrc3*$^{-/-}$ control and infected groups: ## $p<0.01$, #### $p<0.0001$; between *Nlrc3*$^{-/-}$ infected and wild type infected groups: * $p<0.05$, **** $p<0.0001$ by Repeated Measures two-way ANOVA with Tukey's multiple comparisons test). Graph shows pooled results from acute phase (days 0-6 p.i.) and chronic phase (days 14-56 p.i.) studies, expressed as mean ± SEM. During acute phase, results are from four separate experiments, N=22-23 per infected group, during chronic phase, result is from one experiment, N=6-7 per infected group. For control groups, N=4 during acute and chronic phase.

Nlrc3 deficient mice developed aberrant emotional behavior following TMEV infection.

We observed that infected *Nlrc3*$^{-/-}$ mice displayed hypermobility and excitable behavior even after seizures ceased. Therefore, we conducted EPMT to compare locomotor activity and behavioral differences between control and infected groups after seizures

resolved. EPMT is based upon an intricate balance between two main characteristics of mouse behavior, their natural aversion for open and elevated spaces and preference for dark and enclosed spaces, and their inherent curiosity for exploring novel environments [90].

Results from day 17 p.i. demonstrated significantly increased activity among infected *Nlrc3*$^{-/-}$ mice not only in the open arms, but also in the closed arms as indicated by open and closed arm entries (Figure 29B and C) (One way ANOVA with Tukey's multiple comparisons test-open arms entries, between wild type control and *Nlrc3*$^{-/-}$ control: p=0.9605; between wild type control and wild type infected: p=0.9648; between *Nlrc3*$^{-/-}$ control and *Nlrc3*$^{-/-}$ infected: p=0.0010; and between wild type infected and *Nlrc3*$^{-/-}$ infected: p=0.0039) (One way ANOVA with Tukey's multiple comparisons test-closed arms entries, between wild type control and *Nlrc3*$^{-/-}$ control: p=0.2918; between wild type control and wild type infected: p=0.8430; between *Nlrc3*$^{-/-}$ control and *Nlrc3*$^{-/-}$ infected: p=0.0040; and between wild type infected and *Nlrc3*$^{-/-}$ infected: p=0.0235). As shown in figure 29A, infected *Nlrc3*$^{-/-}$ mice also spent significantly more time in the open arms than control *Nlrc3*$^{-/-}$ mice and infected wild type mice (One way ANOVA with Tukey's multiple comparisons test-% time spent on open arms, between wild type control and *Nlrc3*$^{-/-}$ control: p=0.9910; between wild type control and wild type infected: p=0.9906; between *Nlrc3*$^{-/-}$ control and *Nlrc3*$^{-/-}$ infected: p=0.0018; and between wild type infected and *Nlrc3*$^{-/-}$ infected: p=0.0035). To confirm our findings, we repeated the test on day 34 p.i. The second EPMT showed similar results with respect to significantly

increased activity among infected *Nlrc3*$^{-/-}$ mice in the open arms (Figure 29D and E) (One way ANOVA with Tukey's multiple comparisons test-open arms entries, between wild type control and Nlrc3$^{-/-}$ control mice: p=0.9917; between wild type control and wild type infected mice: p=0.9903; between Nlrc3$^{-/-}$ control and Nlrc3$^{-/-}$ infected mice: p=0.0531; and between wild type infected and Nlrc3$^{-/-}$ infected mice: p=0.0385) (One way ANOVA with Tukey's multiple comparisons test-% time spent on open arms, between wild type control and *Nlrc3*$^{-/-}$ control mice: p=0.9947; between wild type control and wild type infected mice: p=0.9846; between *Nlrc3*$^{-/-}$ control and *Nlrc3*$^{-/-}$ infected mice: p=0.0427; and between wild type infected and *Nlrc3*$^{-/-}$ infected mice: p=0.0252). As shown in figure 29F, the activity of infected *Nlrc3*$^{-/-}$ mice in the closed arms was not different in comparison to mice from other groups (One way ANOVA with Tukey's multiple comparisons test-closed arms entries, between wild type control and *Nlrc3*$^{-/-}$ control: p=0.4690; between wild type control and wild type infected: p=0.6393; between *Nlrc3*$^{-/-}$ control and *Nlrc3*$^{-/-}$ infected: p=0.0801; and between wild type infected and *Nlrc3*$^{-/-}$ infected: p=0.1210). Thus, our results showed that *Nlrc3*$^{-/-}$ mice developed aberrant emotional behavior (anxiolytic) and increased locomotor activity following infection.

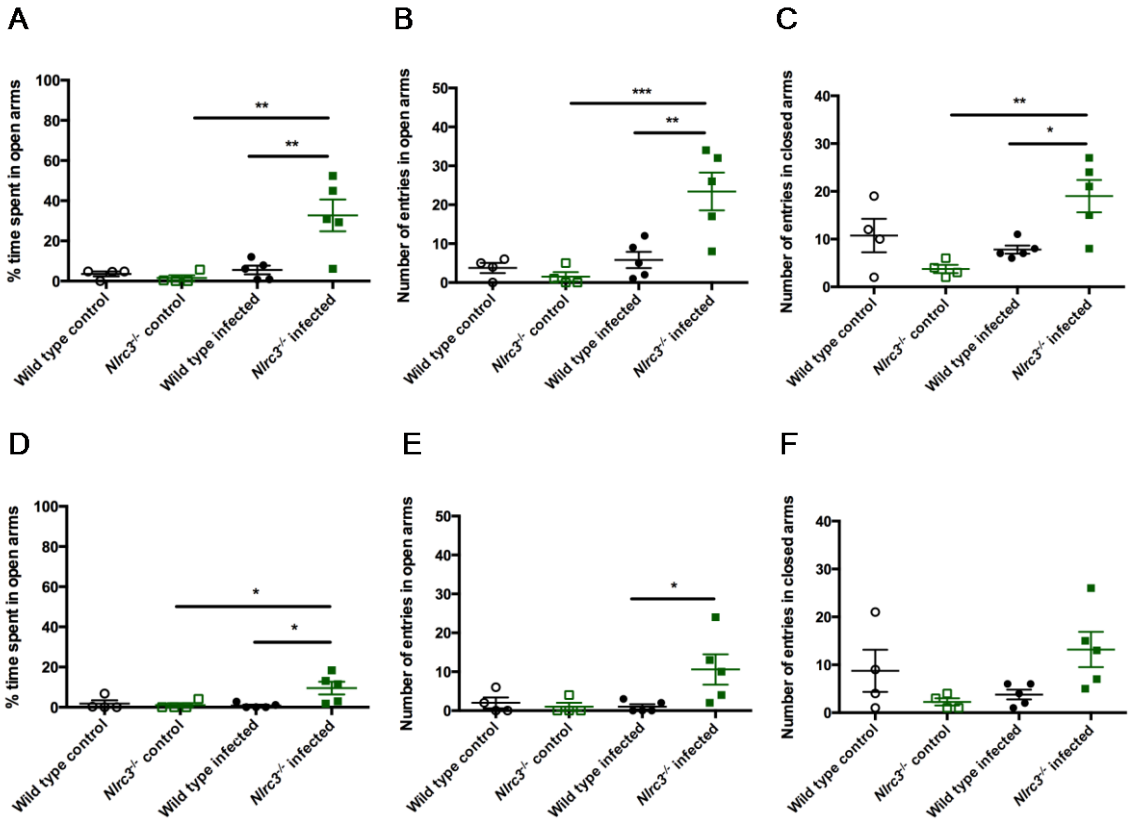

Figure 29 Nlrc3 deficient mice developed aberrant emotional behavior following TMEV infection. We conducted EPMT to determine behavioral abnormalities among infected mice during chronic phase. Graphs A-C are from study conducted on day 17 p.i., and graphs D-F are from study conducted on day 34 p.i. The EPMT results show that *Nlrc3*$^{-/-}$ infected mice spent significantly more time exploring the open arms, and had significantly higher open and closed arms entries than the other groups, indicating hypermobility and development of anxiolytic behavior. The % time spent in open arms was calculated as (time spent in open arms/time spent in open and closed arms) x 100. The number of entries in open and closed arms was recorded manually at the time of the experiment. Graphs show results expressed as mean ± SEM, N=4 per control group and N=5 per infected group. (* $p<0.05$, ** $p<0.01$, *** $p<0.001$ by one-way ANOVA with Tukey's multiple comparisons test).

Seizures in the chronic phase were not mediated by neuro-inflammation.

Previous studies reported that activation and infiltration of innate immune cells into the CNS may contribute to the development of acute seizures [21, 97]. Therefore, we wanted to determine whether chronic inflammation played a role in instigating epileptic seizures. For this purpose, we analyzed leukocyte populations in the brain and CLNs at week 30

p.i. In both infected groups (Figure 30A), the leukocyte profile from the brain showed minimal or no activation of peripheral immune cells (Unpaired t test with Welch's correction, CD45.2 intermediate CD11b+: p=0.1748; CD45.2 high CD11b+: p=0.3600; CD45.2 high Gr1+: p=0.6368; CD45.2 high NK1.1+: p=0.2596; CD45.2 high CD11c+: p=0.5029; CD45.2 high CD8+: p=0.7768; CD45.2 high CD4+: p=0.3304; and CD45.2 high B220+: p=0.3767). In the case of CLNs (Figure 30B), no significant differences were seen between the infected groups, but we found a higher expression of adaptive immune cells (CD45.2 high CD4+ [T helper cells], CD45.2 high CD8+ [Cytotoxic T cells], and CD45.2 high B220+ [B cells]) than other cell types in both groups (Unpaired t test with Welch's correction, CD45.2 high CD11b+: p=0.0128; CD45.2 high Gr1+: p=0.7619; CD45.2 high NK1.1+: p=0.4597; CD45.2 high CD11c+: p=0.1389; CD45.2 high CD8+: p=0.3393; CD45.2 high CD4+: p=0.0903; and CD45.2 high B220+: p=0.2279). Consequently, we eliminated the role of inflammation in causing epileptic seizures following TMEV infection.

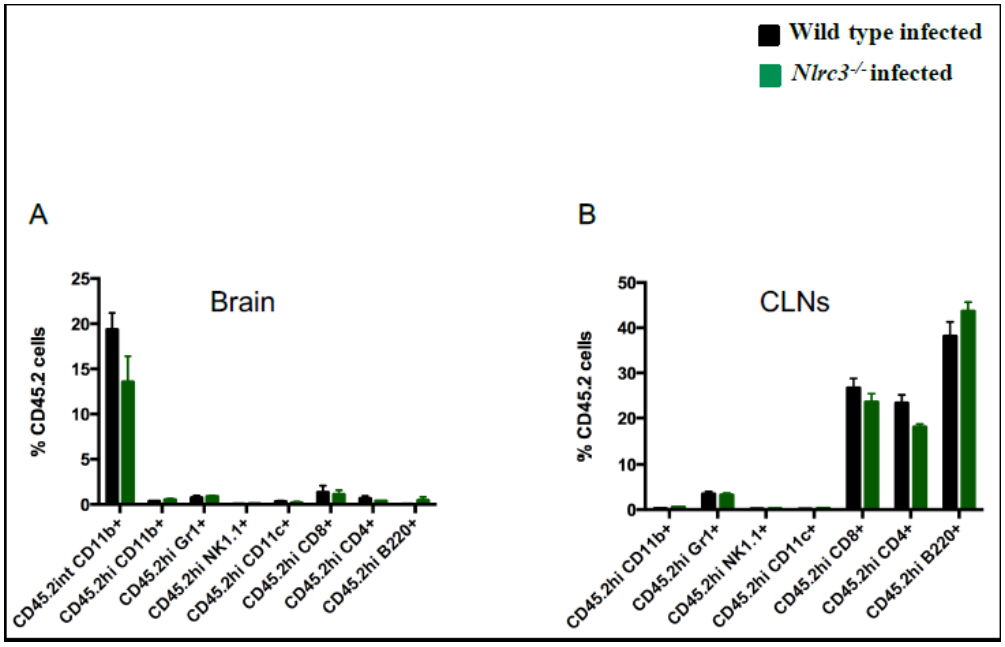

Figure 30 Seizures in the chronic phase were not mediated by neuro-inflammation. To determine whether chronic inflammation contributed to epileptic seizures, innate and adaptive leukocyte populations were analyzed from brain and CLNs of infected mice at week 30 p.i. Surprisingly, we found minimal or no expression of peripheral immune cells in the brain during the chronic phase. In addition, the expression levels of leukocytes populations from brain and CLNs were similar between the infected groups, indicating that epileptic seizures were not the result of chronic inflammation. Graphs show results expressed as mean ± SEM, N=3 per infected group. (Unpaired t test with Welch's correction).

Nlrc3 deficient mice sustain their resistance to demyelinating disease following TMEV infection.

Wild type mice are known to be resistant to TMEV-induced demyelinating disease of the CNS [43,130]. To investigate whether infected *Nlrc3*$^{-/-}$ mice develop chronic inflammation or demyelinating lesions in the spinal cord, we compared spinal cord histology between the two infected groups at week 30 p.i. Like the wild type mice, no lesions or active inflammation was recorded from spinal cords of *Nlrc3*$^{-/-}$ mice in the chronic phase. Our results indicate that *Nlrc3* gene did not alter the resistance of C57BL/6 mice to demyelinating disease of the CNS (Figure 31A and B).

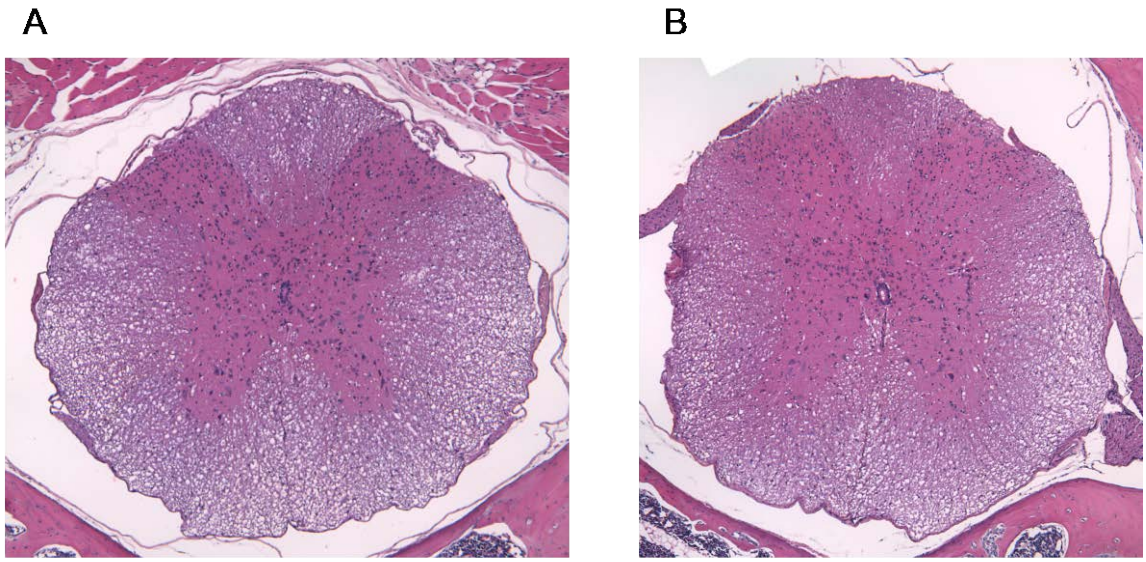

Figure 31 Nlrc3 deficient mice sustain their resistance to demyelinating disease following TMEV infection. To assess the effect of the *Nlrc3* gene on susceptibility of C57BL/6 mice to TMEV-induced demyelinating disease, the spinal cords from *Nlrc3*$^{-/-}$ mice were collected at week 30 p.i., stained with H&E and compared to that of wild type mice. A and B are the representative images (100x) of the thoracic segment of the spinal cord from wild type and *Nlrc3*$^{-/-}$ mice, respectively. Unlike in the susceptible SJL mice, we did not find any pathological condition in the spinal cords from either *Nlrc3*$^{-/-}$ or wild type group, indicating that the *Nlrc3* gene does not regulate the resistance of C57BL/6 mice to TMEV-induced demyelinating disease.

Discussion

The immune system plays an important role in defense against microbial infection and wound healing. However, dysregulated and heightened immune activity in response to infection may cause inflammatory disorders and autoimmune diseases. Therefore, the right balance between the functions of pro- and anti-inflammatory mediators is vital for maintaining homeostasis. NLRs are intracellular pattern recognition receptors that play an essential part in innate immunity. Several NLRs (such as NLR, domain containing 2 [NOD2]) initiate early, non-specific immune responses against infection, while others

(such as NLR family member X1 [NLRX1]) participate in restoring immune responses to basal levels after microbial clearance [135].

Studies on NLRC3 have only recently been started and the current literature implicates its role in downregulating immune responses. Conti, Davis and colleagues [61] found that NLRC3 expression significantly reduces upon T-cell receptor (TCR)- and CD28-dependent stimulation of primary T cells, while addition of exogenous NLRC3 significantly downregulates the induction of signaling pathways (e.g. NF-κB, activator protein-1 [AP-1], and Nuclear factor of activated T-cells [NFAT]), and downstream inflammatory molecules (e.g. IL-2 and CD25) in activated T cells. Thus, they proposed that NLRC3 plays a role in limiting the activation and signaling of T cells. Schneider, Zimmermann et al. [66] demonstrated an inhibitory effect of NLRC3 on TLR-dependent signaling, which is mediated by impairing the activation of TRAF6, a TLR signaling adaptor molecule. They further found that wild type mice administered with lipopolysaccharide (LPS), a TLR4 ligand, have reduced expression of *Nlrc3* mRNA in their peritoneal cells, but *Nlrc3* expression levels return to basal levels at later time-points. Furthermore, LPS-stimulated macrophages from *Nlrc3*$^{-/-}$ mice have increased production of TRAF6, NF-κB, and pro-inflammatory cytokines (TNF, IL-6, and IL-1β) compared to wild type macrophages at early time-points. This effect diminishes at later time-points. *In vivo* studies showed that LPS-treated *Nlrc3*$^{-/-}$ mice develop increased intensity of inflammation and clinical illness compared to wild type mice; thus, they showed a protective role for Nlrc3 in the LPS-induced mouse model of endotoxic shock.

Zhang, Mo and others [67] found that NLRC3 blocks the association between STING and TANK-binding kinase 1 (TBK1), thereby reducing the activation of STING-dependent innate immune signaling (NF-κB and IRF3) under basal conditions and in case of infection against cytosolic DNA, and DNA viruses. They also found that bone marrow-derived macrophages (BMDMs) and mouse embryonic fibroblasts (MEFs) from *Nlrc3* deficient mice have increased production of type I IFN, IL-6 and TNF, and reduced viral load in response to DNA viruses such as Herpes simplex virus-1 (HSV-1). However, they did not find similar responses against RNA viruses, such as Sendai virus (SeV) and vesicular stomatitis virus (VSV). Moreover, HSV-1-infected *Nlrc3*$^{-/-}$ mice exhibit increased inflammation (increased production of IFN-1, TNF-a, IL-6), faster recovery in terms of body weight, and reduced viral load compared to wild type mice. Karki, Man, et al. [68] found that Nlrc3 expression significantly decreases in the tumor tissue of wild type mice with colitis-associated colorectal cancer. In addition, *Nlrc3*$^{-/-}$ mice show increased susceptibility to colitis and colorectal tumorigenesis as they develop pronounced weight loss, damage to the colon, tumor growth, and inflammation in comparison to wild type mice. *Nlrc3*$^{-/-}$ mice also have increased expression levels of innate immune cells (macrophages, NK cells, and neutrophils), pro-inflammatory cytokines (IL-1β, IL-6, TNF, etc.) and chemokines (macrophage chemoattractant protein-1 [MCP-1], monocyte inflammatory protein-1α [MIP-1α], etc.) and increased activation of immune signaling pathways in colon tissue. Thus, they proposed that Nlrc3 protects mice against colitis and colorectal tumorigenesis by reducing the activation of mTOR-signaling pathways at earlier time-points, thereby decreasing cellular proliferation and stem-cell-derived

organoid formation at later time-points. Since, wild type mice with normal expression of Nlrc3 are not completely tumor free, we assume that Nlrc3 provides partial protection against tumor development. In addition, Gültekin, Erin and Özören [60, 146] found that NLRC3 blocks the formation of NLRP3 and NLRC4 inflammasomes, thus decreases the production of IL-1β and IL-18 cytokines.

Libbey, Kennett and group have reported that wild type mice develop acute seizures following TMEV infection, and the proportion of mice affected with seizures vary based on the amount of TMEV used [35]. In the current study, we found that 5.0 x 10^4 pfu of BeAn strain of TMEV induced seizures in ~71% of wild type mice, while the same viral titers caused seizures in all *Nlrc3*$^{-/-}$ mice following infection. Stewart, Wilcox et al. further found that infected wild type mice are known to recover from acute symptomatic seizures after a week p.i. and clear virus within a month p.i., but video-electroencephalogram (VEEG) monitoring has shown that 40-64% of them proceed to develop spontaneous behavioral seizures and 100% of them exhibit epileptiform activity during 2nd, 4th and 7th month p.i. [36]. In our present study, the weekly examinations of mice during the chronic phase (until week 30 p.i.) showed that only one of the 12 infected wild type mice displayed behavioral seizures, while *Nlrc3* deficiency led to behavioral seizures in five of the 12 infected mice. Future studies using VEEG monitoring may help us provide results that are more accurate.

In line with past studies [34], we found that TMEV infection induced acute weight loss among wild type mice in comparison to their controls, and infected mice completely recovered by week 2 p.i. TMEV infection in *Nlrc3*$^{-/-}$ mice also resulted in significant acute weight loss compared to their controls. However, infected *Nlrc3*$^{-/-}$ mice had higher gain in body weight and therefore better recovery than infected wild type mice in spite of increased seizures occurrences.

Using behavioral tests, such as open-field and light/dark box, Umpierre, et al. found that TMEV-infected wild type mice develop anxiety-like symptoms after acute seizures resolve [38]. However, using a different behavioral test (EPMT) we were unable to find any behavioral or locomoter abnormality among wild type infected mice. The difference in results from infected wild type mice could be due to the use of different TMEV strains, behavioral tests, or time at which the tests were conducted. Furthermore, *Nlrc3*$^{-/-}$ mice displayed significant aberrations in locomotor activity and behavioral symptoms that resembled anxiolytic activity, signifying a peculiar role of Nlrc3 gene in regulating mouse behavior that is highlighted post infection.

Moreover, we discovered that epileptic seizures were not the result of chronic inflammation in the CNS, as neither the wild type group nor the *Nlrc3*$^{-/-}$ group showed pertinent immune cell infiltration into the CNS at week 30 p.i. Additionally, the infected groups did not show any significant differences in the leukocyte populations draining the CLNs. Since acute seizures are largely mediated by acute elevation in the activation and

infiltration of innate immune cells in the CNS [21], our chronic phase results support the idea that the mechanisms of induction of acute and chronic seizures are different in this experimental model. Wild type mice exhibit hippocampal sclerosis and glial scarring in the chronic phase [36]; hence, our next step would be to analyze the extent of neuronal damage and glial activation in the hippocampus of *Nlrc3*$^{-/-}$ mice in chronic phase. Examination of spinal cord histology at week 30 p.i. did not show demyelinating lesions in wild type or *Nlrc3*$^{-/-}$ mice, indicating that *Nlrc3* gene does not alter the resistance of wild type mice to TMEV-induced demyelinating disease.

Here we found that in contrast to wild type mice, all the *Nlrc3*$^{-/-}$ mice exhibited pronounced seizures in the acute phase and about half of them developed spontaneous seizures in the chronic phase. Our study showed that Nlrc3 protects mice from TMEV-induced acute seizures and epilepsy to an extent. Acute pronounced inflammation contributes to initiation of acute seizures in wild type mice. Increased incidence of acute seizures in *Nlrc3*$^{-/-}$ mice could be due to suppression of the inhibitory role of Nlrc3 on acute inflammatory mediators, which requires further research. Taken together, our study identified an anti-inflammatory target in the innate immune system, which mitigates both acute seizures and epilepsy induced by TMEV infection. Future studies using Nlrc3 agonists may help to discover potential anti-epileptic drugs.

CHAPTER V

CONCLUSIONS

Epilepsy is a complex neurological disease characterized by unprovoked seizures [2], and is often associated with psychosocial impairments [98]. There is no existing cure for epilepsy. Symptomatic treatment is available to suppress seizure frequency, but current medications still fail to prevent seizures in 30% of the affected population. Therefore, further studies are required to better understand the pathophysiology of seizures, and to delineate more promising therapeutic targets [6,7].

TMEV-induced murine model of epilepsy

The TMEV-induced epilepsy in C57BL/6 mice was first reported by the Fujinami group almost a decade ago [34]. Since then, studies have been conducted to investigate the effects of distinct leukocytes subtypes, cytokines, and chemokines, etc. in the development of acute seizures and epilepsy. Past studies have revealed that the local glial cells (microglia and astrocytes) in the brain become activated in response to TMEV infection. Activated glial cells secrete pro-inflammatory cytokines and chemokines to activate and attract non-resident or peripheral immune cells to the site of insult (hippocampus). Although, the brain is considered as “immuno-privileged”, the dysregulated local immune responses disrupt the integrity of the BBB and cause leakage of peripheral immune cells into the CNS. The infiltrating immune cells such as macrophages,

granulocytes, etc. contribute to already heightened immune responses, pose a grave threat to the viability of neurons, and lead to acute seizures. The infected mice successfully clear virus from the CNS within a month p.i., but the overzealous acute inflammation, hippocampal damage and seizures themselves render mice susceptible to subsequent chronic seizures (epilepsy) [20,21,34,35,78,97].

TMEV-induced demyelinating disease model

TMEV infection induces a biphasic disease in SJL mice, where acute poliomyelitis-like symptoms appear in the early phase and demyelinating disease of the CNS occurs in the late phase. In the early phase, mice usually develop flaccid paralysis, while in the late phase of the disease, mice develop a waddling gait, body tremors, inactivity, impaired righting reflex, etc. Virus is mainly found in neurons in the early phase, while virus continues to persist in macrophages, astrocytes, and oligodendrocytes in the late phase of the disease [24,71,72,75,76]. The increased activation and expansion of T regulatory cells [147], and increased expression of anti-inflammatory cytokine (IL-10) [148] in the CNS of SJL mice could contribute to the inefficiency of T cell responses in mediating viral clearance. The late phase of the disease is characterized by pronounced mononuclear cell infiltration in the leptomeninges and white matter accompanied with primary demyelination in the spinal cord [24,71]. Since the clinical features of the demyelinating disease resemble with human multiple sclerosis (MS), TMEV-infected SJL mouse model has been extensively used to study the pathogenesis of MS.

To further analyze the virus-specific effects on the disease pathogenesis, Oleszak, Leibowitz et al. isolated and characterized two plaque-sized variants, DA-D_S and DA-C_L, of the DA strain of TMEV. Both variants were found genetically stable but they had different growth kinetics and neurovirulence in SJL mice. They found that DA-D_S plaque-sized variant was highly neurovirulent, had higher viral growth, and induced more severe demyelinating disease than the parental DA virus. In contrast to DA-D_S and parental DA virus, the DA-C_L plaque-sized variant yielded lower titers, and was unable to induce any clinical disease, even though it persisted in the CNS of SJL mice [80].

Virulence and pathogenicity of plaque-sized variants of DA strain in epilepsy

To determine the virus-specific effects in the pathogenesis of epilepsy, we infected C57BL/6 mice with either DA-D_S or DA-C_L, and compared the disease pathogenesis with sham-infected mice. We found that the DA-D_S variant induced acute seizures in ~94% of infected mice, while the DA-C_L variant induced seizures in ~12% of infected mice Besides experiencing severe seizures, the DA-D_S-infected mice also exhibited significantly higher sickness scores (non-epileptic clinical illness), and increased weight loss, viral burden in the CNS, neuro-edema, neuro-inflammation, hippocampal damage and anxiety-like symptoms than the DA-C_L-infected mice. However, spatial-associated memory was found to be impaired in both DA-D_S- and DA-C_L- infected mice. Unlike the parental DA virus-infected mice, we found high seizure occurrence and minimal phenotypic variability among the DA-D_S-infected mice. Therefore, we propose that the

DA-D_S-induced epilepsy model would be better suited to understand the disease pathogenesis and to test potential therapeutic drugs for treating epilepsy.

Moreover, upon comparing the genome sequences of DA-D_S and DA-C_L variants, we found three coding differences at the protein level, in the Leader (L), L*, and 2C proteins. The ability to impair the innate host immune response (IFN production) in certain cell types by either Leader or L* contributes to viral evasion of the host immune response and viral persistence [118,123,124,126,127]. Thus, we suggest that the mutations in the Leader and L* proteins of DA-C_L resulted in the attenuated phenotype of the DA-C_L variant in the C57BL/6 mouse model of epilepsy. Further studies are required to understand the distinct effects of the leader and L* proteins.

Implication of NLRs in neurological diseases

The NLRs are the intracellular microbial sensors, broadly classified as pro-inflammatory or anti-inflammatory based upon their role in inflammation [48]. Their expression has been found in brain cells, such as microglia [149], astrocytes [150], neurons [151], pericytes [142], and endothelial cells [143]. Moreover, several NLRs have been implicated in neurological diseases; e.g. NLR family, pyrin domain containing 1 (NLRP1) [152] and NLR family, pyrin domain containing 3 (NLRP3) [153] in Alzheimer's disease; NLRP3 in multiple sclerosis [154]; NLR family, CARD domain containing 4 (NLRC4), absent in melanoma 2 (AIM2) [155], and NLRP1 [156] in stroke; NLRP1 in traumatic brain injury [157]; NLRC5 in

bipolar disorder [158]; etc. With respect to epilepsy, the NLRP1 inflammasome has been suggested to promote neuronal death and chronic spontaneous seizures in an electrically-induced rat model of epilepsy. However, investigators did not find any changes in the occurrence of acute seizures upon NLRP1 silencing [145]. Here, we studied the effects of *Nlrc5* and *Nlrc3* genes, in the pathogenesis of, and susceptibility to, TMEV (BeAn strain)-induced mouse model of epilepsy using *Nlrc5*$^{-/-}$ and *Nlrc3*$^{-/-}$ mice.

The role of *Nlrc5* gene in TMEV-induced experimental model of epilepsy

The clinical studies showed that upon TMEV infection, *Nlrc5*$^{-/-}$ group showed a significant decrease in the proportion of mice suffering from seizures, and exhibited lower sickness scores and weight loss when compared with wild type mice. Flow cytometry studies from day 3 p.i. showed a significant increase in the expression levels of CD45.2 high CD11b+ cells (macrophages, granulocytes) and CD45.2 high Gr+ cells (granulocytes), but a significant reduction in the expression levels of CD45.2 high NK1.1+ cells (NK cells) in the brains from *Nlrc5*$^{-/-}$ infected mice compared to wild type infected mice. Using immunohistochemistry, we found a significant decrease in the number of astrocytes in the hippocampus of *Nlrc5*$^{-/-}$ infected mice than wild type infected mice on day 7 p.i. The gene expression studies using brains from *Nlrc5*$^{-/-}$ infected mice showed a significant reduction in the mRNA levels for the genes involved in the MHC class I pathway (*H2-Kb*, *β_2m*, and *Tap1*), *Il-1β*, *Ifn-β*, and *iNOS* compared to the wild type infected mice on day 7 p.i. However, *Nlrc5*$^{-/-}$ and wild type infected

mice showed no differences in mRNA levels for the genes involved in the MHC class II pathway (*H2-Aa*, *Ciita*), *TMEV*, *Il-6*, *Tnf-α*, *Ifn-γ*, *Mcp-1*, *Rantes*, and *Mip-2*. In addition, wild type infected mice showed a significant increase in the mRNA expression of *Nlrc5* compared to wild type control mice. Taken together, we found that in the wild type mice, the presence of intact Nlrc5 promotes seizures, sickness behavior, and weight loss by exacerbating neuroinflammation following infection with TMEV. As reported by other groups [54,55,57,59,138,144], activated Nlrc5 may modulate inflammation by regulating NF-κB - and IFN-signaling pathways and/or by regulating inflammasomes formed by other NLRs upon TMEV infection. However, further studies are required to understand these interactions. Nonetheless, our findings suggest a pro-inflammatory role of *Nlrc5* gene in *in vivo* model of TMEV-induced epilepsy.

The role of *Nlrc3* gene in TMEV-induced experimental model of epilepsy

With regards to Nlrc3, our studies determined an anti-epileptic effect of *Nlrc3* gene in TMEV-induced epilepsy. The clinical studies following infection showed that *Nlrc3*$^{-/-}$ mice had a significant increase in the susceptibility to TMEV-induced epilepsy. All *Nlrc3*$^{-/-}$ infected mice developed acute seizures, while ~30% of wild type infected mice remained seizure free during the first week p.i. In addition, *Nlrc3*$^{-/-}$ infected group had increase in the frequency of spontaneous seizures when compared with wild type infected group. We found minimal or no infiltration of peripheral leukocytes into the brain of wild type and *Nlrc3*$^{-/-}$ mice at week 30 p.i. Therefore, we suggest that unlike

acute seizures, chronic seizures do not correlate with the infiltration of peripheral leukocytes into the CNS. However, neuronal damage caused by acute phase inflammation may predispose mice to epilepsy. Additionally, we identified the development of aberrant behavior (anxiolytic) and hypermobility in *Nlrc3*$^{-/-}$ mice following infection, which was not found in wild type infected group.

Karki, Man, *et al.* recently proposed a protective role of Nlrc3 in the mouse model of colitis and colorectal tumorigenesis by suppressing the activation of mTOR-signaling pathway, and subsequently downregulating cellular proliferation. They found that affected wild type mice showed reduced expression of *Nlrc3* in their tumor tissue compared to control mice. However, the disease pathogenesis in *Nlrc3*$^{-/-}$ mice worsened as these mice developed more colon tumors and had increased damage to their colon. Furthermore, *Nlrc3*$^{-/-}$ mice showed a significant increase in the expression levels of innate immune cells (macrophages, NK cells, and neutrophils), pro-inflammatory cytokines (IL-1β, IL-6, TNF, etc.) and chemokines (macrophage chemoattractant protein-1 [MCP-1], monocyte inflammatory protein-1α [MIP-1α], etc.) and increased activation of immune signaling pathways in colon tissue in comparison to the wild type mice [68].

Notably, mTOR signaling pathway was also found to be activated in the chemoconvulsant (kainic acid [KA])-induced rodent model of epilepsy by two different groups. Shacka, Lu and colleagues found an acute activation of mTOR pathway in the

hippocampi of mice treated with KA [159], while Zeng, Rensing *et al.* found a biphasic activation of mTOR pathway in rats following KA treatment. An early phase of mTOR activation was seen in hippocampi and neocortex immediately after the onset of acute seizures, and mTOR activation lasted roughly until the resolution of acute seizures. A delayed phase of mTOR activation occurred in hippocampus alone that coincided with the period of epileptogenesis. Furthermore, they found that affected rats that were pretreated with Rapamycin, a mTOR inhibitor, had reduced activation of mTOR in both early and delayed phases, which consequently decreased the frequency of spontaneous seizures, and reduced neuronal death, neurogenesis, and mossy fiber sprouting. The affected rats that were treated with rapamycin within 24 hours after the resolution of KA-induced status epilepticus, had reduced mTOR activation in the chronic phase and decreased development of mossy fiber sprouting and frequency of spontaneous seizures. In addition, pretreatment with Rapamycin did not affect the seizure phenotype in the acute phase [160]. Like in the KA-induced model of epilepsy, the mTOR pathway could be of relevance in the TMEV-induced model of epilepsy. Since Nlrc3 strongly downregulates mTOR pathway, the hyper-susceptibility to TMEV-induced epilepsy seen among *Nlrc3*$^{-/-}$ infected mice could be a result of the inhibition of Nlrc3-mediated suppression of mTOR pathway. Future studies demonstrating the interaction between Nlrc3 and mTOR signaling pathway in TMEV infection would give us better insight into the role of Nlrc3 in the development of epilepsy.

Inflammation is essential for host defense against microbial infection and restoring homeostasis. Therefore, an appropriate balance is required between pro-inflammatory and anti-inflammatory mediators in response to injury or infection. However, dysregulated immune responses generated against TMEV infection lead to increased hippocampal pathology and seizures in C57BL/6 mice. Our findings suggest that mutated viruses may have altered neurovirulence, and can modulate host immune responses, causing subsequent alterations in disease pathogenesis. The differences between seized and non-seized mice following infection would aid in narrowing down the search for the critical factors that are of paramount importance in epilepsy. We also found unique and distinct effects of *Nlrc5* and *Nlrc3* genes in TMEV-induced epilepsy. The *Nlrc5* gene was found to be pro-inflammatory, as its deficiency suppressed neuro-inflammation and protected the infected C57BL/6 mice from seizures. On the other hand, the *Nlrc3* gene was found to be anti-inflammatory, as its deficiency significantly increased the susceptibility of C57BL/6 mice to acute and chronic seizures. Here, we found two potential inflammatory targets that could mitigate epilepsy. Future trials to test treatments downregulating the effects of *Nlrc5* gene or promoting the effects of *Nlrc3* gene may prove beneficial in further controlling seizures.

Future directions

TMEV-induced epilepsy in C57BL/6 mice proves to be an excellent model to study epileptogenesis, and mechanism of acute and chronic forms of seizures. Using plaque-

sized variants of DA strain, we found that mutated virus can significantly alter disease phenotype and can successfully modulate host inflammatory components. Therefore, future studies are required to investigate the specific effects of mutated viral proteins in regulating virulence and disease pathogenesis. We also identified the unique and contrasting roles of Nlrc5 and Nlrc3 in epilepsy development. We showed that Nlrc5 is a positive regulator of inflammation and seizures, while Nlrc3 serves as check-point to suppress both acute and chronic seizures. In addition, Nlrc3 regulates anxiolytic-behavior in mice under pathological conditions. Future studies determining the temporal expression and localization of Nlrc5 and Nlrc3 in the CNS would help in clarifying the mechanism of action of NLRs in epilepsy. To conclude, we found that both the virus and inflammation generated in response to virus infection are critical for the development of seizures. However, the exact cause of seizure onset at day 3 p.i. and the abrupt cessation of seizures at day 7 p.i. needs to be further elucidated.

REFERENCES

1 Hirtz, D. *et al.* How common are the “common” neurologic disorders? *Neurology* **68**, 326-337 (2007).

2 Fisher, R. S. *et al.* ILAE official report: a practical clinical definition of epilepsy. *Epilepsia* **55**, 475-482, doi:10.1111/epi.12550 (2014).

3 Fisher, R. S. *et al.* Operational classification of seizure types by the International League Against Epilepsy: Position Paper of the ILAE Commission for Classification and Terminology. *Epilepsia* **58**, 522-530 (2017).

4 Control, C. f. D. & Prevention. Epilepsy in adults and access to care--United States, 2010. *MMWR. Morbidity and mortality weekly report* **61**, 909 (2012).

5 Ngugi, A. K. *et al.* Incidence of epilepsy A systematic review and meta-analysis. *Neurology* **77**, 1005-1012 (2011).

6 Harward, S. C. & McNamara, J. O. in *Issues in Clinical Epileptology: A View from the Bench* 243-251 (Springer, 2014).

7 Cunliffe, V. T. *et al.* Epilepsy research methods update: Understanding the causes of epileptic seizures and identifying new treatments using non-mammalian model organisms. *Seizure* **24**, 44-51 (2015).

8 Berg, A. T. *et al.* Revised terminology and concepts for organization of seizures and epilepsies: report of the ILAE Commission on Classification and Terminology, 2005-2009. *Aktuelle Neurologie* **37**, 120-130 (2010).

9 Annegers, J. F., Rocca, W. A. & Hauser, W. A. in *Mayo Clinic Proceedings.* 570-575 (Elsevier).

10 Getts, D. R., Balcar, V. J., Matsumoto, I., Müller, M. & King, N. J. Viruses and the immune system: their roles in seizure cascade development. *Journal of neurochemistry* **104**, 1167-1176 (2008).

11 Misra, U. K., Tan, C. T. & Kalita, J. Viral encephalitis and epilepsy. *Epilepsia* **49**, 13-18 (2008).

12 Cole, A. J. Is epilepsy a progressive disease? The neurobiological consequences of epilepsy. *Epilepsia* **41**, S13-S22 (2000).

13 Kandratavicius, L. *et al.* Animal models of epilepsy: use and limitations. *Neuropsychiatric disease and treatment* **10**, 1693 (2014).

14 Stables, J. P. *et al.* Models for epilepsy and epileptogenesis: report from the NIH workshop, Bethesda, Maryland. *Epilepsia* **43**, 1410-1420 (2002).

15 Pekny, M., Wilhelmsson, U. & Pekna, M. The dual role of astrocyte activation and reactive gliosis. *Neuroscience letters* **565**, 30-38, doi:10.1016/j.neulet.2013.12.071 (2014).

16 Nguyen, M. D., Julien, J.-P. & Rivest, S. Innate immunity: the missing link in neuroprotection and neurodegeneration? *Nature Reviews Neuroscience* **3**, 216-227 (2002).

17 Ballabh, P., Braun, A. & Nedergaard, M. The blood–brain barrier: an overview: structure, regulation, and clinical implications. *Neurobiology of disease* **16**, 1-13 (2004).

18 Marchi, N., Granata, T., Ghosh, C. & Janigro, D. Blood–brain barrier dysfunction and epilepsy: pathophysiologic role and therapeutic approaches. *Epilepsia* **53**, 1877-1886 (2012).

19 Vezzani, A., French, J., Bartfai, T. & Baram, T. Z. The role of inflammation in epilepsy. *Nature reviews neurology* **7**, 31-40 (2011).

20 Libbey, J. E., Kennett, N. J., Wilcox, K. S., White, H. S. & Fujinami, R. S. Interleukin-6, produced by resident cells of the central nervous system and infiltrating cells, contributes to the development of seizures following viral infection. *J Virol* **85**, 6913-6922, doi:10.1128/jvi.00458-11 (2011).

21 Cusick, M. F., Libbey, J. E., Patel, D. C., Doty, D. J. & Fujinami, R. S. Infiltrating macrophages are key to the development of seizures following virus infection. *J Virol* **87**, 1849-1860, doi:10.1128/jvi.02747-12 (2013).

22 Coulter, D. A. & Steinhäuser, C. Role of astrocytes in epilepsy. *Cold Spring Harbor perspectives in medicine* **5**, a022434 (2015).

23 Vezzani, A., Ravizza, T., Balosso, S. & Aronica, E. Glia as a source of cytokines: implications for neuronal excitability and survival. *Epilepsia* **49**, 24-32 (2008).

24 Lipton, H. L. & Canto, M. C. Theiler's virus-induced central nervous system disease in mice. *UCLA forum in medical sciences*, 263-277 (1976).

25 Buenz, E. J. & Howe, C. L. Picornaviruses and cell death. *Trends in microbiology* **14**, 28-36 (2006).

26 Young, E. E. *et al.* Chronic social stress impairs virus specific adaptive immunity during acute Theiler's virus infection. *Journal of neuroimmunology* **254**, 19-27 (2013).

27 Theiler, M. & Gard, S. ENCEPHALOMYELITIS OF MICE : III. EPIDEMIOLOGY. *The Journal of experimental medicine* **72**, 79-90 (1940).

28 Lipton, H. L. Characterization of the TO strains of Theiler's mouse encephalomyelitis viruses. *Infection and immunity* **20**, 869-872 (1978).

29 Daniels, J. B., Pappenheimer, A. M. & Richardson, S. Observations on encephalomyelitis of mice (DA strain). *The Journal of experimental medicine* **96**, 517-530 (1952).

30 Theiler, M. & Gard, S. ENCEPHALOMYELITIS OF MICE : I. CHARACTERISTICS AND PATHOGENESIS OF THE VIRUS. *The Journal of experimental medicine* **72**, 49-67 (1940).

31 Lipton, H. L. Theiler's virus infection in mice: an unusual biphasic disease process leading to demyelination. *Infection and immunity* **11**, 1147-1155 (1975).

32 Theiler, M. SPONTANEOUS ENCEPHALOMYELITIS OF MICE, A NEW VIRUS DISEASE. *The Journal of experimental medicine* **65**, 705-719 (1937).

33 Lorch, Y., Friedmann, A., Lipton, H. L. & Kotler, M. Theiler's murine encephalomyelitis virus group includes two distinct genetic subgroups that differ pathologically and biologically. *J Virol* **40**, 560-567 (1981).

34 Libbey, J. E. *et al.* Seizures following picornavirus infection. *Epilepsia* **49**, 1066-1074, doi:10.1111/j.1528-1167.2008.01535.x (2008).

35 Libbey, J. E., Kennett, N. J., Wilcox, K. S., White, H. S. & Fujinami, R. S. Lack of correlation of central nervous system inflammation and neuropathology with the development of seizures following acute virus infection. *Journal of virology* **85**, 8149-8157 (2011).

36 Stewart, K.-A. A., Wilcox, K. S., Fujinami, R. S. & White, H. S. Development of Post-infection Epilepsy Following Theiler Virus Infection of C57BL/6 Mice. *Journal of neuropathology and experimental neurology* **69**, 1210 (2010).

37 Smeal, R. M. *et al.* The activity within the CA3 excitatory network during Theiler's virus encephalitis is distinct from that observed during chronic epilepsy. *Journal of neurovirology* **18**, 30-44 (2012).

38 Umpierre, A. D. *et al.* Impaired cognitive ability and anxiety-like behavior following acute seizures in the Theiler's virus model of temporal lobe epilepsy. *Neurobiology of disease* **64**, 98-106 (2014).

39 Kim, B. S., Palma, J. P., Kwon, D. & Fuller, A. C. Innate immune response induced by Theiler's murine encephalomyelitis virus infection. *Immunologic research* **31**, 1-12 (2005).

40 Drescher, K. M., Murray, P. D., David, C. S., Pease, L. R. & Rodriguez, M. CNS Cell Populations are Protected from Virus-Induced Pathology by Distinct Arms of the Immune System. *Brain pathology* **9**, 21-31 (1999).

41 D LINDSLEY, M., PATICK, A. K., PRAYOONWIWAT, N. & RODRIGUEZ, M. in *Mayo Clinic Proceedings.* 829-838 (Elsevier).

42 Pullen, L. C., Miller, S. D., Dal Canto, M. C. & Kim, B. S. Class I-deficient resistant mice intracerebrally inoculated with Theiler's virus show an increased T cell response to viral antigens and susceptibility to demyelination. *European journal of immunology* **23**, 2287-2293 (1993).

43 Rodriguez, M. *et al.* Abrogation of resistance to Theiler's virus-induced demyelination in H-2b mice deficient in beta 2-microglobulin. *The Journal of Immunology* **151**, 266-276 (1993).

44 Libbey, J. E., Kirkman, N. J., Wilcox, K. S., White, H. S. & Fujinami, R. S. Role for complement in the development of seizures following acute viral infection. *Journal of virology* **84**, 6452-6460 (2010).

45 Meissner, T. B. *et al.* NLR family member NLRC5 is a transcriptional regulator of MHC class I genes. *Proceedings of the National Academy of Sciences* **107**, 13794-13799 (2010).

46 Meissner, T. B., Li, A. & Kobayashi, K. S. NLRC5: a newly discovered MHC class I transactivator (CITA). *Microbes and Infection* **14**, 477-484 (2012).

47 Lupfer, C. & Kanneganti, T.-D. Unsolved mysteries in NLR biology. *Frontiers in immunology* **4** (2013).

48 Allen, I. C. Non-inflammasome forming NLRs in inflammation and tumorigenesis. *Frontiers in immunology* **5** (2014).

49 Biswas, A., Meissner, T. B., Kawai, T. & Kobayashi, K. S. Cutting edge: impaired MHC class I expression in mice deficient for Nlrc5/class I transactivator. *The Journal of Immunology* **189**, 516-520 (2012).

50 Yao, Y. *et al.* NLRC5 regulates MHC class I antigen presentation in host defense against intracellular pathogens. *Cell research* **22**, 836-847 (2012).

51 Robbins, G. R. *et al.* Regulation of class I major histocompatibility complex (MHC) by nucleotide-binding domain, leucine-rich repeat-containing (NLR) proteins. *Journal of Biological Chemistry* **287**, 24294-24303 (2012).

52 Neerincx, A., Rodriguez, G. M., Steimle, V. & Kufer, T. A. NLRC5 controls basal MHC class I gene expression in an MHC enhanceosome-dependent manner. *The Journal of Immunology* **188**, 4940-4950 (2012).

53 Ranjan, P. *et al.* NLRC5 interacts with RIG-I to induce a robust antiviral response against influenza virus infection. *European journal of immunology* (2014).

54 Neerincx, A. *et al.* A role for the human nucleotide-binding domain, leucine-rich repeat-containing family member NLRC5 in antiviral responses. *Journal of Biological Chemistry* **285**, 26223-26232 (2010).

55 Kuenzel, S. *et al.* The nucleotide-binding oligomerization domain-like receptor NLRC5 is involved in IFN-dependent antiviral immune responses. *The journal of immunology* **184**, 1990-2000 (2010).

56 Cui, J. *et al.* NLRC5 negatively regulates the NF-κB and type I interferon signaling pathways. *Cell* **141**, 483-496 (2010).

57 Tong, Y. *et al.* Enhanced TLR-induced NF-κB signaling and type I interferon responses in NLRC5 deficient mice. *Cell research* **22**, 822-835 (2012).

58 Kumar, H. *et al.* NLRC5 deficiency does not influence cytokine induction by virus and bacteria infections. *The Journal of Immunology* **186**, 994-1000 (2011).

59 Davis, B. K. *et al.* Cutting edge: NLRC5-dependent activation of the inflammasome. *The Journal of Immunology* **186**, 1333-1337 (2011).

60 Gültekin, Y., Eren, E. & Özören, N. Overexpressed NLRC3 Acts as an Anti-Inflammatory Cytosolic Protein. *Journal of innate immunity* **7**, 25-36 (2015).

61 Conti, B. J. *et al.* CATERPILLER 16.2 (CLR16. 2), a novel NBD/LRR family member that negatively regulates T cell function. *Journal of Biological Chemistry* **280**, 18375-18385 (2005).

62 Sha, Z. *et al.* NOD-like subfamily of the nucleotide-binding domain and leucine-rich repeat containing family receptors and their expression in channel catfish. *Developmental & Comparative Immunology* **33**, 991-999 (2009).

63 Li, M. *et al.* Expression profiles of NODs in channel catfish (Ictalurus punctatus) after infection with Edwardsiella tarda, Aeromonas hydrophila, Streptococcus iniae and channel catfish hemorrhage reovirus. *Fish & shellfish immunology* **33**, 1033-1041 (2012).

64 Cuvillier-Hot, V., Boidin-Wichlacz, C., Slomianny, C., Salzet, M. & Tasiemski, A. Characterization and immune function of two intracellular sensors, HmTLR1 and HmNLR, in the injured CNS of an invertebrate. *Developmental & Comparative Immunology* **35**, 214-226 (2011).

65 Shiau, C. E., Monk, K. R., Joo, W. & Talbot, W. S. An anti-inflammatory NOD-like receptor is required for microglia development. *Cell reports* **5**, 1342-1352 (2013).

66 Schneider, M. *et al.* The innate immune sensor NLRC3 attenuates Toll-like receptor signaling via modification of the signaling adaptor TRAF6 and transcription factor NF-[kappa] B. *Nature immunology* **13**, 823-831 (2012).

67 Zhang, L. *et al.* NLRC3, a member of the NLR family of proteins, is a negative regulator of innate immune signaling induced by the DNA sensor STING. *Immunity* **40**, 329-341 (2014).

68 Karki, R. *et al.* NLRC3 is an inhibitory sensor of PI3K–mTOR pathways in cancer. *Nature* (2016).

69 Lipton, H. L., Kim, B. S., Yahikozawa, H. & Nadler, C. F. Serological evidence that Mus musculus is the natural host of Theiler's murine encephalomyelitis virus. *Virus research* **76**, 79-86 (2001).

70 Lipton, H. L. Persistent Theiler's murine encephalomyelitis virus infection in mice depends on plaque size. *The Journal of general virology* **46**, 169-177, doi:10.1099/0022-1317-46-1-169 (1980).

71 Lipton, H. L. & Dal Canto, M. C. Chronic neurologic disease in Theiler's virus infection of SJL/J mice. *Journal of the neurological sciences* **30**, 201-207 (1976).

72 Lipton, H. L. & Dal Canto, M. C. Susceptibility of inbred mice to chronic central nervous system infection by Theiler's murine encephalomyelitis virus. *Infection and immunity* **26**, 369-374 (1979).

73 Libbey, J. E., Kennett, N. J., Wilcox, K. S., White, H. S. & Fujinami, R. S. Lack of correlation of central nervous system inflammation and neuropathology with the development of seizures following acute virus infection. *J Virol* **85**, 8149-8157, doi:10.1128/jvi.00730-11 (2011).

74 Lipton, H. & Melvold, R. Genetic analysis of susceptibility to Theiler's virus-induced demyelinating disease in mice. *The Journal of Immunology* **132**, 1821-1825 (1984).

75 Lipton, H. L. & Canto, C. Contrasting effects of immunosuppression on Theiler's virus infection in mice. *Infection and immunity* **15**, 903-909 (1977).

76 Sethi, P. & Lipton, H. Location and distribution of virus antigen in the central nervous system of mice persistently infected with Theiler's virus. *British journal of experimental pathology* **64**, 57 (1983).

77 Rodriguez, M., Leibowitz, J. L. & Lampert, P. W. Persistent infection of oligodendrocytes in Theiler's virus-induced encephalomyelitis. *Annals of neurology* **13**, 426-433 (1983).

78 Stewart, K. A., Wilcox, K. S., Fujinami, R. S. & White, H. S. Development of postinfection epilepsy after Theiler's virus infection of C57BL/6 mice. *Journal of neuropathology and experimental neurology* **69**, 1210-1219, doi:10.1097/NEN.0b013e3181ffc420 (2010).

79 Chamorro, M., Aubert, C. & Brahic, M. Demyelinating lesions due to Theiler's virus are associated with ongoing central nervous system infection. *Journal of virology* **57**, 992-997 (1986).

80 Oleszak, E. L., Leibowitz, J. L. & Rodriguez, M. Isolation and characterization of two plaque size variants of Theiler's murine encephalomyelitis virus (DA strain). *The Journal of general virology* **69 (Pt 9)**, 2413-2418, doi:10.1099/0022-1317-69-9-2413 (1988).

81 Kirkman, N. J., Libbey, J. E., Wilcox, K. S., White, H. S. & Fujinami, R. S. Innate but not adaptive immune responses contribute to behavioral seizures following viral infection. *Epilepsia* **51**, 454-464, doi:10.1111/j.1528-1167.2009.02390.x (2010).

82 Stewart, K. A., Wilcox, K. S., Fujinami, R. S. & White, H. S. Theiler's virus infection chronically alters seizure susceptibility. *Epilepsia* **51**, 1418-1428, doi:10.1111/j.1528-1167.2009.02405.x (2010).

83 Ohara, Y. *et al.* Molecular cloning and sequence determination of DA strain of Theiler's murine encephalomyelitis viruses. *Virology* **164**, 245-255 (1988).

84 Racine, R. J. Modification of seizure activity by electrical stimulation. II. Motor seizure. *Electroencephalogr Clin Neurophysiol* **32**, 281-294 (1972).

85 Welsh, C., Tonks, P., Nash, A. & Blakemore, W. The effect of L3T4 T cell depletion on the pathogenesis of Theiler’s murine encephalomyelitis virus infection in CBA mice. *J. Gen. Virol* **68**, 1659-1667 (1987).

86 Benson, M. J., Manzanero, S. & Borges, K. Complex alterations in microglial M1/M2 markers during the development of epilepsy in two mouse models. *Epilepsia* **56**, 895-905, doi:10.1111/epi.12960 (2015).

87 Young, E. E. *et al.* Chronic restraint stress during early Theiler's virus infection exacerbates the subsequent demyelinating disease in SJL mice: II. CNS disease severity. *Journal of neuroimmunology* **220**, 79-89 (2010).

88 Howe, C. L. *et al.* Hippocampal protection in mice with an attenuated inflammatory monocyte response to acute CNS picornavirus infection. *Scientific reports* **2**, 545, doi:10.1038/srep00545 (2012).

89 Pino, P. A. & Cardona, A. E. Isolation of brain and spinal cord mononuclear cells using percoll gradients. *Journal of visualized experiments: JoVE* (2011).

90 Komada, M., Takao, K. & Miyakawa, T. Elevated plus maze for mice. *Journal of visualized experiments : JoVE,* doi:10.3791/1088 (2008).

91 Jiang, Y. *et al.* Ketogenic diet attenuates spatial and item memory impairment in pentylenetetrazol-kindled rats. *Brain research* **1646**, 451-458, doi:10.1016/j.brainres.2016.06.029 (2016).

92 Moinfar, Z., Dambach, H. & Faustmann, P. M. Influence of drugs on gap junctions in glioma cell lines and primary astrocytes in vitro. *Frontiers in physiology* **5**, 186, doi:10.3389/fphys.2014.00186 (2014).

93 Frohman, M. A., Dush, M. K. & Martin, G. R. Rapid production of full-length cDNAs from rare transcripts: amplification using a single gene-specific oligonucleotide primer. *Proceedings of the National Academy of Sciences of the United States of America* **85**, 8998-9002 (1988).

94 Biolabs, N. E. NEB Tm Calculator v1.9.7.

95 Dossi, E., Vasile, F. & Rouach, N. Human astrocytes in the diseased brain. *Brain Research Bulletin* (2017).

96 Sofroniew, M. V. Molecular dissection of reactive astrogliosis and glial scar formation. *Trends in neurosciences* **32**, 638-647 (2009).

97 Howe, C. L., Lafrance-Corey, R. G., Sundsbak, R. S. & Lafrance, S. J. Inflammatory monocytes damage the hippocampus during acute picornavirus infection of the brain. *Journal of neuroinflammation* **9**, 50, doi:10.1186/1742-2094-9-50 (2012).

98 Bell, B., Lin, J. J., Seidenberg, M. & Hermann, B. The neurobiology of cognitive disorders in temporal lobe epilepsy. *Nature Reviews Neurology* **7**, 154-164 (2011).

99 Kanner, A. M. Epilepsy and mood disorders. *Epilepsia* **48**, 20-22 (2007).

100 Vogel-Ciernia, A. & Wood, M. A. Examining object location and object recognition memory in mice. *Current protocols in neuroscience*, 8.31. 31-38.31. 17 (2014).

101 Stewart, K.-A. A., Wilcox, K. S., Fujinami, R. S. & White, H. S. Development of postinfection epilepsy after Theiler's virus infection of C57BL/6 mice. *Journal of Neuropathology & Experimental Neurology* **69**, 1210-1219 (2010).

102 Buenz, E. J., Rodriguez, M. & Howe, C. L. Disrupted spatial memory is a consequence of picornavirus infection. *Neurobiology of disease* **24**, 266-273 (2006).

103 Buenz, E. J. *et al.* Apoptosis of hippocampal pyramidal neurons is virus independent in a mouse model of acute neurovirulent picornavirus infection. *The American journal of pathology* **175**, 668-684 (2009).

104 Engel Jr, J. Mesial temporal lobe epilepsy: what have we learned? *The Neuroscientist* **7**, 340-352 (2001).

105 Cendes, F. Mesial temporal lobe epilepsy syndrome: an updated overview. *Journal of Epilepsy and Clinical Neurophysiology* **11**, 141-144 (2005).

106 Curia, G. *et al.* Pathophysiogenesis of mesial temporal lobe epilepsy: is prevention of damage antiepileptogenic? *Current medicinal chemistry* **21**, 663-688 (2014).

107 Barker-Haliski, M. L. *et al.* Evaluating an etiologically relevant platform for therapy development for temporal lobe epilepsy: Effects of carbamazepine and valproic acid on acute seizures and chronic behavioral comorbidities in the Theiler's murine encephalomyelitis virus mouse model. *Journal of Pharmacology and Experimental Therapeutics* **353**, 318-329 (2015).

108 Bauer, J. *et al.* Astrocytes are a specific immunological target in Rasmussen's encephalitis. *Annals of neurology* **62**, 67-80 (2007).

109 Taylor, J. *et al.* Patients with epilepsy: cognitively compromised before the start of antiepileptic drug treatment? *Epilepsia* **51**, 48-56 (2010).

110 Tellez-Zenteno, J. F., Patten, S. B., Jetté, N., Williams, J. & Wiebe, S. Psychiatric comorbidity in epilepsy: a population-based analysis. *Epilepsia* **48**, 2336-2344 (2007).

111 Bannerman, D. *et al.* Regional dissociations within the hippocampus—memory and anxiety. *Neuroscience & Biobehavioral Reviews* **28**, 273-283 (2004).

112 Fanselow, M. S. & Dong, H.-W. Are the dorsal and ventral hippocampus functionally distinct structures? *Neuron* **65**, 7-19 (2010).

113 van Eyll, O. & Michiels, T. Non-AUG-initiated internal translation of the L* protein of Theiler's virus and importance of this protein for viral persistence. *J Virol* **76**, 10665-10673 (2002).

114 Michiels, T., Jarousse, N. & Brahic, M. Analysis of the leader and capsid coding regions of persistent and neurovirulent strains of Theiler's virus. *Virology* **214**, 550-558, doi:10.1006/viro.1995.0066 (1995).

115 Roos, R. P., Kong, W. P. & Semler, B. L. Polyprotein processing of Theiler's murine encephalomyelitis virus. *J Virol* **63**, 5344-5353 (1989).

116 Pevear, D. C., Calenoff, M., Rozhon, E. & Lipton, H. L. Analysis of the complete nucleotide sequence of the picornavirus Theiler's murine encephalomyelitis virus indicates that it is closely related to cardioviruses. *J Virol* **61**, 1507-1516 (1987).

117 Kong, W. P. & Roos, R. P. Alternative translation initiation site in the DA strain of Theiler's murine encephalomyelitis virus. *J Virol* **65**, 3395-3399 (1991).

118 van Pesch, V., van Eyll, O. & Michiels, T. The leader protein of Theiler's virus inhibits immediate-early alpha/beta interferon production. *J Virol* **75**, 7811-7817 (2001).

119 Chen, H. H., Kong, W. P. & Roos, R. P. The leader peptide of Theiler's murine encephalomyelitis virus is a zinc-binding protein. *J Virol* **69**, 8076-8078 (1995).

120 Kong, W. P., Ghadge, G. D. & Roos, R. P. Involvement of cardiovirus leader in host cell-restricted virus expression. *Proc Natl Acad Sci U S A* **91**, 1796-1800 (1994).

121 Sorgeloos, F., Jha, B. K., Silverman, R. H. & Michiels, T. Evasion of antiviral innate immunity by Theiler's virus L* protein through direct inhibition of RNase L. *PLoS Pathog* **9**, e1003474, doi:10.1371/journal.ppat.1003474 (2013).

122 Takano-Maruyama, M., Ohara, Y., Asakura, K. & Okuwa, T. Leader (L) and L* proteins of Theiler's murine encephalomyelitis virus (TMEV) and their regulation of the virus' biological activities. *J Neuroinflammation* **3**, 19, doi:10.1186/1742-2094-3-19 (2006).

123 Delhaye, S., van Pesch, V. & Michiels, T. The leader protein of Theiler's virus interferes with nucleocytoplasmic trafficking of cellular proteins. *J Virol* **78**, 4357-4362 (2004).

124 Ricour, C. *et al.* Inhibition of mRNA export and dimerization of interferon regulatory factor 3 by Theiler's virus leader protein. *J Gen Virol* **90**, 177-186, doi:10.1099/vir.0.005678-0 (2009).

125 Ciomperlik, J. J., Basta, H. A. & Palmenberg, A. C. Three cardiovirus Leader proteins equivalently inhibit four different nucleocytoplasmic trafficking pathways. *Virology* **484**, 194-202, doi:10.1016/j.virol.2015.06.004 (2015).

126 Chen, H. H., Kong, W. P., Zhang, L., Ward, P. L. & Roos, R. P. A picornaviral protein synthesized out of frame with the polyprotein plays a key role in a virus-induced immune-mediated demyelinating disease. *Nat Med* **1**, 927-931 (1995).

127 Ghadge, G. D., Ma, L., Sato, S., Kim, J. & Roos, R. P. A protein critical for a Theiler's virus-induced immune system-mediated demyelinating disease has a cell type-specific antiapoptotic effect and a key role in virus persistence. *J Virol* **72**, 8605-8612 (1998).

128 van Eyll, O. & Michiels, T. Influence of the Theiler's virus L* protein on macrophage infection, viral persistence, and neurovirulence. *J Virol* **74**, 9071-9077 (2000).

129 Bureau, J.-F. *et al.* Mapping loci influencing the persistence of Theiler's virus in the murine central nervous system. *Nature genetics* **5**, 87-91 (1993).

130 Clatch, R. J., Melvold, R. W., Miller, S. D. & Lipton, H. L. Theiler's murine encephalomyelitis virus (TMEV)-induced demyelinating disease in mice is influenced by the H-2D region: correlation with TEMV-specific delayed-type hypersensitivity. *The Journal of Immunology* **135**, 1408-1414 (1985).

131 Bureau, J. *et al.* The interaction of two groups of murine genes determines the persistence of Theiler's virus in the central nervous system. *Journal of virology* **66**, 4698-4704 (1992).

132 Bröer, S. *et al.* Viral mouse models of multiple sclerosis and epilepsy: Marked differences in neuropathogenesis following infection with two naturally

occurring variants of Theiler's virus BeAn strain. *Neurobiology of Disease* **99**, 121-132 (2017).

133 Ting, J. P.-Y. *et al.* The NLR gene family: a standard nomenclature. *Immunity* **28**, 285-287 (2008).

134 Biswas, A. & Kobayashi, K. S. Regulation of intestinal microbiota by the NLR protein family. *International immunology* **25**, 207-214 (2013).

135 Coutermarsh-Ott, S., Eden, K. & Allen, I. C. Beyond the inflammasome: regulatory NOD-like receptor modulation of the host immune response following virus exposure. *Journal of General Virology* **97**, 825-838 (2016).

136 Kong, X., Yuan, Z. & Cheng, J. The function of NOD-like receptors in central nervous system diseases. *Journal of neuroscience research* (2016).

137 Benko, S., Magalhaes, J. G., Philpott, D. J. & Girardin, S. E. NLRC5 limits the activation of inflammatory pathways. *The Journal of Immunology* **185**, 1681-1691 (2010).

138 Triantafilou, K., Kar, S., van Kuppeveld, F. J. & Triantafilou, M. Rhinovirus-induced calcium flux triggers NLRP3 and NLRC5 activation in bronchial cells. *American journal of respiratory cell and molecular biology* **49**, 923-934 (2013).

139 Racine, R. J. Modification of seizure activity by electrical stimulation: II. Motor seizure. *Electroencephalography and clinical neurophysiology* **32**, 281-294 (1972).

140 Mendez-Fernandez, Y. V., Hansen, M. J., Rodriguez, M. & Pease, L. R. Anatomical and cellular requirements for the activation and migration of virus-

specific CD8+ T cells to the brain during Theiler's virus infection. *Journal of virology* **79**, 3063-3070 (2005).

141 Staehli, F. *et al.* NLRC5 deficiency selectively impairs MHC class I-dependent lymphocyte killing by cytotoxic T cells. *The Journal of Immunology* **188**, 3820-3828 (2012).

142 Nyúl-Tóth, Á. *et al.* Expression of pattern recognition receptors and activation of the non-canonical inflammasome pathway in brain pericytes. *Brain, Behavior, and Immunity* (2017).

143 Nagyőszi, P. *et al.* Regulation of NOD-like receptors and inflammasome activation in cerebral endothelial cells. *Journal of neurochemistry* **135**, 551-564 (2015).

144 Guo, X. *et al.* Respiratory syncytial virus infection upregulates NLRC5 and major histocompatibility complex class I expression through RIG-I induction in airway epithelial cells. *Journal of virology* **89**, 7636-7645 (2015).

145 Tan, C.-C. *et al.* NLRP1 inflammasome is activated in patients with medial temporal lobe epilepsy and contributes to neuronal pyroptosis in amygdala kindling-induced rat model. *Journal of neuroinflammation* **12**, 18 (2015).

146 Eren, E., Berber, M. & Özören, N. NLRC3 protein inhibits inflammation by disrupting NALP3 inflammasome assembly via competition with the adaptor protein ASC for pro-caspase-1 binding. *Journal of Biological Chemistry*, jbc. M116. 769695 (2017).

147 Richards, M. H. *et al.* Virus expanded regulatory T cells control disease severity in the Theiler's virus mouse model of MS. *Journal of autoimmunity* **36**, 142-154 (2011).

148 Herder, V. *et al.* Interleukin-10 expression during the acute phase is a putative prerequisite for delayed viral elimination in a murine model for multiple sclerosis. *Journal of neuroimmunology* **249**, 27-39 (2012).

149 Burm, S. M. *et al.* Inflammasome-induced IL-1β secretion in microglia is characterized by delayed kinetics and is only partially dependent on inflammatory caspases. *Journal of Neuroscience* **35**, 678-687 (2015).

150 Minkiewicz, J., Rivero Vaccari, J. P. & Keane, R. W. Human astrocytes express a novel NLRP2 inflammasome. *Glia* **61**, 1113-1121 (2013).

151 Wang, Y.-C. *et al.* Acid-sensing ion channel 1a contributes to the effect of extracellular acidosis on NLRP1 inflammasome activation in cortical neurons. *Journal of neuroinflammation* **12**, 246 (2015).

152 Tan, M. *et al.* Amyloid-β induces NLRP1-dependent neuronal pyroptosis in models of Alzheimer's disease. *Cell death & disease* **5**, e1382 (2014).

153 Halle, A. *et al.* The NALP3 inflammasome is involved in the innate immune response to amyloid-β. *Nature immunology* **9**, 857-865 (2008).

154 La Rosa, F. *et al.* Up-regulation of Nod Like Receptors-3 signaling in multiple sclerosis disease. *Journal of Neuroimmunology* **275**, 87 (2014).

155 Denes, A. *et al.* AIM2 and NLRC4 inflammasomes contribute with ASC to acute brain injury independently of NLRP3. *Proceedings of the National Academy of Sciences* **112**, 4050-4055 (2015).

156 Abulafia, D. P. *et al.* Inhibition of the inflammasome complex reduces the inflammatory response after thromboembolic stroke in mice. *Journal of Cerebral Blood Flow & Metabolism* **29**, 534-544 (2009).

157 de Rivero Vaccari, J. P. *et al.* Therapeutic neutralization of the NLRP1 inflammasome reduces the innate immune response and improves histopathology after traumatic brain injury. *Journal of Cerebral Blood Flow & Metabolism* **29**, 1251-1261 (2009).

158 Pacifico, R. & Davis, R. Transcriptome sequencing implicates dorsal striatum-specific gene network, immune response and energy metabolism pathways in bipolar disorder. *Molecular psychiatry* (2016).

159 Shacka, J. J. *et al.* Kainic acid induces early and transient autophagic stress in mouse hippocampus. *Neuroscience letters* **414**, 57-60 (2007).

160 Zeng, L.-H., Rensing, N. R. & Wong, M. The mammalian target of rapamycin signaling pathway mediates epileptogenesis in a model of temporal lobe epilepsy. *Journal of Neuroscience* **29**, 6964-6972 (2009).